Summer 8-23-2019

Fractures, Fluids, and Metamorphism: Shear Zone Initiation in the Marcy Anorthosite Massif, Adirondacks, New York, USA

James Hodge
University of Maine, jloganhodge@gmail.com

Recommended Citation

FRACTURES, FLUIDS, AND METAMORPHISM: SHEAR ZONE INITIATION IN THE

MARCY ANORTHOSITE MASSIF, ADIRONDACKS, NEW YORK, USA

By

James Hodge

B.S. College of Saint Rose, 2017

A Thesis

Submitted in Partial Fulfillment of the

Requirements for the Degree of

Master of Science

(in Earth and Climate Sciences)

The Graduate School

The University of Maine

August 2019

Advisory Committee:

Scott Johnson, Professor and Director School of Earth and Climate Sciences, Advisor

Chris Gerbi, Professor School of Earth and Climate Sciences, Advisor

Alicia Cruz-Uribe, Professor School of Earth and Climate Sciences

Martin Yates, Professor School of Earth and Climate Sciences

FRACTURES, FLUIDS, AND METAMORPHISM: SHEAR ZONE INITIATION IN THE

MARCY ANORTHOSITE MASSIF, ADIRONDACKS, NEW YORK, USA

By James Hodge

Thesis Advisors: Dr. Scott Johnson, Dr. Chris Gerbi

An Abstract of the Thesis Presented
in Partial Fulfillment of the Requirements for the
Degree of Master of Science
(in Earth and Climate Sciences)
August 2019

Localized shear zones are important rheological features that influence deformation behavior throughout the Earth's middle-to-lower crust. Therefore, the processes through which shear zones initiate and localize remains an important geologic question. The study of strain localization and shear zone initiation is made difficult due to continued deformation overprinting the microstructures which lead to initiation and obfuscating the context in which localization occurred. The Marcy anorthosite in the Adirondack Highlands, New York, is a nominally granulite-facies, plagioclase-rich massif cut by centimeter-to-meter scale shear zones which provides a natural example of shear zone localization within the middle-to-lower crust. My work focuses on the microstructural examination of shear zones at Bennies Brook within the Marcy massif to construct the sequence of geologic events which lead to shear zone initiation. I used field observations combined with optical and electron microscope observations and electron probe geochemistry to investigate how microstructural conditions changed over time as the sequence progressed, as well as explore the tectonic implications of shear zone development within the massif. My results suggest that the initiation of viscous shearing was facilitated by a combination of physical and chemical weakening during exhumation. The country rock

anorthosite was pervasively fractured and/or crushed which increased permeability sufficiently to allow for the infiltration of chlorine-rich hydrothermal fluids, primarily along centimeter-wide brittle fault zones where permeability was greatest. These fluids triggered the retrograde replacement of plagioclase feldspar to scapolite and pyroxene to amphibole and quartz. This weakened the rock through the introduction of the relatively weak minerals as well as an associated reduction in grain size. In the planar zones of greatest metasomatism, this weakening was sufficient for viscous shearing to initiate. The relative timing and orientation of the shear zones supports previous work suggesting that the Adirondack Highlands underwent exhumation associated with orogenic collapse during the Ottawan orogeny (ca. 1080–1000 Ma).

TABLE OF CONTENTS

LIST OF TABLES

LIST OF FIGURES

CHAPTER 1

INTRODUCTION

1.1. Purpose of Study

Why am I studying this geologic problem, and what can I contribute?

Understanding the microscale processes by which the Earth's middle-to-lower crust deforms is an important step in understanding macro scale tectonic features. Of particular importance are the mechanisms by which strain is able to localize into discrete, long-lived shear zones that accommodate crustal displacement along plate boundaries and detachment zones during orogenic cycles (Kenkmann & Dresen, 2002; Regenauer-Lieb & Yuen, 2004; Warren & Hirth, 2006; Platt & Behr, 2011; Bercovici & Ricard, 2012; Montési, 2013; Gueydan et al., 2014). In addition to providing information about past tectonic activity, macro scale shear zones at depth can drive fault zone movement at and near the Earth's surface, often representing a threat to nearby human populations. However, despite being a fundamental aspect of Earth's deformation behavior at depth and an association with seismic events, the underlying chemical and geophysical processes that drive the localization and development of shear zones are still not definitively understood. Because the middle-to-lower crust comprises mostly plagioclase-rich mafic rocks, studying strain localization processes in these rock types is of particular importance (Ji & Mainprice, 1990; Rybacki & Dresen, 2004; Bürgmann & Dresen, 2008; Svahnberg & Piazolo, 2010; Menegon et al., 2013; Okudaira et al., 2017; Putnis et al., 2017). Current knowledge of the processes that contribute to strain localization in these and other rocks comes from field investigations, laboratory experiments, and numerical modeling. In the field, much

work has been done examining shear zones cutting metamorphosed crystalline rocks in outcrop that have been exhumed from depth. These studies generally use *in-situ* mapping techniques to characterize and develop a structural context for a work site, then focus on microstructural analyses to determine the dominant deformation mechanisms and/or construct a geochronological timeline (Kenkmann & Dresen, 2002; Mancktelow & Pennacchioni, 2005, Warren & Hirth, 2006; Marsh et al., 2009; Svahnberg & Piazolo, 2010; Okudaira et al., 2017). Experimental laboratory work has primarily focused on testing deformation using compression and shear apparatuses. This research has been instrumental to the understanding of deformation mechanisms by allowing for the derivation of empirical flow laws and constraints on dominant creep regimes, with attention often focused on grain size variability and creep mechanisms (Tullis & Yund, 1991; Post and Tullis, 1999; Stünitz & Tullis, 2001; Marti et al., 2018). Finally, the last two decades have seen the advancing use of numerical modeling in examining structural, tectonic, and rheological problems. Numerical models utilize experimentally-derived flow laws, crystallographic attributes, and other empirical data to produce various models of factors such as grain-size evolution and bulk strength of solid Earth material under stress (Mancktelow, 2002; Misra & Mandal, 2007; Cook et al., 2014; Gueydan et al., 2014; Cross et al., 2015; Gerbi et al., 2016; Xu & Zhang, 2018). Despite this considerable body of work investigating strain localization and shear zone formation using multiple methods, there are still aspects that are not well characterized. As much of the literature on strain localization is concerned with the rheological evolution of shear zones, a notable knowledge gap exists regarding the processes through which viscous shear zones initiate in the middle-lower crust.

In this study, I seek to fill some of this knowledge gap by analyzing natural shear zones formed in the interior of the anorthositic Marcy massif, Adirondacks, New York to determine the
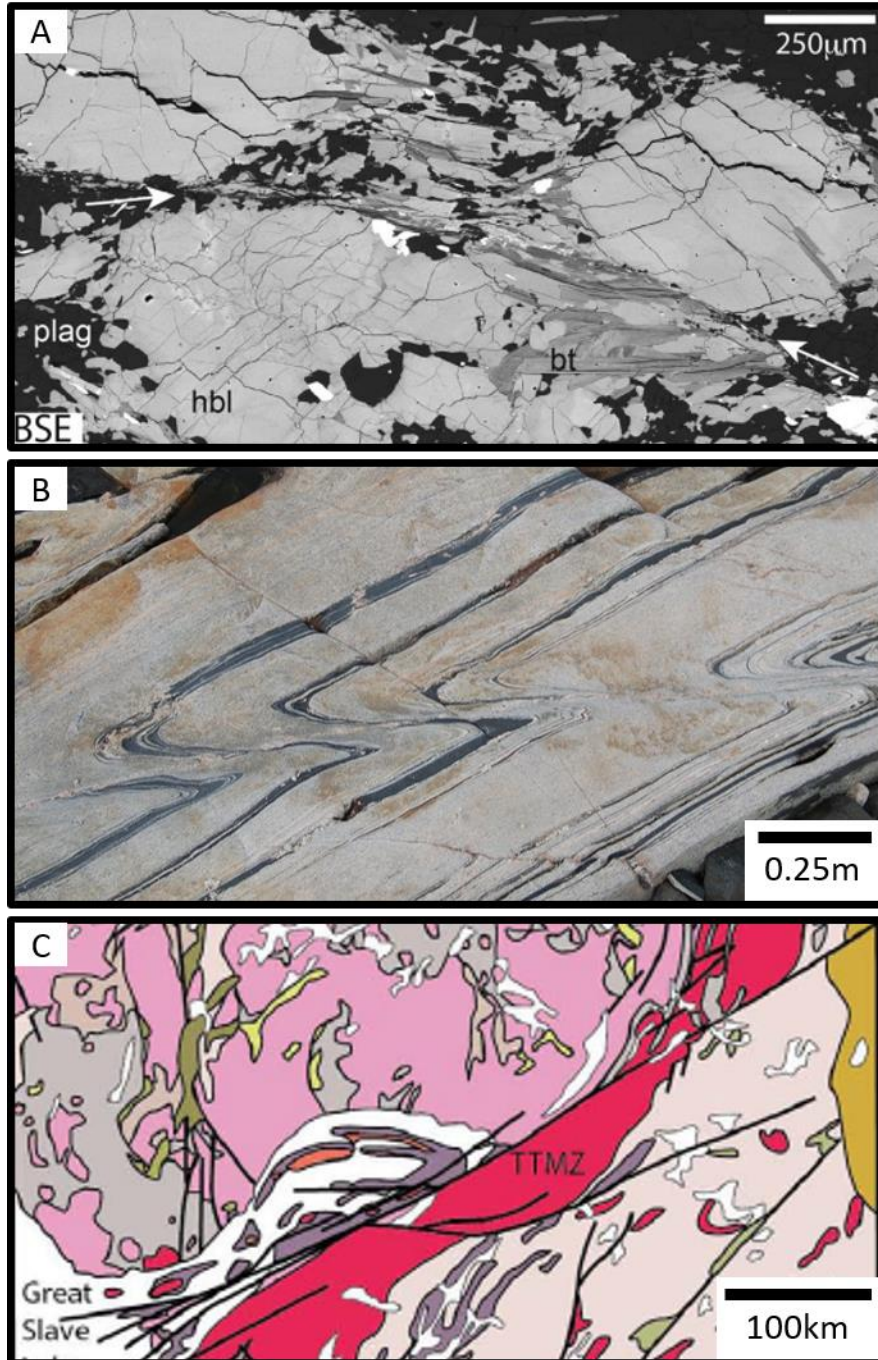
Figure 1.1.   Comparison of several examples of shear zones on varying scales. (A) Micro-scale shear zone cutting through amphibolite-facies gneiss, Fjordland, New Zealand (Gerbi et al., 2016). (B) Meso-scale shear zone displacing mafic and felsic bands of granulite-facies gneiss. Parry Sound, Ontario (Photograph from Chris Gerbi). (C) Macro-scale Great Slave Lake shear zone displacing various rock bodies in the Northern Territories of Canada (Fossen & Cavalcante, 2017).

mechanisms by which viscous strain localization initiates and evolves. The Marcy massif is a plagioclase-rich body that has undergone granulite-facies metamorphism during an orogenic event, followed by amphibolite-facies metamorphism during exhumation, and is now exposed at the Earth's surface (McLelland et al., 1996). The Marcy anorthosite and surrounding rocks constitute the Adirondack Highlands, the southern-most extent of the Grenville Province which runs primarily along the coast of eastern Canada. The Highlands have been investigated throughout the past century for insight into the Grenville orogenic cycle, which impacted much of the eastern coast of North America from ca. 1150-950 Ma, and are a typical example of amphibolite-granulite facies terranes (Buddington, 1939; Valley & O'Neil, 1982; Mezger et al., 1991; McLelland et al., 1996; Clechenko & Valley, 2003; Storm & Spear, 2005; Seifert et al., 2010; Peck et al., 2018; Regan et al., 2019). However, due to a lack of accessible outcrops, relatively little existing work has focused on deformational microstructures within the massif interior. Therefore, my goals in this study are two-fold. First, I analyze and document deformational and metamorphic microstructures within the Marcy massif to better characterize strain localization processes in meta-anorthosite. Second, I relate these microstructures to the broader Adirondack context, which helps to characterize the deformational history of this geologically important region.

1.2. Shear Zone Formation and Evolution

Where do shear zones form, what drives their formation, and how does their rheology evolve through space and time?

The localization of strain into discrete shear features within the Earth's crust has been thoroughly documented across all scales, from micro-shear zones to tectonic plate boundaries

4

(Figure 1.1) (Poirier, 1980; White et al., 1980; Kirby, 1985; Segall & Simpson, 1986; Mancktelow, 2002, Warren & Hirth, 2006; Marsh et al., 2009; Linckens et al., 2011; Goncalves et al., 2012; Gerbi et al., 2016; Fossen & Cavalcante, 2017). Although the ubiquitous nature of localization throughout nearly every rock type and regime provides countless opportunity for studying these features, hence the large amount of existing literature, this ubiquity also means that conditions of shear zone development are variable and extracting universally applicable information from any given instance can be difficult. Therefore, the driving processes by which strain localizes still represent an important rheological question (Tullis & Yund, 1991; Post and Tullis, 1999; Montési, 2013; Czaplińska et al., 2015; Shulman, 2016; Marti et al., 2018).

Shear zone formation can be partitioned into two phases: initial brittle and/or viscous failure in response to external stresses, and the subsequent development of that initial deformation into a zone of localized strain (Tullis & Yund, 1987; Mancktelow & Pennacchioni 2005; Fusseis et al., 2006; Goncalves et al., 2012; Fossen & Cavalcante, 2017). In the brittle regime, deformation occurs essentially instantaneously resulting in discrete fractures from microscale crack networks to crustal/lithospheric scale fault zones and/or cataclastic flow of brittle fragments. Initiation of brittle deformation is dependent on the ratio of the applied stress to the rock's tensile/shear strength, and the propagation of these features is described by fracture mechanics. In the viscous regime, nucleation is followed by viscous creep governed by material-dependent flow laws. This behavior manifests as narrowing with increased strain if controlled by strain-weakening processes or broadening if controlled by strain-strengthening processes (Mitra, 1978; White et al., 1980; Means, 1995; Warren & Hirth, 2006; Linckens et al., 2011; Goncalves et al., 2012; Fossen & Cavalcante, 2017). Once strain is initiated, a variety of parameter-dependent deformation mechanisms partition strain into shear zones which can have a wide

variety of behaviors based on deformation conditions, rock type, and dominant creep

mechanism. Whether or not a given rock will deform through brittle failure or viscous creep

depends both on internal properties (mineral types, topology, grain size) and external properties

(differential stress, strain rate, temperature, pressure, fluid access) (Passchier & Trouw, 2005;

Bürgmann & Dresen, 2008; Shulman, 2016). Because temperature and pressure are important

factors in determining deformation behavior regardless of other variables, certain regimes tend to

dominate at different depths in Earth's crust (Figure 1.2). However, the impact of other internal

and external factors is becoming increasingly recognized, and the partitioning of the crust into

definitive deformation regimes is idealized (Fitz Gerald & Stünitz, 1993; Stünitz et al., 2003;

Brander et al., 2012; Hertgen et al., 2017). Often in the case of viscous strain-weakening

systems, deformation is dominated by dislocation creep, which reduces grain size through
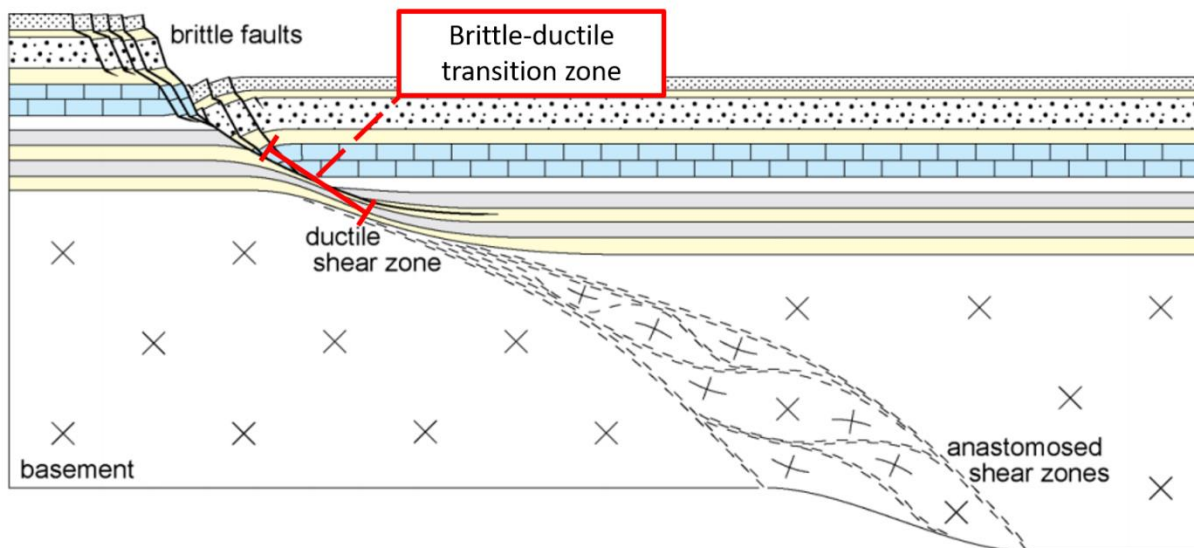
Figure 1.2. Idealized cross-section of a fault system through Earth's continental crust. Deformation mechanisms change from brittle faulting in the upper crust to primarily viscous deformation in the middle crust. In the lower crust, strain widens into anastomosing mylonite zones. Though coexistence of brittle to viscous behavior is often thought to be confined to a relatively narrow transition zone in the middle crust based on typical temperature and pressure gradients, the position and extent of this zone can vary based on rock type, tectonic setting, and fluid access. Modified from Ramsay (1980).

dynamic recrystallization processes such as grain-boundary movement. This response decreases the energy in the system by eliminating crystal lattice dislocations associated with high elastic energy (Passchier & Trouw, 2005). These forms of creep are driven by differential stress and strain rate but are insensitive to grain size. However, with continued deformation, grain size will become small enough (2–10 µm) that grain-size sensitive creep mechanisms such as grain-boundary diffusion become more efficient and the system will weaken (Tullis & Yund, 1991; Braun et al., 1999; Warren & Hirth, 2006).

The mechanisms by which strain localization nucleates remains difficult to study because initial conditions are inevitably overprinted by the subsequent development of a shear zone. To circumvent the obstacle of overprinting deformation, a spatial strain gradient must be present. If an increase in strain exists over a given area, it can serve as a general proxy for increasing strain over time, assuming that high-strain areas passed through the same microstructural history as low-strain areas (Ramsay, 1980; Johnson et al., 2004). This allows for the initiation of localization to be examined. Numerical modelling is also a useful tool for looking at initiation conditions without the worry of any textural overprinting. Modelling has been instrumental in showing that in rocks, which are elastically and viscously heterogenous at the grain scale, localization can occur due to the heterogenous distribution of microscale stresses under a homogenous macroscale stress, especially in polymineralic systems (Cook et al., 2014; Gerbi et al, 2016). These microscale stresses are created by strength heterogeneities, from varying mineral types, crystal orientations, and rheologically distinct inclusions (Mancktelow, 2002; Misra & Mandal, 2007; Gerbi et al, 2016).

1.3. Retrograde Metamorphic Weakening

What impact can retrograde metamorphism have on the strength of rocks in the lower crust?

The abundance of plagioclase-rich, granulite-facies provinces within the Earth's lower crust makes them important when considering geodynamics and tectonics. These rock bodies typically have a very low fluid content as a result of high-grade metamorphic reactions and dehydration melting (Thompson, 1982; Harlov, 2012), giving them a relatively high strength. When these dry rocks are exhumed or otherwise transported to lower temperature conditions, they become progressively farther out of equilibrium, as retrograde reactions typically require fluid to initiate, and diffusion timescales are long. However, there is evidence of granulite bodies retrogressed to amphibolite-facies mineral assemblages through metasomatic processes facilitated by the presence of fluid (Kullered & Erambert, 1999; Mukai et al., 2014; Kusebauch
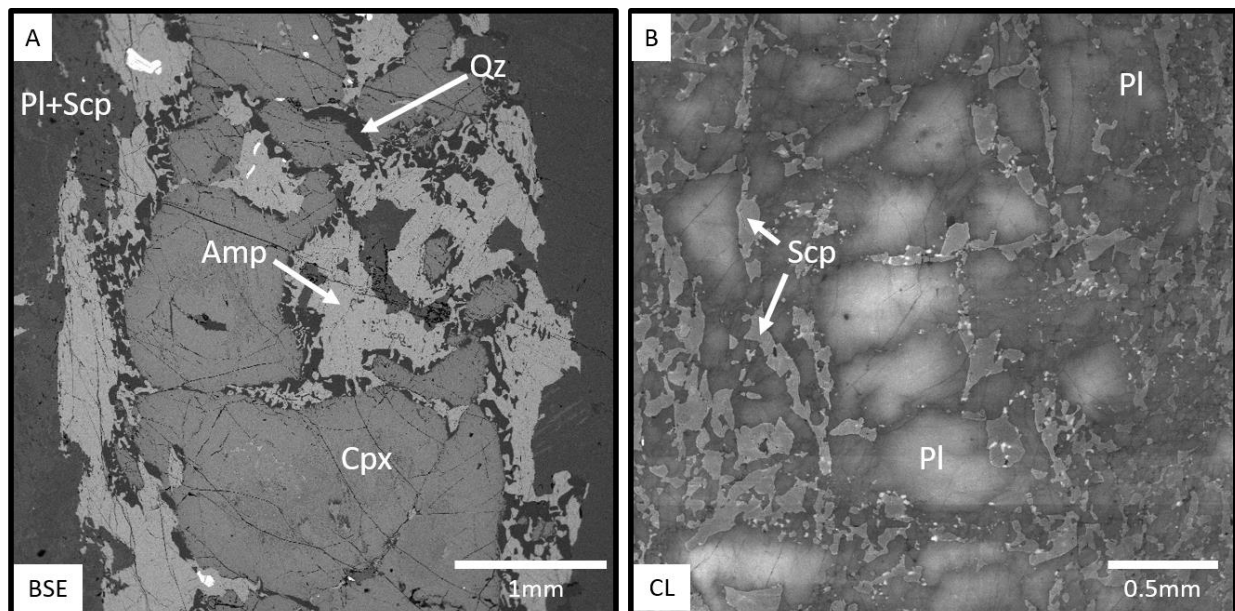
Figure 1.3.   Examples of retrograde replacement. Replacement reaction microstructures in a granulite facies anorthosite that lead to grain-size reduction and growth of relatively weak minerals, Adirondacks, New York. (A) Amphibole + quartz symplectite replacing pyroxene. (B) Scapolite replacing plagioclase along grain boundaries and triple junctions.

et al., 2015; Okudaira et al., 2017; Putnis et al., 2017; Centrella et al., 2018; Condit & Mahan, 2018). A common explanation of this is an increased permeability within the granulite body allowing for the infiltration of fluids which facilitate diffusion/mass-transfer processes and trigger retrograde reactions to equilibrate the rock to lower-grade conditions. As part of the retrograde process, strong mineral assemblages such as plagioclase and pyroxene transition to much weaker assemblages such as quartz, amphibole, and mica. The transition to lower-grade assemblages is also commonly accompanied by a grain-size reduction as modal abundances shift and new grains form (Figure 1.3). The combination of these processes typically lowers the strength of the rock (Brodie & Rutter, 1987; Fitz Gerald & Stünitz, 1993; Stünitz & Tullis, 2001; de Ronde, et al., 2005; Holyoke & Tullis, 2006; Marsh et al., 2009; Goncalves et al., 2012; Jamtveit et al., 2016; Centrella et al., 2018; Marti et al., 2018).

1.4. Geologic Setting

What are the tectonic and metamorphic histories of the Adirondack Highlands, and how do the structures at my study site reflect them?

The Adirondack Highlands region constitutes the southern-most extent of the Grenville province which runs primarily along the coast of eastern Canada and is the result of a prolonged and complex collisional tectonic period from approximately 1300–950 Ma, during which volcanic arcs accreted to the eastern coast of Laurentia (Figure 1.4) (McLelland, 1989; Rivers & Corrigan, 2000; Rivers, 2008). The region has been studied throughout the past century to understand the complex regional tectonic and metamorphic history (Buddington, 1939; Valley & O'Neil, 1982; Mezger et al., 1991; McLelland et al., 1996; Clechenko & Valley, 2003; Storm &

Spear, 2005; Seifert et al., 2010; Peck et al., 2018; Regan et al., 2019), with a particular focus on

the ca. 3000 km^2 Marcy anorthosite massif.

1.4.1. Tectonic and Polymetamorphic History

The Marcy massif is part of the voluminous Adirondack anorthosite-mangerite-

charnockite-granite (AMCG) suite (Figure 1.4). Members of this suite were likely derived

bimodally during delamination of the lithosphere ca. 1150 Ma (McLelland et al., 2004), with
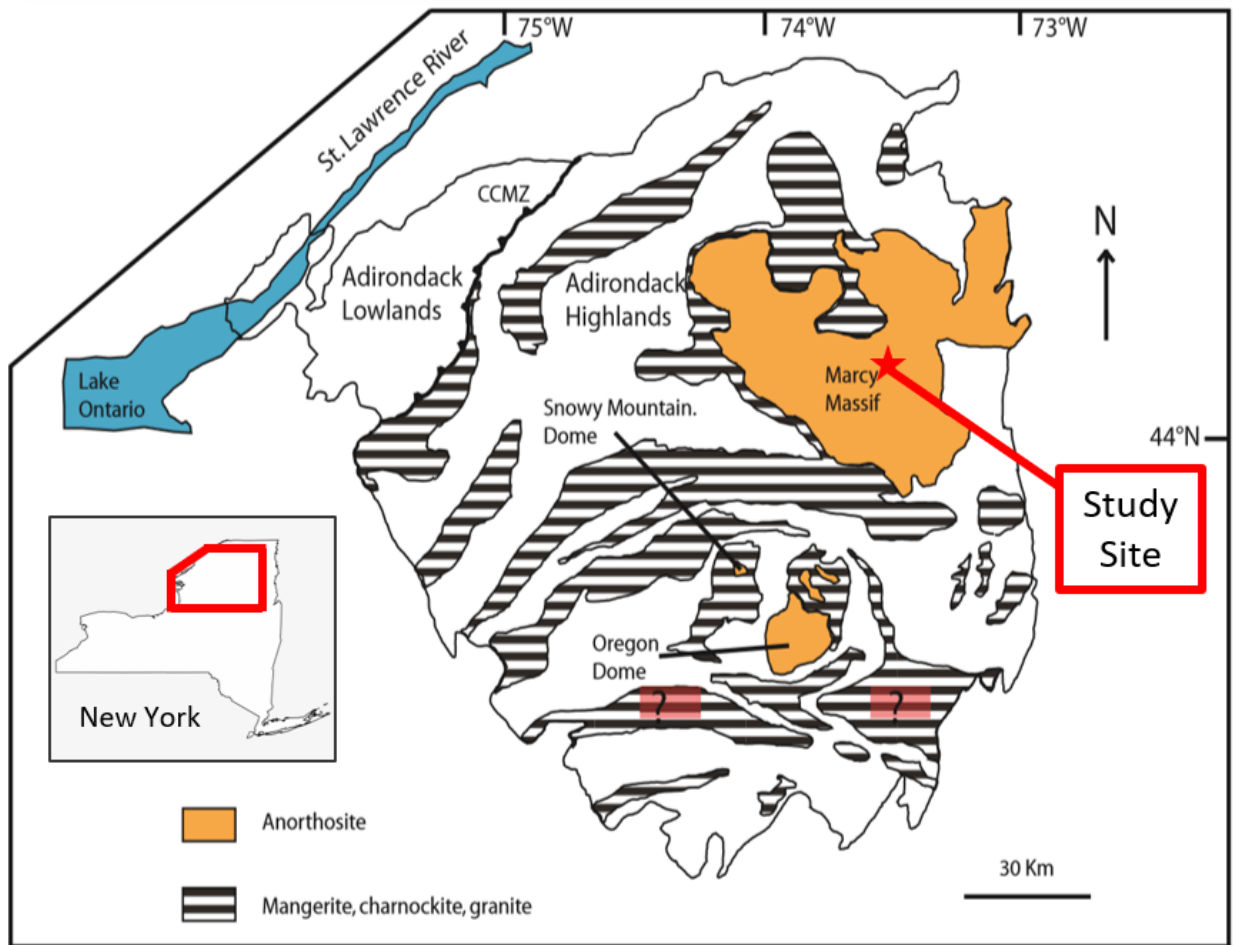
Figure 1.4.   Map of the Adirondack region of upstate New York showing the Marcy Massif
and the study site location. Black-and-white-striped zones are other igneous bodies within the
Adirondack Highlands coeval with the Marcy anorthosite. Areas in white are mostly meta-
igneous and meta-sedimentary gneisses, marbles, and skarns. Adapted from Regan et al. (2011).

10

anorthositic and gabbroic rocks sourced by fractional crystallization of the asthenosphere and more felsic members sourced by anatexis of continental crust. If so, the suite is coeval but not comagmatic (McLelland et al., 2004; Seifert et al., 2010; Regan et al., 2011; Regan et al., 2019). The timing of the emplacement has been reliably determined to be ca. 1150 Ma during the Shawinigan orogeny (McLelland et al., 2004). However, the depth of this emplacement has been difficult to confirm. $\delta^{18}O$ values of skarns along the massif margin indicate that meteoric water
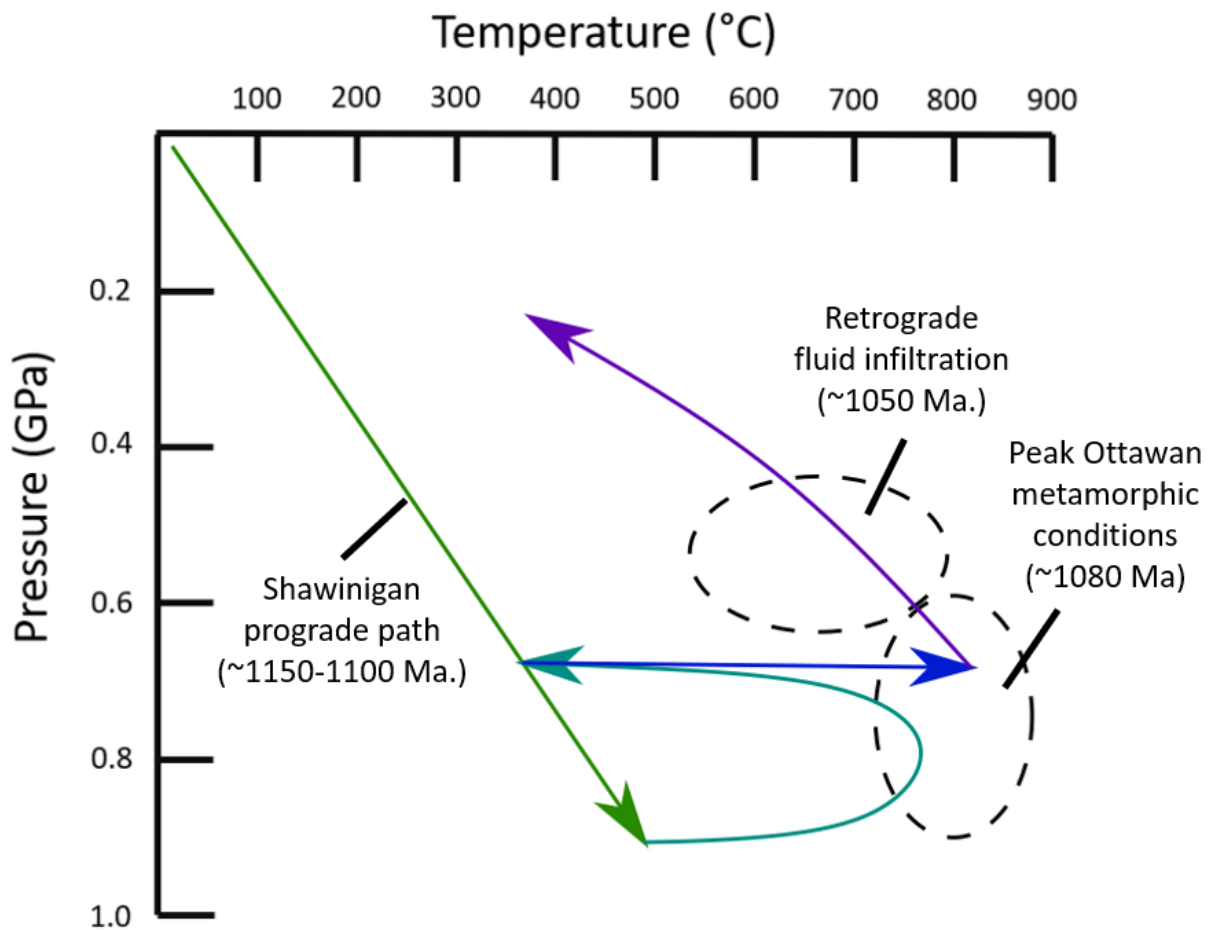
Figure 1.5. Proposed pressure-temperature path for the Marcy massif during the Grenville orogeny. P-T path from the Shawinigan phase (~1150 Ma.) to the late Ottawan phase (~1020 Ma.) of the Grenville orogeny adapted from Regan et al. (2019) based on work from Spear & Markussen (1997), Storm & Spear (2005), and Peck et al. (2018). Emplacement of the massif in the lower-middle crust was followed by granulite-facies metamorphism, isobaric cooling and reheating back to granulite-facies, then a period of igneous intrusions and fluid infiltration related to exhumation and extension on the retrograde path.

mixed with magmatic fluids during contact metamorphism (Valley & O'Neil, 1982), leading to an initial hypothesis that the anorthosite could not have crystallized deeper than 10km from the surface (Valley & O'Neil, 1982; Clechenko & Valley, 2003). However, with current knowledge about meteoric water mobility in ductile orogenic belts, as well as refined pressure-temperature modelling, recent work suggests that emplacement in the middle-lower crust was more likely followed by isobaric cooling and reheating (Regan et al., 2019).

Emplacement was followed by heating and subsequent metamorphism under granulite-facies conditions of ~800 MPa and 800°C during the onset of the Ottawan orogeny ca. 1080 Ma (Figure 1.5) (Bohlen et al., 1985; Mezger et al., 1991; Spear & Markussen, 1997; Storm & Spear, 2005). While contraction continued to the northwest, the Adirondack Highlands region underwent orogenic collapse ca. 1050 Ma (Rivers, 2008; McLelland & Selleck, 2011;Wong et al., 2012; Peck et al., 2018; Regan et al., 2019). NW/SE extension was facilitated by the
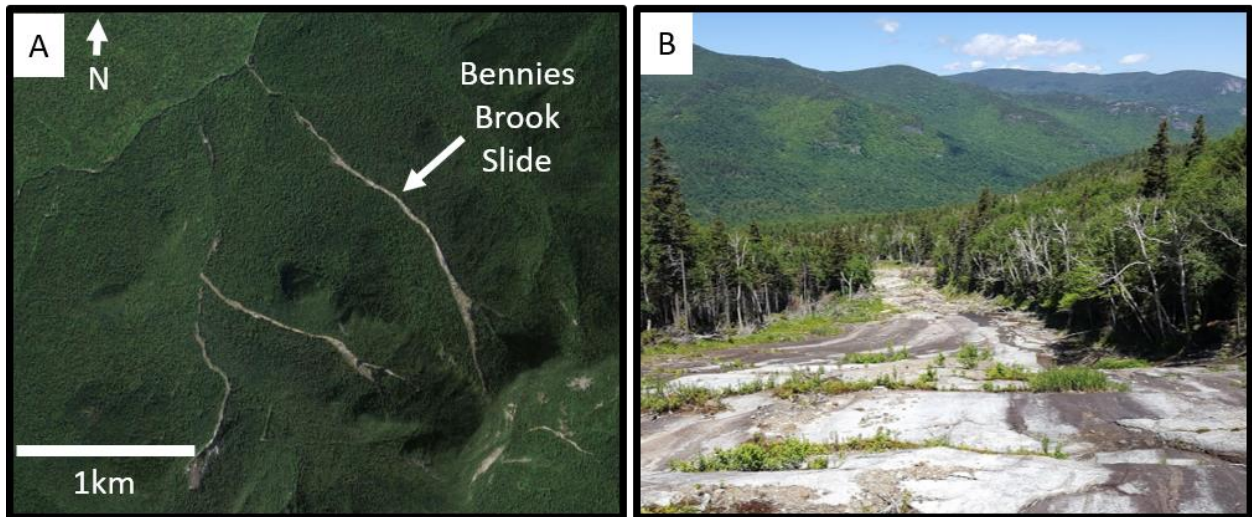
Figure 1.6.   Study Site Location. (A) Vertical satellite view of Adirondack landslides caused by Hurricane Irene in 2011. (B) Part of the study site for this work along the slide at Bennies Brook looking downslope to the northwest.

Carthage-Colton shear zone to the NW, separating the Highlands from the lowlands region, and the East Adirondack shear zone to the SE. The timing of the extension is supported by dated igneous bodies such as the LMG (Lyon Mountain Granite), which is interpreted to have been emplaced during this extension period (Selleck, 2005; McLelland & Selleck, 2011; Valley et al., 2011: Regan et al., 2019), as well as various pegmatitic veins, ore bodies, and other fluid-derived features in the Highlands (Selleck, 2005; McLelland & Selleck, 2011; Valley et al., 2011: Chiarenzelli et al., 2018). This indicates that the late Ottawan was a time of significant change for the Marcy massif and neighboring rocks.

Though the massif is nominally anorthosite, mineral abundances are not homogenous throughout the massif, with meter-scale zones of gabbro and gabbronorite distributed throughout. (Regan et al., 2019). In several areas, metamorphic alteration of the anorthosite has also been identified, locally introducing metasomatic assemblages that include chlorite, amphibole, scapolite, apatite, and biotite (Morrison & Valley, 1988; Morrison & Valley, 1991; Spear & Markussen, 1997). On its margins the Marcy massif is in contact with various metapelitic and igneous gneisses and skarns, as well as other units of the AMCG suite (McLelland et al., 2004).

1.4.2. Study Site

Samples were collected from the Bennies Brook slide, an exposed landslide scarp near the center of the massif, ~10km south of the northern margin, in the high peak area of the Adirondack Highlands (Figure 1.6). Landslide scarps are plentiful within this region of the Highlands (Mackenzie, 2017), but they are commonly located on near-vertical, cliff-like slopes rendering field work next to impossible. The Bennies Brook site is a relatively shallow slope for much of its ~2km length, and thus provides an opportunity to investigate the Marcy massif

interior. Within the study site the anorthosite is cut by mylonitized granitic dikes and shear zones varying from millimeter- to meter-scale. The anorthosite also hosts various meter-scale gabbroic patches with increased pyroxene abundance relative to the anorthosite and at least one gabbroic dike with sheared anorthosite along its margins. Dikes and shear zones form a mutually off-setting conjugate set at ~280°W and ~350°W suggesting that granitic dike intrusions and shear zone development are coeval (Fossen & Cavalcante, 2017; Regan et al., 2019). The timing of these intrusions and deformational events is not well constrained, but plausibly occurred between 1050-1020 Ma during the prolonged orogenic collapse of the Adirondack Highland region.

CHAPTER 2

METHODS

2.1. Sample Collection

Sixteen *in situ* specimens were collected from the Bennies Brook study site using a rock hammer or a 4lb. sledge hammer and chisel. Sample selection was based on their spatial relationship to various shear features in order to best analyze any possible strain gradients. However, due to the limited capability of available tools and the glacially polished nature of the outcrop, only samples that were easily extracted were collected. Despite this complication, all 16 specimens contain at least a section of shear-zone or dike margin. In addition the *in situ* samples, seven float samples were collected.

2.2. Sample Preparation

From these samples, I made 52 thin sections at the University of Maine. After initial inspection using optical microscopy, 20 of the thin sections were prepared for use in scanning electron microscopy and electron probe microanalysis.

2.3. Sample Analysis

2.3.1. Optical Microscopy

Before selection for electron beam analysis, I inspected each thin section using an optical microscope. Further optical inspection of microstructures and high-resolution image capture was

done on a Zeiss Axio Imager M2 microscope using Zeiss ZEN Pro software for image stitching and post-processing.

2.3.2. Scanning Electron Microscopy

I obtained images for visual microstructural analysis using Backscattered electron analysis (BSE) and Monochromatic cathodoluminescence detection (CL) on a Tescan VEGA-II XMU scanning electron microscope (SEM) at the University of Maine using 20-kV accelerating voltage, ~100–600 pA beam current, and 0.1 µm spot size at a working distance of 15 mm. I used Electron dispersive spectroscopy (EDS) to acquire semiquantitative geochemical data for initial mineral identification and analysis. EDS was done on the same SEM instrument using EDAX Genesis software under the same working conditions. I also used Wavelength-dispersive electron probe microanalysis (EPMA) for quantitative geochemical analysis of plagioclase, scapolite, pyroxene, and amphibole. EPMA was done using a Cameca SX-100 microprobe at the University of Maine using a 15-kV accelerating voltage, 10 nA beam current, and 5 µm spot size. Results are reported as the average of 2–5 grains within a thin section, with 10 points per grain.

CHAPTER 3

STRUCTURAL OBSERVATIONS

What sort of rocks, minerals, and structures did I observe in the field and under the microscope?

The purpose of this chapter is to document outcrop- and microscale structural observations made utilizing optical and scanning electron microscopy, and to present geochemical data to quantify mineral compositions. These observations serve to characterize the host anorthosite and the localized strain features found within the boundaries of the Bennies Brook study site. However, only the shear features have been studied in detail, as all *in situ* samples were gathered no further than 30cm from a shear feature. Igneous textures and composition are variable at the mesoscale, and due to the scarcity of meter-scale structural mapping across much of the massif interior, the nature of this heterogeneity is not well documented outside the boundaries of the study site. Therefore, any textural or compositional characterization of the anorthosite at the Bennies Brook site might not be representative of the total massif and is thus presented as the original host rock only relative to the shear structures that cut it.

3.1. Field Observations

What sort of structures did I orient and document in the field, and how are they spatially related?

In the field, I observed various features cutting the anorthosite, with many exhibiting shear displacement. The most important of these features are centimeter-wide granitic dikes
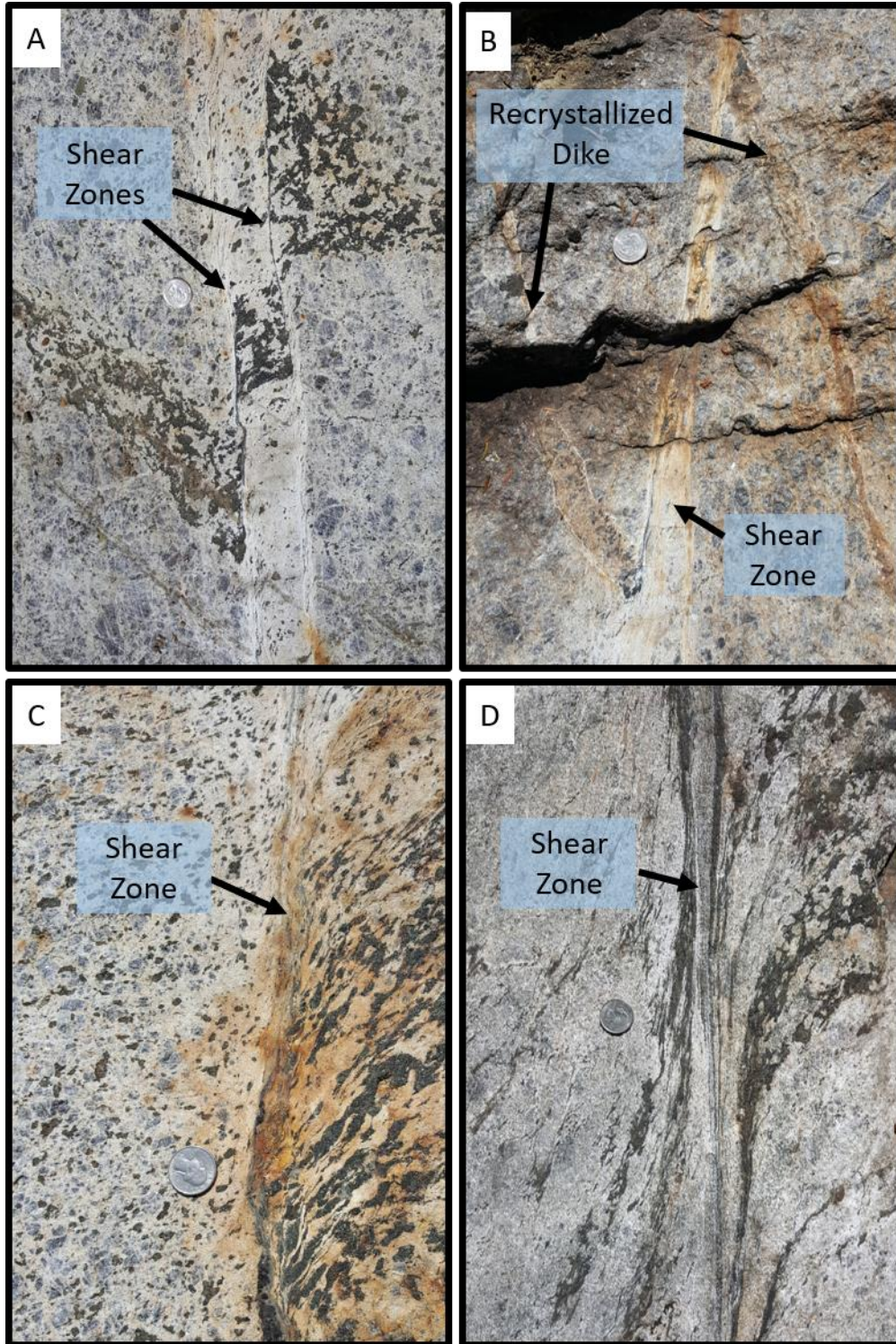
Figure 3.1. Photographs of anorthosite shear zones in the field. US quarter coin for scale in all images. (A) Parallel pair of left-lateral shear zones displacing a gabbroic band. (B) Left-lateral shear zone displacing a granulite-facies dike. (C) Left-lateral shear zone cross-cutting gabbroic patch. (D) Left-lateral shear zone cross-cutting gabbroic bands.
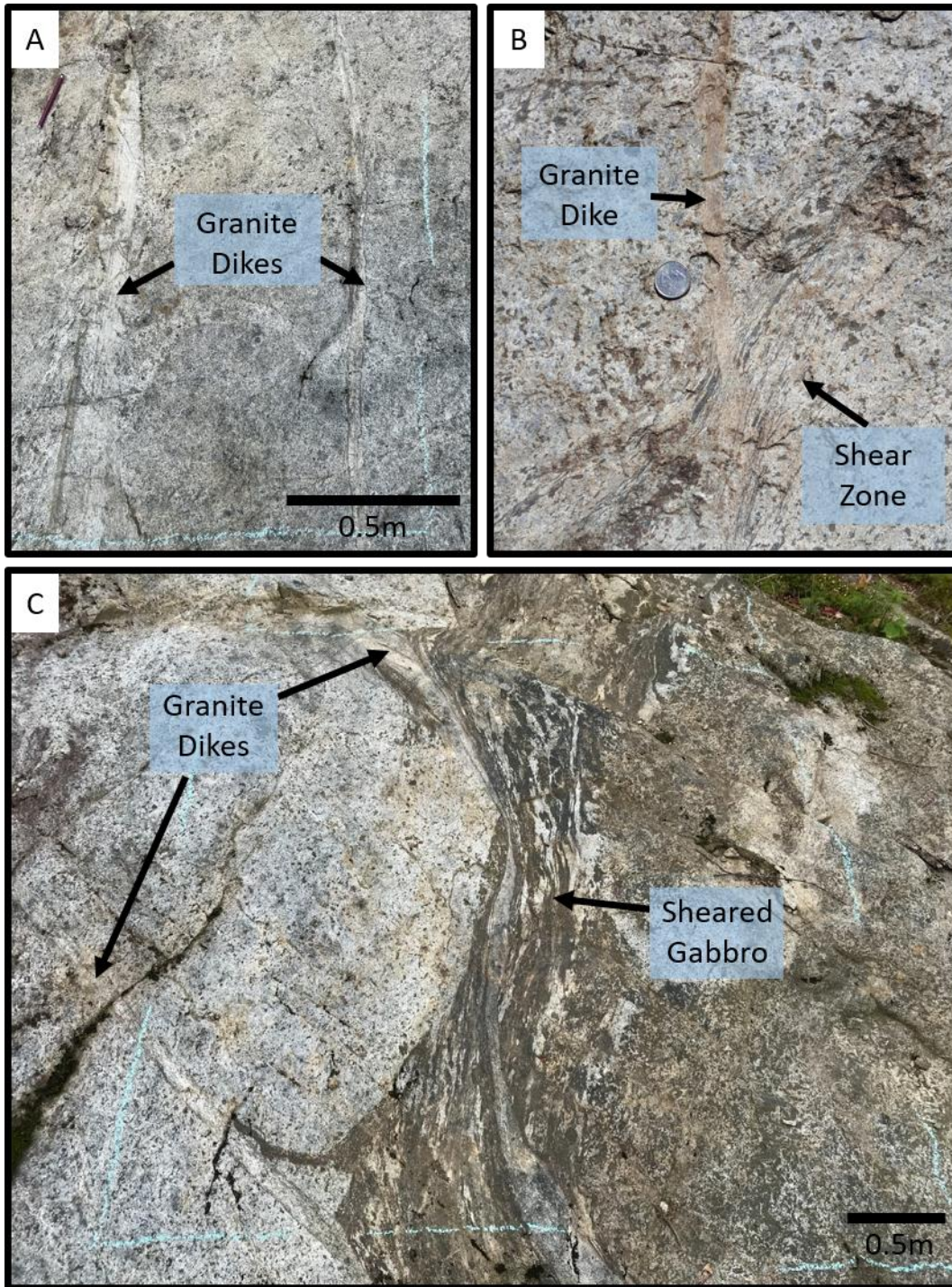
Figure 3.2. Photographs of dikes in the field. (A) Parallel pair of granitic dikes (B) Left-laterally sheared granitic dike complexly cross-cutting shear zone with ambiguous sense of shear. US quarter coin for scale. (C) Parallel pair of left-laterally sheared granitic dikes mutually offsetting right-lateral gabbroic shear zone.

(Figure 3.1) and centimeter-meter wide anorthosite shear zones (Figure 3.2). Granitic dikes dip steeply and appear fine-grained and thoroughly sheared internally with no apparent deformation in the host anorthosite along the contact margins. Shear zones within the anorthosite also dip near-vertically and are commonly made clear by offsetting various gabbroic zones, which are distributed heterogeneously throughout the study site.

Both dikes and shear zones predominantly strike ~290°, with occasional shear zones striking ~350° as documented by Regan et al., (2019) (Figure 3.3). Shear zones and dikes striking 290° show a left-lateral sense of shear, and shear zones striking 350° show right-lateral sense of shear. Where sets of dikes and shear zones cross they appear to be mutually-offsetting (Figure 3.2b-c). A single cm-wide gabbroic dike was also observed to strike ~290° but did not cross any other shear feature where exposed. Other planar features were observed, in various orientations, but extensive recrystallization obscures deformation mechanisms and structural relationships. These features likely represent older, granulite-facies deformation events. Therefore, these features were not investigated thoroughly.

3.2. Microscale Observations

What sort of structures did I observe only by using optical and scanning electron microscopy, and how were they distributed?

To investigate the origin of the shear features observed in the field, I gathered samples proximal to the features and examined the deformational and metamorphic microstructures. For the purpose of characterization and structural interpretation, I qualitatively split shear zones and their margins into four planar zones roughly parallel to the apparent plane of shearing based on
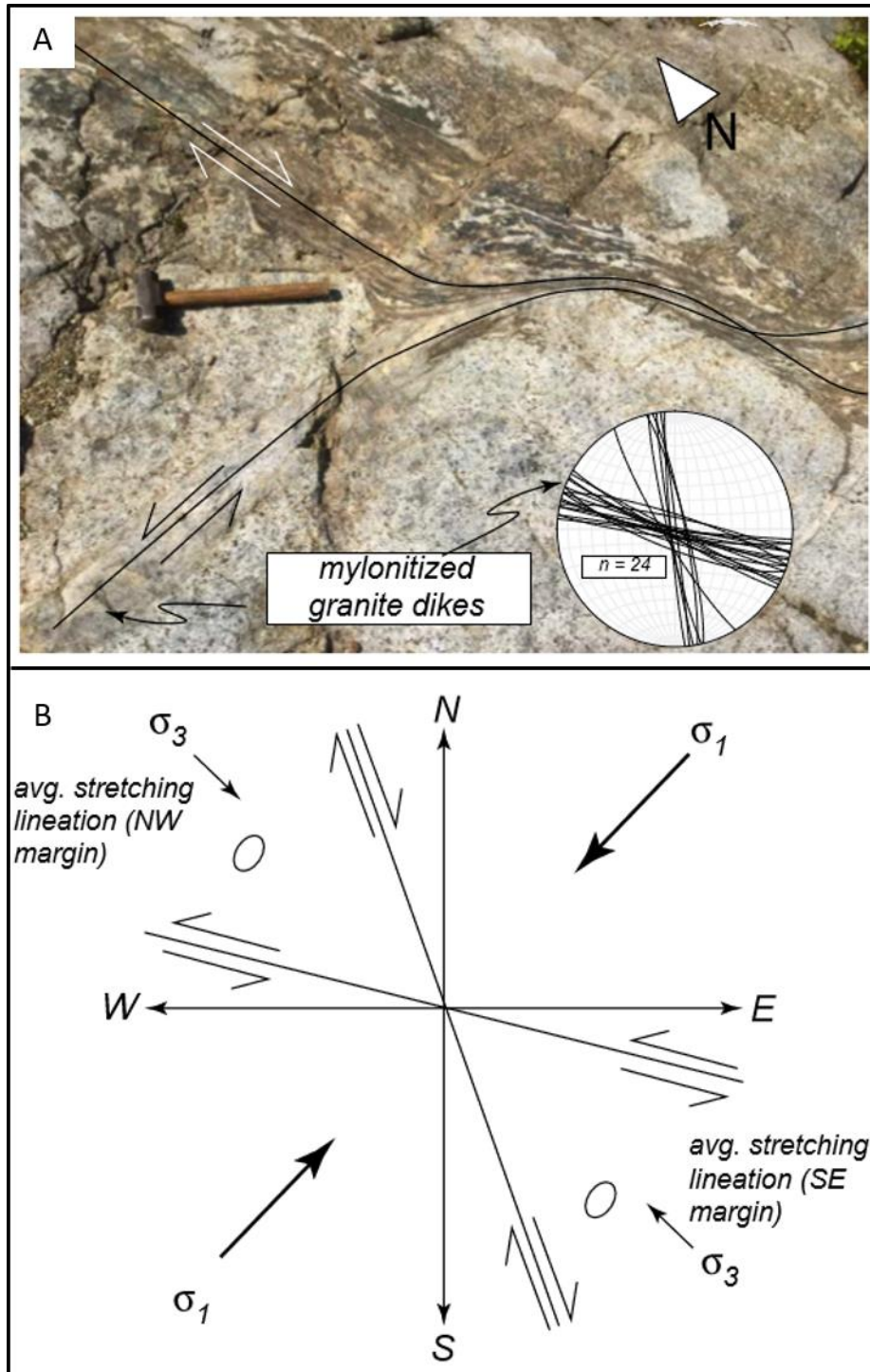
Figure 3.3. Orientation of shear zones and mylonitized granite dikes within the Marcy massif from Regan et al. (2019). (A) Photograph and data showing the same set of features shown in figure 3.2.C and a stereonet diagram of shear zones and mylonitized granite dike orientations. (B) generalized stress orientations resulting in the conjugate systems observed at Bennies Brook.

mineral abundances and grain sizes. These zones represent an increase in strain from Zone I to

Zone IV (Figure 3.4) approaching the shear zone core and allow us to investigate the evolution

of a shear zone across the strain gradient. I also distinguish between two plagioclase types

(Figure 3.3). I define Type A as plagioclase phenocrysts up to 15 cm in diameter that appear dark

grey to navy blue in hand sample and have a cloudy blue-grey tint in thin section under plain-

polarized light. These grains commonly show extensive deformation twinning and anti-perthitic

exsolution lamellae. I define Type B as fine-grained plagioclase that appears an ivory or chalky
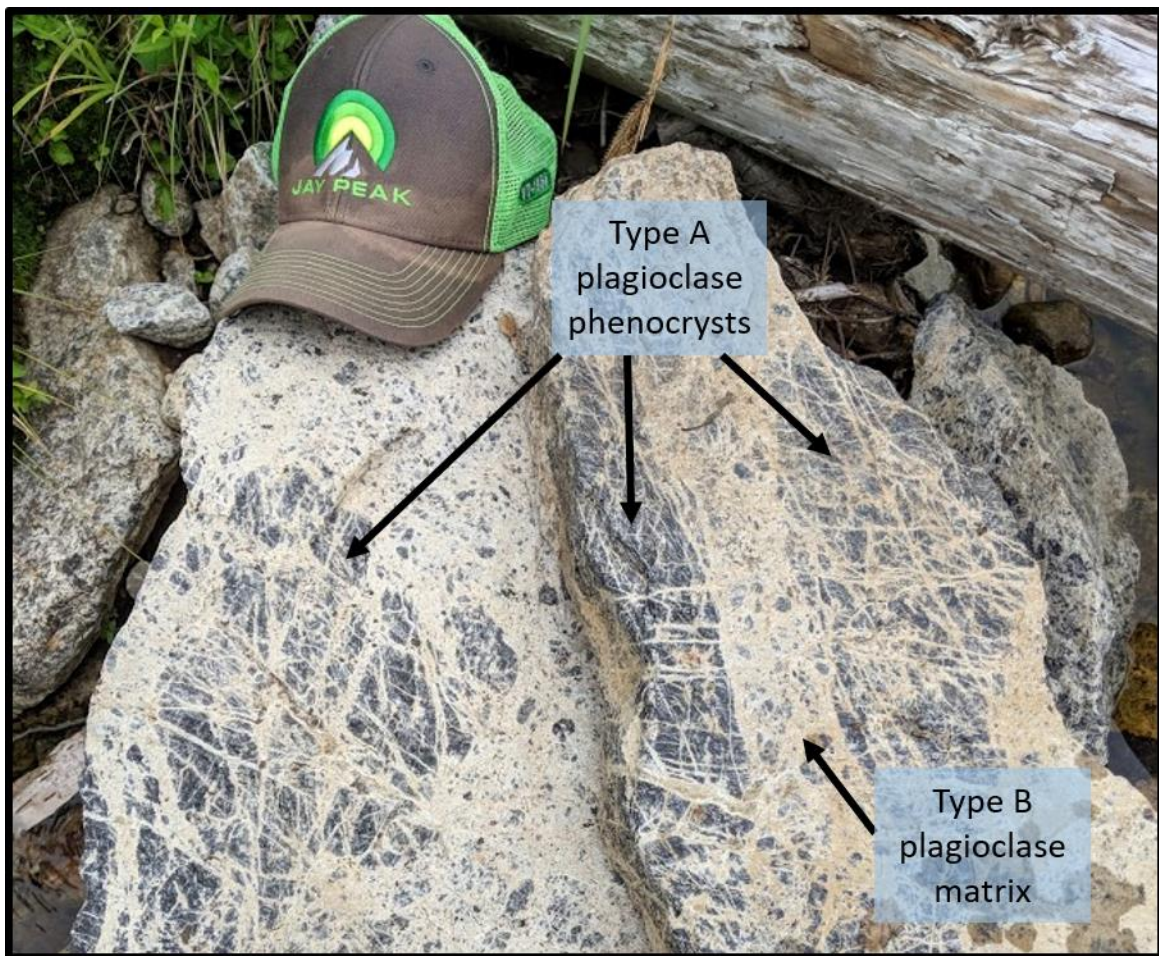
Figure 3.4. Photograph showing contrast between Type A and Type B plagioclase. Dark grey Type A plagioclase phenocrysts are cross-cut by fine-grained, ivory Type B plagioclase which fills fractures and constitutes much of the matrix. Hat for scale.

Zone I	Coarse-grained matrix of 90% plagioclase with interspersed clinopyroxene clusters. Garnet and iron oxides are present with garnet tending to rim clinopyroxenes.
Zone II	Plagioclase grains (%50-90) with scapolite (10-50%) along grain-boundaries and junctions in a mid-sized matrix (50-1000microns) surrounding clinopyroxene clusters (1-5mm) rimmed by amphibole and fine-grained quartz.
Zone III	Variably sized (10-1000microns) mix of plagioclase (~10-30%) and scapolite (~70-90%) grains surrounding interspersed clinopyroxene phenocrysts (1-5mm) rimmed by amphibole and fine-grained quartz.
Zone IV	Evenly distributed mix of fine-grained (10-50microns) plagioclase (~30-50%) and scapolite (~50-70%), with narrow ribbons of entrained amphibole and quartz parallel to direction of shear.

Table 3.1. Summary of microstructural zones associated with shear features at Bennies Brook. Zone I represents the furthest zone from the shear zone core, and zone IV the shear zone core.

Abbreviation	Mineral
Pl	Plagioclase Feldspar
Qz	Quartz
Scp	Scapolite
Cpx	Clinopyroxene
Amp	Amphibole
Ksp	Potassium Feldspar
Grt	Garnet
Ilm	Ilmenite

Table 3.2. Mineral abbreviations after Whitney & Evans (2010).

white in hand sample and colorless in thin section under plain-polarized light. Across the study

site, Type A grains are surrounded by a matrix of Type B grains, and commonly are crosscut by

narrow, planar zones of Type B plagioclase. I discuss the origin and relationship between these

two plagioclase types further in the next chapter.

3.2.1. Zone I (Host Anorthosite)

Zone I represents the textures and mineral abundances of the anorthosite ~20 cm from a

shear zone core and beyond (Figure 3.5). This zone is characterized by less than 10 modal %

scapolite, a lack of other metasomatic minerals (amphibole, biotite, apatite), the presence of

garnet as small porphyroblasts within the matrix and as rims around pyroxene clusters, and

abundant Type A plagioclase phenocrysts approximately 0.5–2cm in diameter. Type B

plagioclase grains vary from approximately 5–150mm in diameter in the matrix, and on the finer
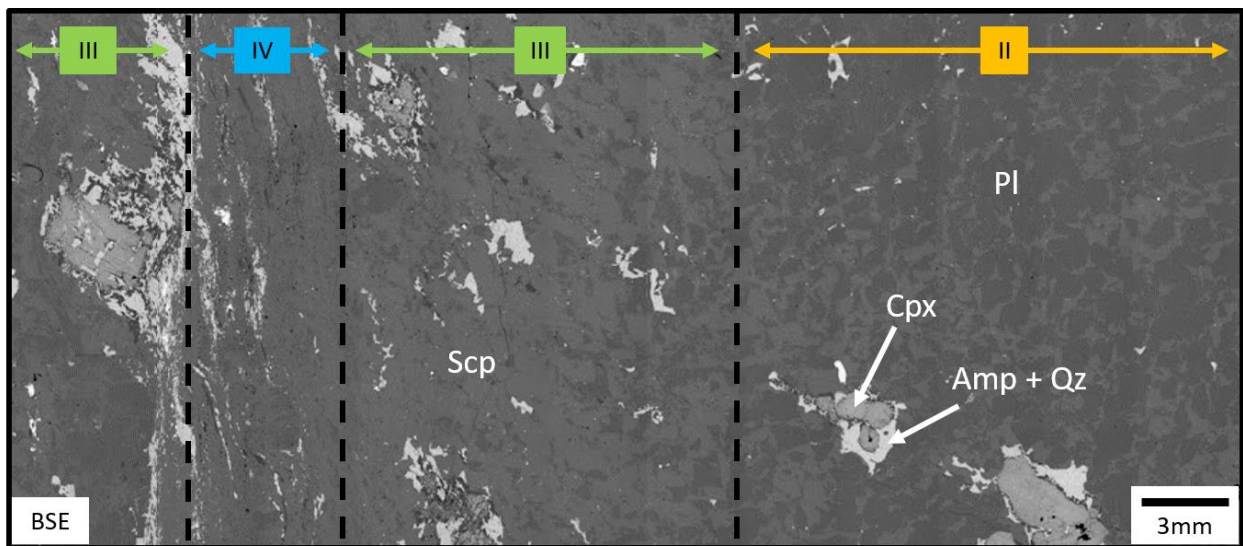
Figure 3.5.   Representative examples of zones II-IV with increasing proximity to a shear zone. Full thin section backscattered electron image. As proximity increases, modal abundance of metasomatic minerals (scapolite, amphibole, quartz) increases, and grain size decreases. Zone I lies further from the shear zone and is not represented in this thin section. However, the same microstructural trends of increasing grain size and decreasing metasomatic minerals continue with distance from the shear zone core (Zone IV).

end of that range when appearing in fractures and kink bands in large Type B grains. Other

mineral grains are variable but range from approximately 0.5–10mm. All grains appear equant to

sub-equant, regardless of size or mineral.

Zone I microstructures are typical of Marcy anorthosite analyzed elsewhere, with a

bimodal plagioclase grain size distribution between large Type A phenocrysts (no more than

20%) and finer Type B grains in the matrix and crosscutting larger grains. Within this zone,
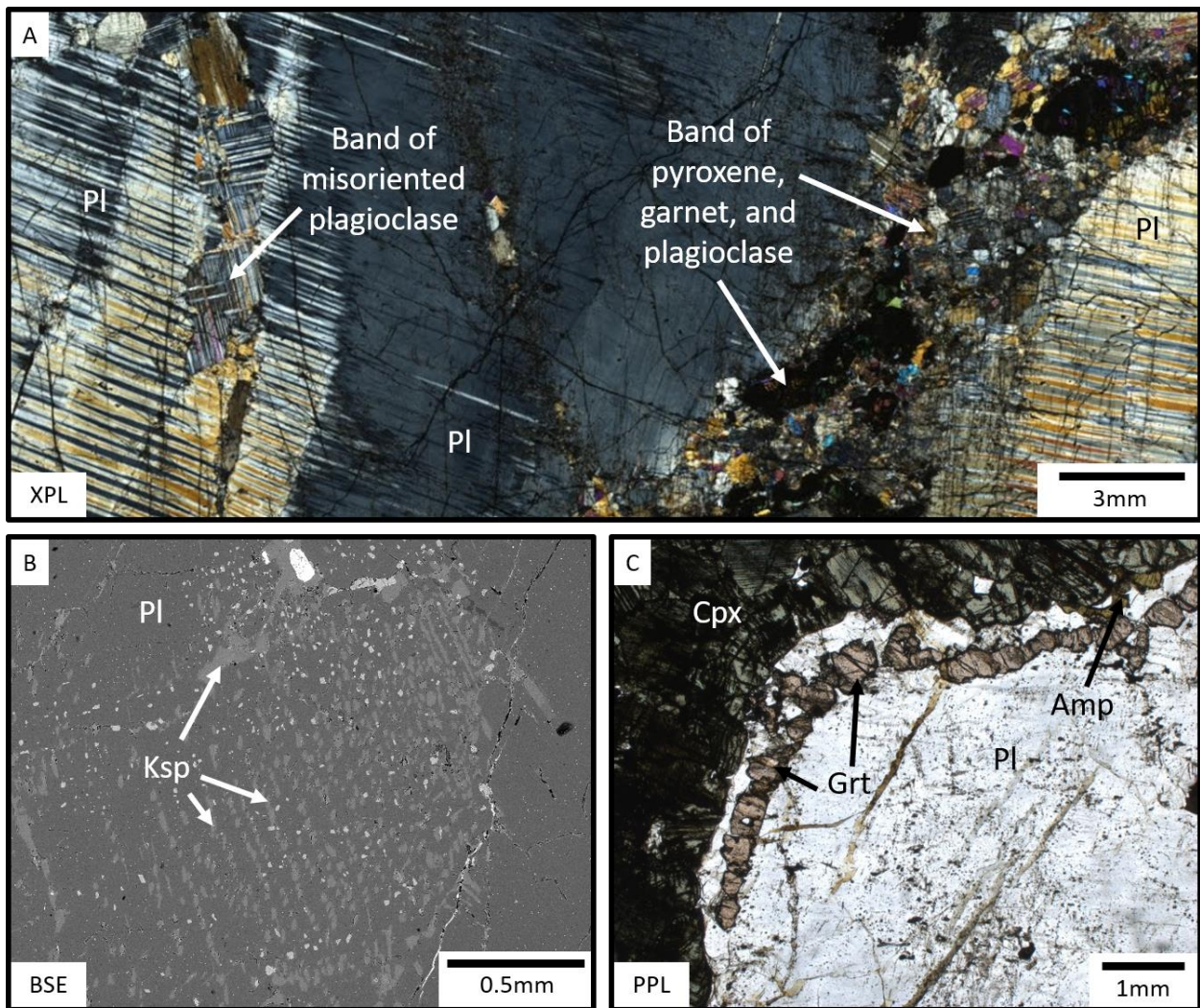
Figure 3.6. Images of microstructures characteristic of zone I. (A) Photomicrograph of Type A phenocrysts with a cross-cutting band of misoriented plagioclase grains and matrix of Type B plagioclase, garnet, and pyroxene. (B) Type A plagioclase grain exhibiting antiperthitic potassium feldspar exsolution lamellae. (C) Photomicrograph of garnet rimming pyroxene with only a single grain of amphibole suggesting fluid access.

planar features resembling shear zones appear in outcrop. However, under microscope inspection

there is no apparent evidence of strain or deformation associated with them. These features are

commonly rich in garnet, both in the matrix and rimming pyroxene, and iron oxides compared to

the surrounding rock. Due to a lack of microstructural evidence suggesting strain, these features

were left largely unexamined. The mineral abundances present in Zone I approximate the

average mineral abundances of the entire Marcy anorthosite massif with the addition of up to
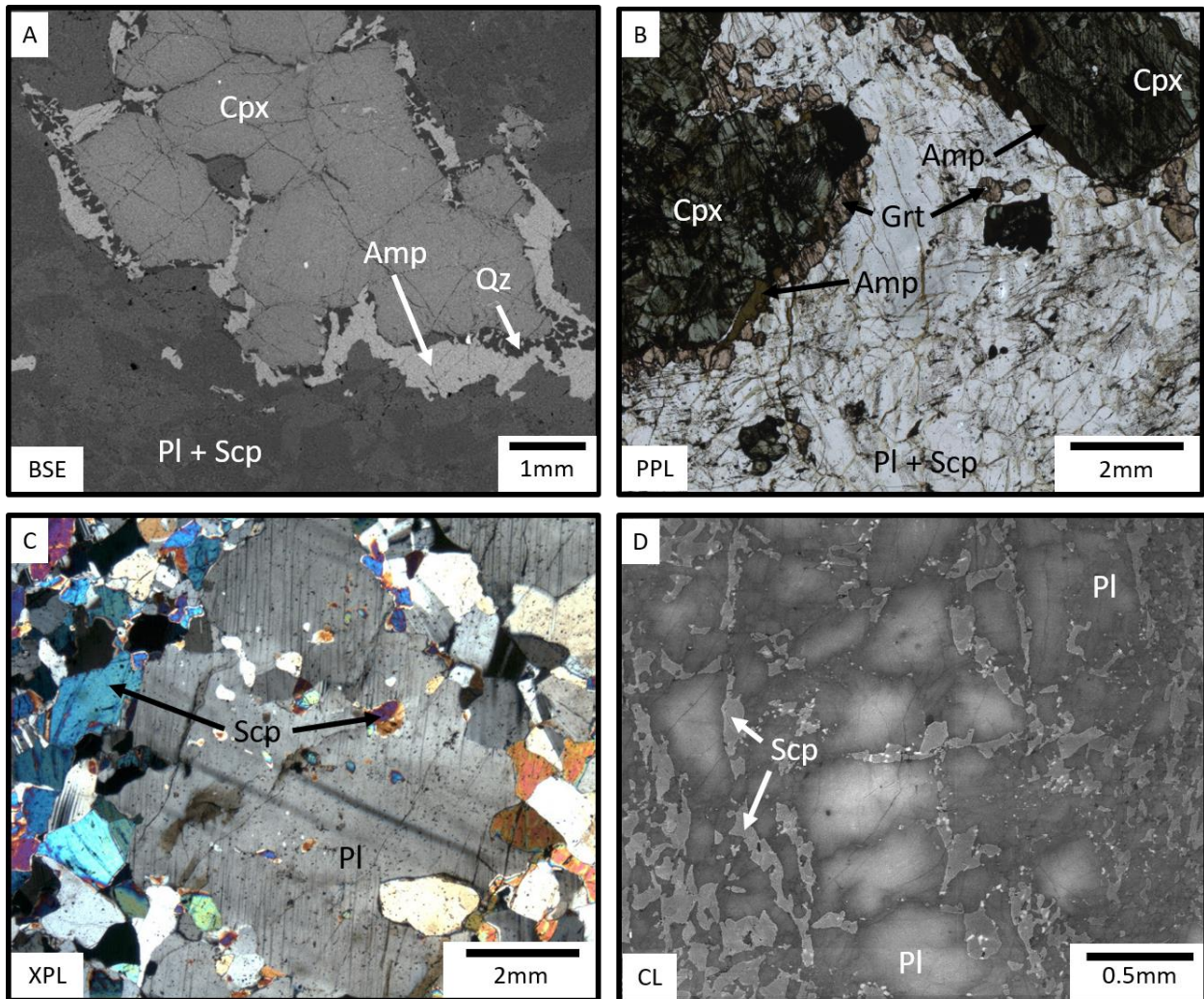
Figure 3.7. Images of microstructures characteristic of zone II. (A) Pyroxene rimmed by amphibole + quartz symplectite in a mixed matrix of plagioclase and scapolite. (B) Photomicrograph of evenly mixed garnet and amphibole with little quartz rimming pyroxene. (C) Type A plagioclase grain with linear sets of scapolite blebs scapolite surrounded by Type B plagioclase + scapolite matrix. (D) Spatial distribution of scapolite strongly indicating replacement of plagioclase along grain boundaries and junctions.

10% scapolite dispersed within the plagioclase matrix and minor amphibole and quartz associated with pyroxene within 0.5 m of a shear zone.

3.2.2. Zone II (Outer Gradient)

Zone II is characterized by 10%–50% scapolite within the plagioclase matrix and the introduction of amphibole and quartz rims around pyroxene, sometimes in conjunction with garnet. This zone generally comprises the area 5–20 cm from the shear zone core.

Microstructurally, Zone II resembles Zone I with increased abundance of metasomatic replacement minerals (Figure 3.6). Grain size is reduced as more scapolite replaces plagioclase along grain boundaries and triple junctions and amphibole + quartz symplectic rims are introduced containing grains as small as 10 µm. The ratio of Type B to Type A plagioclase also increases. The minerals present in Zone II are consistent with Zone I with the exception of greater modal abundances of scapolite and amphibole at the expense of plagioclase and garnet respectively. Scapolite modal abundance increases to up to 50% of the matrix, and the presence of garnet is reduced as pyroxenes instead are primarily rimmed by amphibole +/- quartz.

3.2.3. Zone III (Inner Gradient)

Zone III is characterized by greater than 50% scapolite within the matrix, complete removal of garnet, and widening of symplectic amphibole and quartz rims around pyroxene. Due to the wider symplectic rims and increased abundance of scapolite, grain-size is notably decreased from Zone II (Figure 3.7). This zone generally forms an approximately 5cm-wide zone adjacent to the shear zone core.

27

The microstructures within Zone III show a gradual to marked decrease in grain-size approaching the shear zone core. As in Zone II, this grain-size reduction is the result of metasomatic replacement and the near complete elimination of Type A plagioclase phenocrysts. Some minerals, including scapolite and chlorine-rich biotite, show evidence of crystal-plastic deformation. The dominant mineral in Zone III is scapolite, which has extensively replaced plagioclase. Amphibole and quartz are also present in higher abundances. As with other zones, there does not appear to be any composition gradient regarding any given mineral, but due to changes in modal abundances towards increasing metasomatic minerals, bulk chemistry does change with proximity to the shear zone core (Zone IV). In at least one sample, chlorine-rich biotite is also present in Zone III.
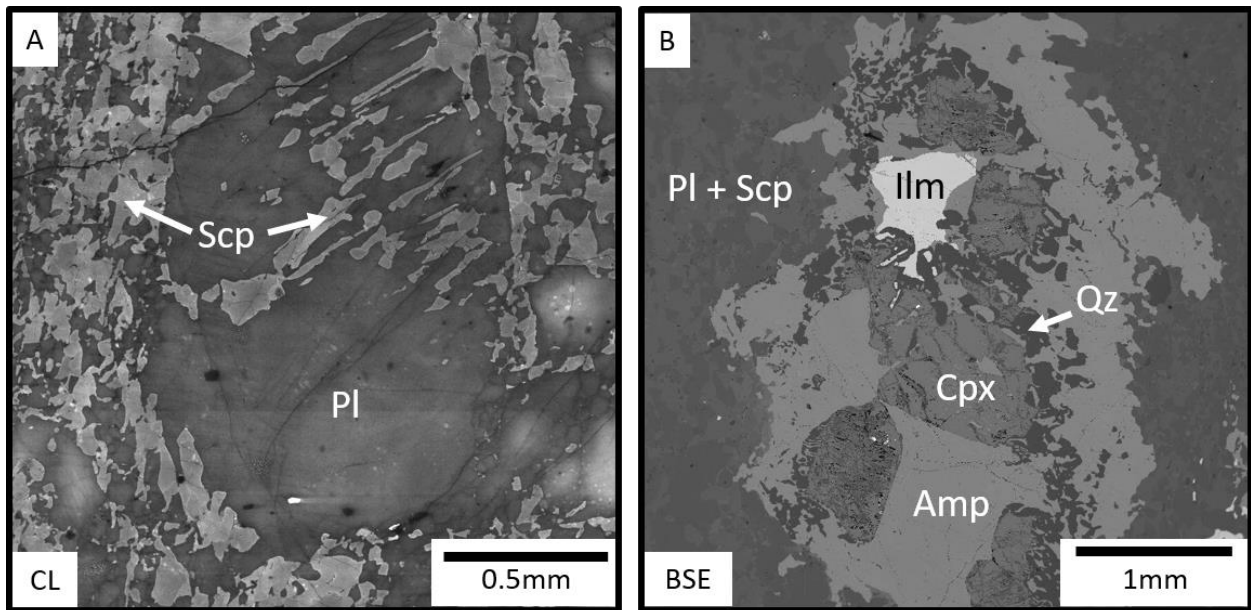
Figure 3.8. Images of microstructures characteristic of zone III. (A) Extensive replacement of plagioclase by scapolite in fine-grained matrix and further replacement within a Type A plagioclase grain in linear, parallel segments possibly crystallographically controlled. (B) Pyroxene and accessory ilmenite with wide corona of amphibole and quartz.

3.2.4. Zone IV (Shear Zone Core)

Zone IV represents the shear zone core which is commonly only a few mm wide. Grain-size of Type B plagioclase and replacement scapolite becomes very fine-grained (5-10 µm diameter) and phases become mixed forming a nearly homogenous distribution of plagioclase and scapolite (Figure 3.8). Every sample studied containing Zone IV also featured one or more rimmed pyroxene immediately adjacent to the shear zone core. Amphibole, biotite, and quartz grains are less abundant than in Zone III, but where rimmed pyroxenes are adjacent to the shear zone core, the rims are truncated, and amphibole, quartz, and biotite grains are entrained into the shear zone. Zone IV comprises mostly plagioclase and scapolite, with some amphibole, quartz, and biotite. Composition once again appears constant within each given mineral population.
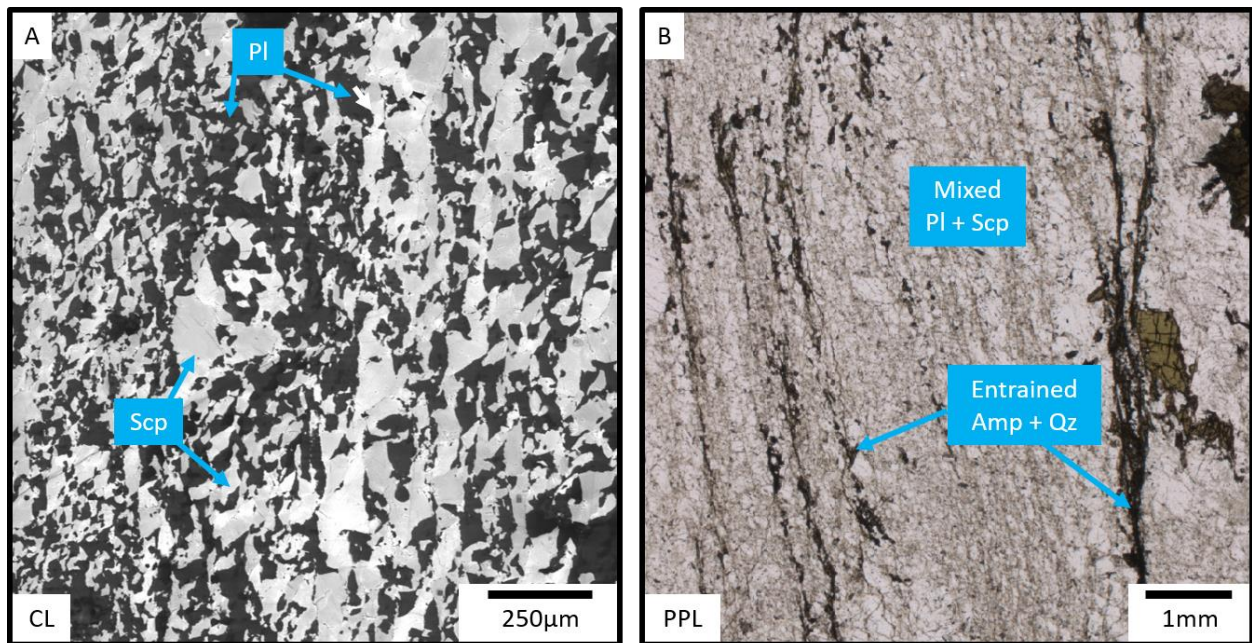
Figure 3.9. Images of microstructures characteristic of zone IV. (A) High-contrast cathodoluminescence image of fine-grained plagioclase and scapolite with distinctly jagged cuspate-lobate grain boundaries in shear zone core. (B) Photomicrograph of fine-grained plagioclase and scapolite as well as entrained ribbons of amphibole and quartz on the margin of a shear zone core.

29

CHAPTER 4

GEOCHEMICAL DATA

What can the composition of the minerals tell us about the metamorphic and deformation history of the rock?

Bulk chemistry at the study site is relatively homogenous with the exception of meter-scale zones of higher mafic mineral content and shear zones that contain retrograde Cl-rich mineral assemblages. Differences in individual mineral compositions are homogenous on the thin section scale, other than some zoning evident in pyroxenes approaching contact with amphibole, but composition tends to vary between samples. I completed EPMA analysis on the dominant minerals in several samples to provide representative chemical compositions and identify variance in composition across the study site.

4.1. Plagioclase

Plagioclase composition is intermediate (An_{40-55}) within the study site (Table 4.1) which is consistent with the accepted composition range for the Marcy Massif (Bohlen et al., 1985; Morrison & Valley, 1991; Seifert et al., 2010). No clear pattern or structure corresponds to composition variance. While a relatively wide compositional range exists across the study site, there is negligible difference in the %An composition between Type A plagioclase and Type B plagioclase grains within a given thin section.

4.2. Scapolite

Scapolite composition is intermediate ($AnEq_{45-60}$) but slightly more calcic than associated plagioclase (Table 4.2). Chlorine weight % is variable from sample to sample with higher Cl

content tending to correlate with higher modal abundance of scapolite, though Cl content stays relatively constant within a given thin section regardless of microstructural Zone.

4.3. Pyroxene

EPMA measurements were only gathered from pyroxene in a single thin section (Table 4.3) and therefore variance across the study site cannot be quantified. However, semiquantitative EDS analysis of other thin sections suggests that this single suite of measurements is representative. Pyroxene is the only mineral that shows grain-scale chemical gradients. At reaction fronts approaching contact with amphibole, Fe content decreases and Mg content increases.

Mineral	Plagioclase			
Sample	BB6-6	BB8-2	BB12-8	BB12-9
Oxide wt. %				
Na_2O	6.46	5.76	5.11	5.38
K_2O	0.46	0.35	0.33	0.33
CaO	8.18	9.50	10.46	10.12
Al_2O_3	26.80	27.64	27.31	28.38
SiO_2	58.29	56.03	56.00	55.87
Total	100.31	99.43	99.30	100.80
Atoms per Formula Unit (8 O)				
Na_2O	0.56	0.49	0.45	0.47
K_2O	0.03	0.02	0.02	0.02
CaO	0.39	0.47	0.51	0.48
Al_2O_3	1.41	1.48	1.46	1.49
SiO_2	2.60	2.52	2.54	2.50
Total	4.99	4.99	4.97	4.96

Table 4.1.   Table of EPMA data for plagioclase representative of various thin sections. BB6-6 contains a mm-wide shear zone. BB8-2 contains a series of anastomosing mm-wide shear zones. BB12-8 and BB12-9 are ~50 mm from a mm-wide shear zone.

Mineral	Scapolite		
Sample	BB6-6	BB8-2	BB12-9
Oxide wt. %			
Cl	2.84	1.88	1.04
Na_2O	6.11	4.93	3.92
K_2O	2.07	1.39	0.99
MgO	-0.12	-0.08	0.16
CaO	10.50	12.83	15.11
MnO	0.00	0.00	0.04
FeO	0.06	0.17	0.52
BaO	0.09	0.08	0.19
Al_2O_3	24.34	25.15	26.17
CO_2	1.32	3.31	3.24
SiO_2	52.77	50.34	48.60
SO_2	0.01	-0.01	0.02
Total	100.00	100.00	100.00
Atoms per Formula Unit (12 Al+Si)			
Cl	0.71	0.48	0.30
Na_2O	1.74	1.44	1.21
K_2O	0.39	0.27	0.22
MgO	-0.03	-0.02	0.02
CaO	1.66	2.06	2.38
MnO	0.00	0.00	0.01
FeO	0.01	0.02	0.05
BaO	0.01	0.00	0.01
Al_2O_3	4.23	4.45	4.60
CO_2	0.29	0.52	0.69
SiO_2	7.77	7.55	7.40
SO_2	0.00	0.00	0.00
Total	16.49	16.77	16.90

Table 4.2.   Table of EPMA data for scapolite representative of various thin sections. CO2 content calculated by difference. BB6-6 contains a mm-wide shear zone. BB8-2 contains a series of anastomosing mm-wide shear zones. BB12-9 is ~50 mm from a mm-wide shear zone.

4.4. Amphibole

Amphibole chemistry also appears slightly variable within the study site but consistent on the thin section scale (Table 4.3). Chlorine content is considerable for amphibole, and differences in weight % across samples show the same correlation to retrograde mineral modal abundance as scapolite.

4.5. Other Minerals

I observed several other minerals, both common (quartz, garnet, ilmenite, and pyrite) and uncommon (orthopyroxene, biotite, apatite), but quantitative EPMA analysis was not performed on these minerals. However, my EDS measurements showed notable chlorine content in both biotite and apatite where present, which indicates those minerals are lesser parts of the same retrograde assemblage as scapolite, quartz, and amphibole.

Mineral	Pyroxene
Sample	BB6-6
Oxide wt. %	
Na_2O	0.54
K_2O	0.00
MgO	10.38
CaO	21.86
MnO	0.48
FeO	12.94
Al_2O_3	3.29
V_2O_3	-0.05
Cr_2O_3	0.02
SiO_2	50.22
TiO_2	0.39
Total	100.13
Atoms per Formula Unit (6 O)	
Na_2O	0.04
K_2O	0.00
MgO	0.53
CaO	0.81
MnO	0.01
FeO	0.37
Al_2O_3	0.52
V_2O_3	0.00
Cr_2O_3	0.00
SiO_2	1.73
TiO_2	0.01
Total	4.02

Mineral	Amphibole	
Sample	BB6-6	BB12-3
Oxide wt. %		
F	0.21	0.35
Cl	4.64	2.97
H_2O	0.49	0.90
Na_2O	0.96	1.09
K_2O	3.33	3.11
MgO	4.44	5.46
CaO	11.18	11.20
MnO	0.30	0.15
FeO	24.48	23.47
BaO	0.19	0.05
Al_2O_3	13.85	13.14
V_2O_3	0.02	0.08
Cr_2O_3	0.00	0.02
SiO_2	35.53	36.83
TiO_2	1.23	1.95
Total	100.86	100.79
O=F , Cl	1.13	0.82
Total	99.72	99.97
Atoms per Formula Unit (23 O)		
F	0.08	0.13
Cl	1.03	0.60
H_2O	0.43	0.72
Na_2O	0.24	0.25
K_2O	0.56	0.47
MgO	0.86	0.97
CaO	1.56	1.44
MnO	0.03	0.02
FeO	2.68	2.35
BaO	0.01	0.00
Al_2O_3	2.13	1.86
V_2O_3	0.00	0.01
Cr_2O_3	0.00	0.00
SiO_2	4.64	4.41
TiO_2	0.12	0.18
Total	14.38	13.42

Table 4.3.   Table of EPMA data for pyroxene and amphibole representative of various thin sections. BB6-6 contains a mm-wide shear zone. BB12-3 is ~50 mm from a mm-wide shear zone.

CHAPTER 5

DISCUSSION

What are my interpretations of the observations and data? How do these interpretations fit into the story and can they answer my geologic questions?

This chapter serves to interpret the various deformational and metamorphic microstructures characterized in the previous chapter. Through this interpretation, a sequence of events leading up to the localization of strain into shear zones will be hypothesized to form the crux of this thesis. The hypothesized timeline will then be compared to events proposed by past and current literature to support its validity. The study area is limited when compared to the total area of the massif, and the heterogenous nature of the massif interior has been noted by this study and others (McLelland, 1989). Therefore, the area for which the microstructural analysis is representative is limited and might not represent the entire anorthosite massif.

5.1. Bimodal Plagioclase

What are the rheological implications of the relationship between the two plagioclase types, and how might they have become different?

One of the most striking features of the Marcy anorthosite in outcrop is the bimodal nature of the plagioclase (Figure 3.3). As noted in a previous chapter, this study defines large, dark grey or navy-blue plagioclase phenocrysts as Type A and fine-grained, ivory colored plagioclase as Type B. Within the study site, modal percentages of Type B plagioclase range from 10% to 80%, varying strongly in abundance across the site. The prevalence and

heterogenous distribution raise an interesting question regarding the origin of the plagioclase differentiation and its implications for the deformation history of the massif. In one of his initial surveys of the massif, Buddington (1939) distinguished the lighter colored, fine-grained matrix as "crushed" plagioclase, implying that the darker phenocrysts are relict grains from which Type B plagioclase was produced through deformation or other mechanisms. Other workers have recognized this bimodality as magmatic rather than tectonic, attributing the texture to cumulate plagioclase laths in a matrix of mobilize crystal-rich mush (McLelland et al., 2004). However, this assessment requires a lack of plagioclase deformation to remain plausible, which might not be accurate based on my microstructural investigation.

Investigation under an optical microscope reveals an important difference between these two plagioclase types (Figure 5.1). The dark navy or grey color of the Type A phenocrysts is caused by pervasive clouds of micro-inclusions (Figure 5.1b), identified as ilmenite and
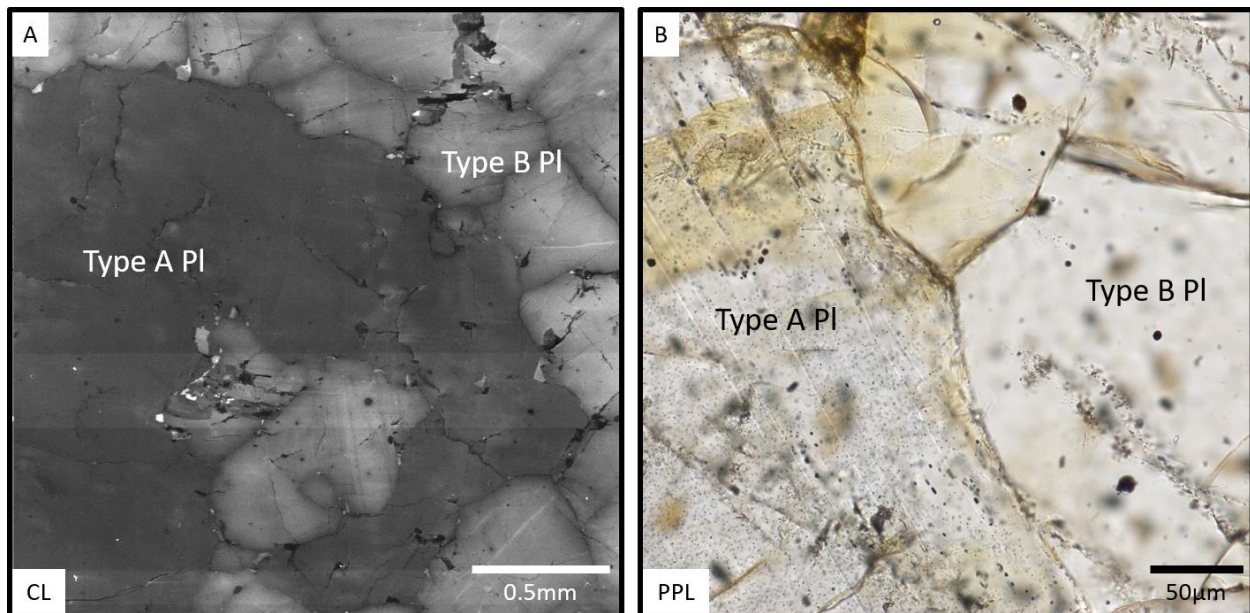
Figure 5.1. Comparison of Type A and Type B plagioclase. (A) CL-dark Type A plagioclase phenocryst surrounded by matrix of finer-grained, CL-bright Type B plagioclase. (B) Photomicrograph of border between Type A and Type B grains showing the cloudy presence of iron oxide micro-inclusions exclusively within Type A plagioclase on left.

magnetite (Wenk et al., 2011). However, Type B plagioclase grains are nearly inclusion-free, and any inclusions present appear to have coalesced into larger inclusions. This observation is corroborated by cathodoluminescence (CL) analysis which shows that Type B grains luminesce more than Type A (Figure 5.1a). Despite a negligible difference in %An between adjacent Type A and Type B plagioclase grains. This might be expected, as the presence of iron is known to quench luminescence (Geake et al., 1977; Mora & Ramseyer, 1992; Mills et al., 2017). However, the lower luminescence of Type A plagioclase appears more uniform than the patchy distribution of Fe-rich micro-inclusions. Therefore, it is possible that this correlation is misleading. Despite the general compositional similarities between Type A and Type B plagioclase, the CL discrepancy might instead be a function of the presence or lack of minor or trace elements which were not measured.

The formation of these Fe-rich inclusions during the cooling of plagioclase feldspar is well documented as an exsolution process occurring post-crystallization (Davis, 1981; Wenk et al., 2011). Thus, it can be inferred that during and immediately following crystallization, only Type A plagioclase was present, and the development of Type B plagioclase was post-emplacement. The close compositional similarity between adjacent Type A and Type B grains suggests that the generation of Type B plagioclase occurred in a dry environment, though it is possible that the dominance of plagioclase buffered the system sufficiently to prevent any compositional changes. The lack or coalescence of microinclusions in Type B plagioclase means it is likely either the product of neocrystallization or recrystallization, eliminating the inclusions. However, the orientation of Type B grains relative to both each other and nearby Type A plagioclase appears highly randomized, with optically-determined misorientation angles between adjacent grains approaching 90º in some cases (Figure 5.2). This observation is inconsistent with

37

recrystallization through subgrain rotation or grain-boundary migration to form Type B

plagioclase (Drury & Urai, 1990; Vernon, 2004). Instead, I propose tensile and shear fracturing

of Type A grains with subsequent neocrystallization of Type B grains in areas of highest strain

energy and fluid access (Ji & Mainprice, 1990; Fitz Gerald & Stünitz, 1993; Kruse et al., 2001;

Stünitz et al., 2003; Ree et al., 2005; Menegon et al., 2013). This is evidenced by the

aforementioned high misorientation angle between adjacent grains, as well as kinking of

plagioclase twins adjacent to some neoblastic bands (Figure 5.2.B) suggesting high amounts of

strain energy associated with the distortion of the crystalline lattice and the growth of scapolite

within these bands indicating the presence of fluid (Figure 5.2). Without EBSD data, the

orientations of the bands relative to the grain is unclear but are likely crystallographically

controlled (Brown & Macaudière, 1984; Stünitz et al., 2003; Brander et al., 2012). Bands of
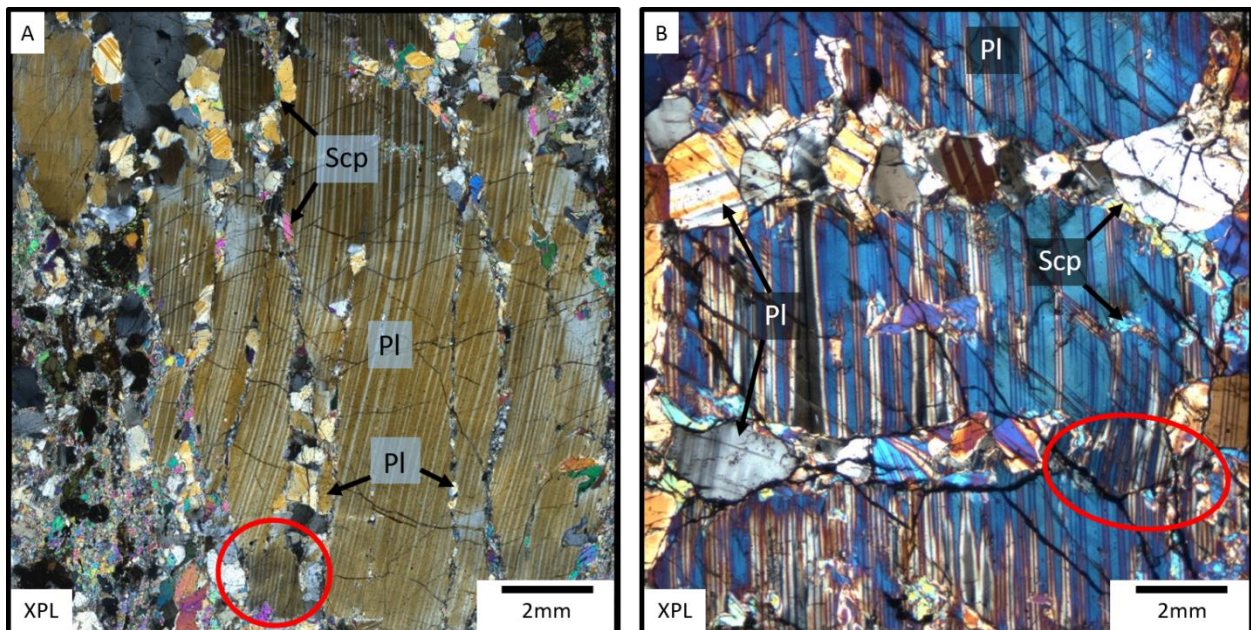
Figure 5.2.   Microphotographs showing bands of neoblastic Type B plagioclase grains within Type A plagioclase phenocrysts. (A) Numerous narrow bands of Type B grains with scapolite cross-cutting relict Type A grain preferentially semi-parallel to bent growth twin planes. Distinctly kinked segment circled in red. (B) Relatively wide bands of Type B grains with scapolite cross-cutting relict Type A grain perpendicular to deformation twins. Distinctly kinked segment shown by red ellipse.

neoblastic Type B plagioclase cross-cutting relict Type A plagioclase phenocrysts throughout the

study site then implies pervasive brittle damage, in agreement with the early description of

"crushed plagioclase" by Buddington (1939). Though previous magmatic interpretations might

not be entirely incorrect, my observations suggest that brittle deformation contributed to the

bimodal texture observed in the Marcy anorthosite.

5.2. Deformation and Metamorphism Timeline

What is my hypothesized sequence of events, and how do my direct observations compare with

those made by prior work?

Previous work determined that after granulite-facies collisional metamorphism during the

onset of the Ottawan orogenic phase ca. 1080 Ma, the Adirondack Highlands region became

gravitationally unstable and orogenic collapse began in the late Ottawan phase, ca. 1050 Ma

(McLelland et al., 1996; Selleck et al., 2005; Rivers, 2008; Wong et al., 2012; Peck et al., 2018)

During this time, the Marcy anorthosite massif was subjected to NW/SE extensional stresses

under amphibolite-facies conditions as the region was exhumed (Selleck et al., 2005; McLelland

& Selleck, 2011; Regan et al., 2019). Based on the microstructural evidence present across the

various shear zones sampled, I hypothesize that these macroscale stresses acting on the

rheologically strong, dry anorthosite caused high levels of strain energy and subsequent brittle

damage throughout much of the massif. I approximate pressure-temperature conditions during

this late Ottawan exhumation to be ~500–600 MPa and 600–650ºC based on comparisons made

to the Ca-amphibole thermobarometry experiments of Apted & Liou (1983), which supports

approximations made by previous work (Figure 1.5) (McLelland et al., 1996; McLelland et al.,

2013; Peck et al., 2018, Regan et al., 2019).

As mentioned in the previous section, brittle damage is most strongly evidenced by the neocrystallization of Type B plagioclase in bands associated with scapolite cross-cutting Type A phenocrysts. However, the presence of anomalous CL-bright traces cutting plagioclase grains (Figure 5.3) might provide further evidence. Lacking other explanation, these traces might represent healed microcracks similar to those documented in quartz by Mills et al., (2017). However, the relative rarity of these features and presence within neoblastic Type B plagioclase prevents them from being definitive evidence. Despite the lack of confidence in this case, cumulative evidence suggests brittle damage on a scale that could plausibly increase the permeability of the massif interior sufficiently to facilitate fluid infiltration into the system.

The brittle damage that occurred drove the extensive generation of neoblastic plagioclase cross-cutting plagioclase phenocrysts and forming the Type B matrix described previously, as well as increasing the local permeability of the rock along brittle faults. This increased
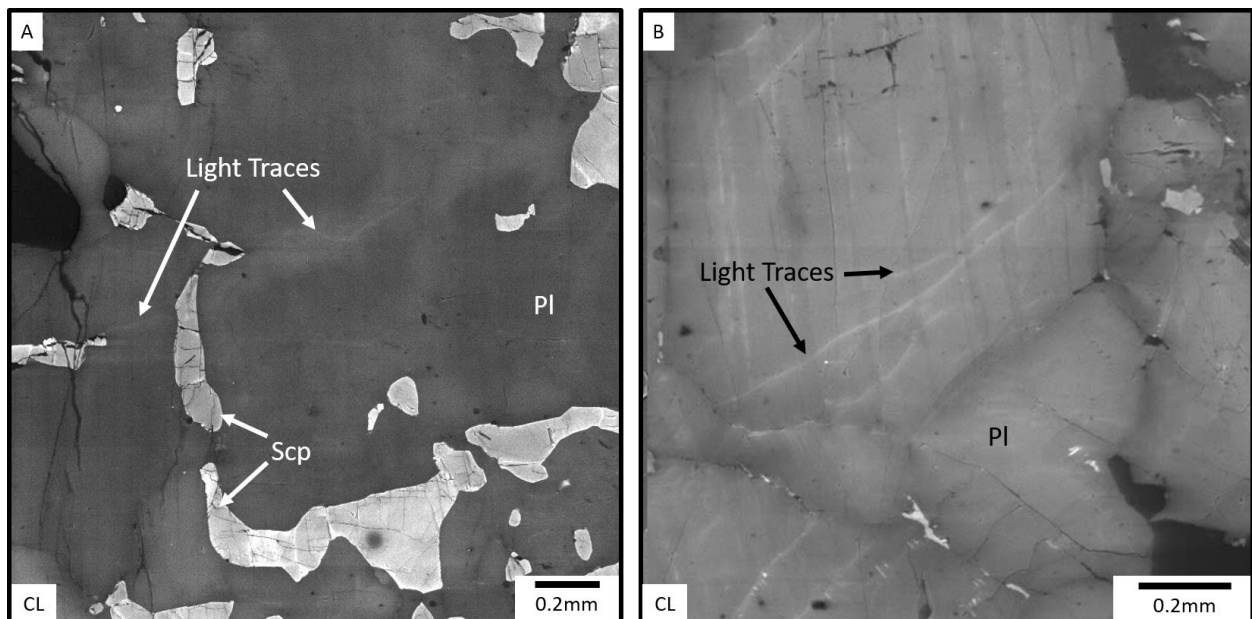
Figure 5.3. Cathodoluminescence images of anomalous bright traces in plagioclase. Traces potentially indicate locations of healed microfractures. (A) Light traces associated with curvilinear scapolite grains within a Type A grain. (B) Light traces cutting a Type B grain.

permeability allowed for the infiltration of fluids into the interior of the massif in conjunction with other igneous intrusions and REE-rich fluid fluxes into the country rock gneisses flanking the massif margins (McLelland et al., 1996; Selleck, 2005; McLelland & Selleck, 2011; Valley et al., 2011: Chiarenzelli et al., 2018; Regan et al., 2019). The presence of fluid in the system triggered metasomatic replacement reactions, fundamentally changing the bulk physical properties of the rock within up to a meter of the zones of highest fluid flux. Scapolite, amphibole, quartz, and biotite were introduced, reducing the strength of the rock through both the addition of weaker minerals such as biotite and quartz into the system and the net reduction of grain-size within the hydrated zones (cf. Fitz Gerald & Stünitz, 1993). This weakening was greatest in areas of greatest metasomatism, which likely correspond with preexisting brittle fractures/faults. As macroscale stresses continued to cause deformation within the Marcy massif, a deformation mechanism switch occurred in these now rheologically weak zones, and subsequent strain was accommodated largely by initiation and growth of localized viscous shear zones (Figure 5.4).

As mentioned previously, grain size throughout the massif tends to be distributed bimodally, with Type A plagioclase megacrysts surrounded, and sometimes crosscut, by Type B plagioclase along with garnet, augite, and other minor minerals (Figure 3.5a). This variability is interpreted to be the product of relict igneous textures overprinted by a brittle deformation event which caused the formation of Type B plagioclase. Approaching shear zones, average grain-size becomes more homogenous as Type A phenocrysts become rarer and smaller and Type B plagioclase modal abundance increases accordingly. The introduction of metasomatic scapolite also lowers the average grain size, as do amphibole-quartz symplectite rims around pyroxene, and the increasing modal abundance of these replacement minerals also serves to reduce grain

size. The grain-size reduction seen approaching shear features (Zones I-III) is therefore

interpreted to be a product of brittle damage heterogeneously increasing permeability followed

by an influx of geothermal fluid which triggered retrograde metasomatic replacement throughout

damage zones, weakening the rock through grain-size reduction and the introduction of relatively

weak minerals. Further grain-size reduction within the shear zone core (Zone IV) is then the

result of viscous creep processes as shear zones preferentially localized in zones of highest

metamorphic weakening. This study supplements a collection of work suggesting that a fluid

influx and associated metasomatic alteration can change the character of a rock body sufficiently

to promote localization (Marsh et al., 2009; Culshaw et al., 2010; Brander et al., 2012;

Goncalves et al., 2012, Mukai et al., 2014; Okudaira et al., 2017, Condit & Mahan, 2018).

Symplectic rims of amphibole and quartz around pyroxene represent microscale areas of

weakness induced by metasomatic replacement both through the relative weakness of the

amphibole and quartz relative to the relict pyroxene and the reduced grain size associated with

the symplectic growth. Every thin section that contained part of a shear zone also contained one

or more pyroxenes whose rims were truncated by the shear zone suggesting that that

microstructure is an important weakening factor (Figure 5.5).

The replacement of plagioclase by scapolite also reduced the grain size though the

introduction of a new phase. However, because little experimental work exists documenting the

physical properties of scapolite, it is difficult to say what effect the replacement of plagioclase by

scapolite had on the strength of the system compared to the addition of amphibole + quartz.

Regardless of how much each replacement reaction weakened the system, microstructural

relationships show that the dominant factor controlling shear zone initiation is the degree of

metasomatic replacement and the grain-size reduction associated with that replacement.

Furthermore, once strain began to localize and grain-size was reduced, the primary plagioclase

and secondary scapolite (as well as entrained amphibole, quartz, and other minerals) became

mixed (Figure 3.8a). This mixed polymineralic distribution within the shear zone core results in
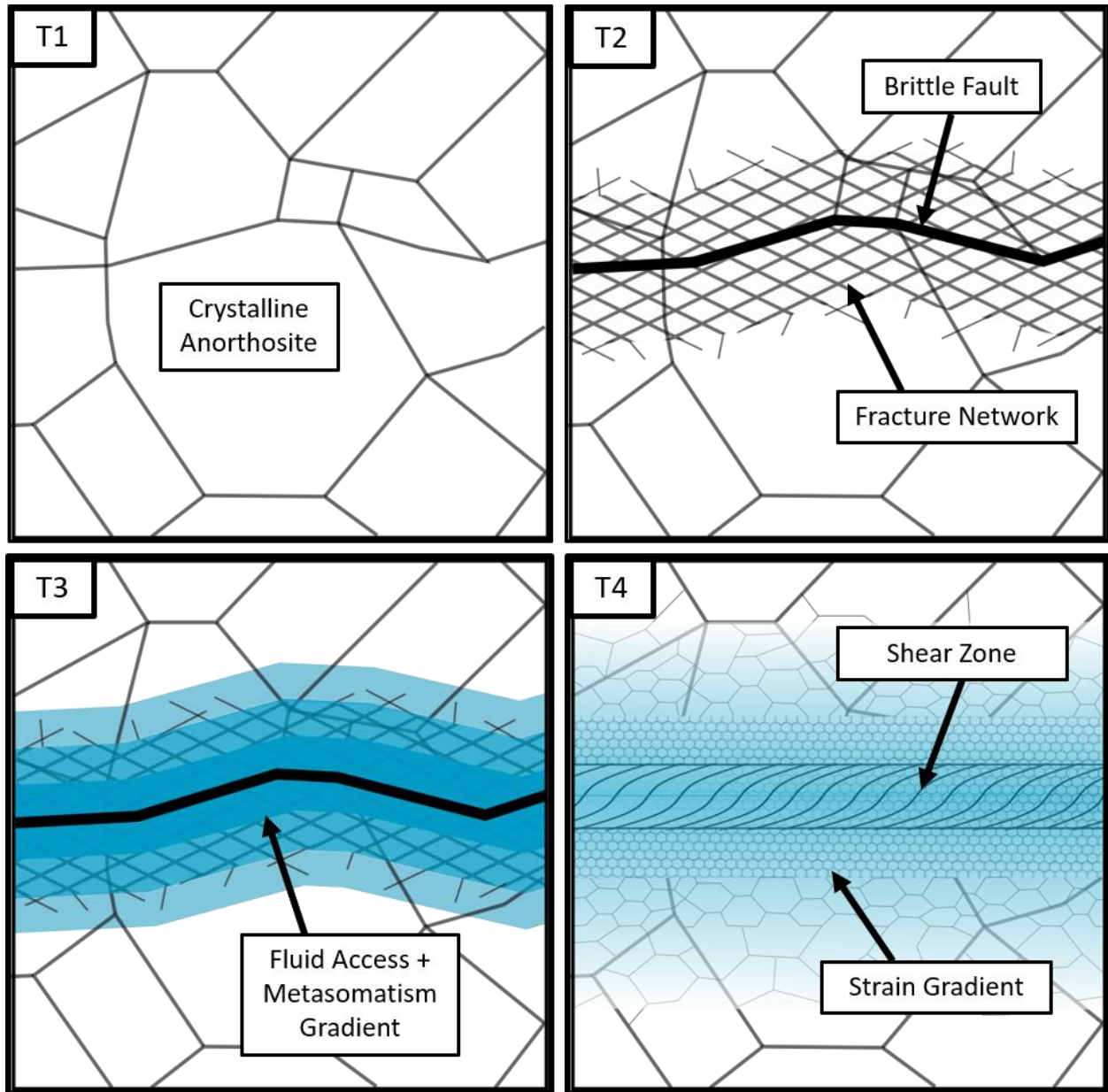
Figure 5.4. Schematic showing hypothesized sequence leading to shear zone initiation. (T1) Crystalline structure pre-deformation. (T2) Brittle fault and lesser radial fractures cut through crystalline rock. (T3) Increased permeability allows for the infiltration of hydrothermal fluid along fractures triggering metasomatic reactions along a gradient. (T4) Viscous shear zone initiates along the planar zone of greatest metasomatic weakening with the strain gradient correlating to the metasomatism gradient.

phase pinning which slows grain-growth and healing causing the shear zone to stay in a grain-size sensitive deformation regime and keeping the zone preferentially weak compared to the surrounding host rock (Ree et al., 2005; Warren & Hirth, 2006; Herwegh et al., 2011; Linckens et al., 2011; Bercovici & Ricard, 2012; Platt, 2015; Viegas et al., 2016). In my samples, though numerous individual grains appear to be less than 10 µm in diameter within Zone IV, the average grain size does not appear to fall below that size, with grains commonly over 100 µm in diameter. Although it is likely that this is a function of late-stage static recrystallization after deformation had ceased due to the irregular grain geometry and size, I cannot confirm that grain-size sensitive creep was the dominate creep mechanism in the shear zone core.
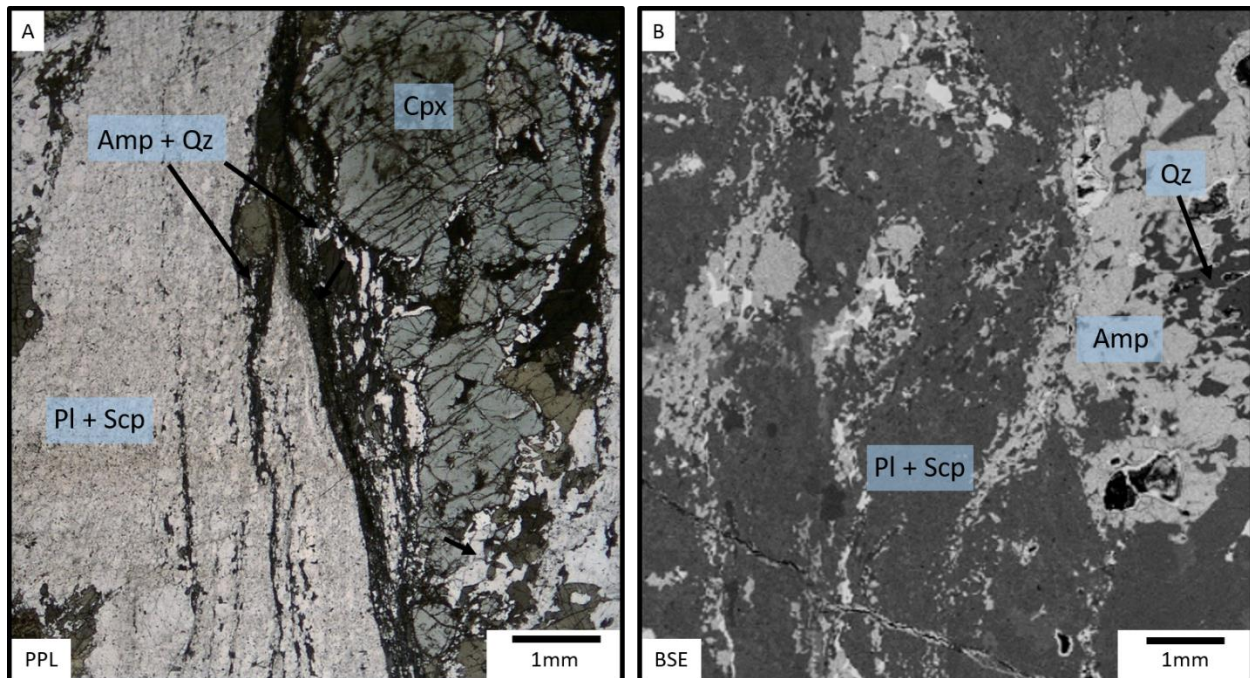
Figure 5.5. Evidence that metasomatic replacement predated shear zone development. (A) Photomicrograph showing a shear zone truncating and entraining the symplectic amphibole + quartz rim around a pyroxene cluster into the shear zone. (B) Sheared amphibole + quartz assemblages on the margin of a shear zone core.

44

5.3. Granulite-Amphibolite Transition

How are retrograde metamorphism and deformation related, and what are the implications of this correlation?

Near investigated shear zones, plagioclase is partially replaced by scapolite along grain boundaries and triple junctions, and clinopyroxene grains/grain clusters are partially replaced by amphibole + quartz symplectic coronas. Biotite and apatite are also present in at least one sample but are not common. Because the Marcy massif is nominally a dry, granulite-facies meta anorthosite, these replacement reactions must be interpreted as a period of fluid access facilitated by an increase in local permeability as interpreted by other workers (e.g., Kullered & Erambert, 1999; Mukai et al., 2014; Okudaira et al., 2017; Centrella et al., 2018; Condit & Mahan, 2018). Evidence for this increased permeability from brittle damage has already been discussed in previous sections. Additionally, modal abundance of metasomatic minerals increase with proximity to shear zone cores, suggesting fluid was introduced preferentially along planes of greatest permeability and fluid access, which are now represented by the cores of viscous shear zones. A temporal correlation can be applied with mafic and granitic dikes that cut the bedrock in similar orientations. These dikes have not been quantitatively dated, but structural relationships suggest that the dikes and shear zones are the result of NW/SE extension, making it likely that they are coeval with igneous bodies such as the Lyon Mountain granite which has been determined to have intruded during orogenic collapse in the late Ottawan phase of the Grenville orogeny ca. 1050 Ma (Selleck, 2005; McLelland & Selleck, 2011; Valley et al., 2011: Regan et al., 2019).

The introduction of halogen-rich minerals such as amphibole, biotite, and scapolite as part of the fluid-assisted retrograde transition from granulite-facies assemblages to amphibolite assemblages in the middle-to-lower-crust is well noted (Kullered & Erambert, 1999; Mukai et al., 2014; Okudaira et al., 2017; Centrella et al., 2018; Condit & Mahan, 2018). The most abundant replacement mineral, presumably due to the abundance of plagioclase, is scapolite. Unfortunately, the stability and material properties of scapolite are poorly understood outside of its solid-solution endmember compositions, marialite ($Na_4Al_3Si_9O_{24}Cl$) and meionite ($Ca_4Al_6Si_6O_{24}CO_3$) (Deer et al., 1992; Teertstra & Sherriff, 1997; Almeida & Jenkins, 2017). These endmembers mirror the sodic and calcic endmembers of plagioclase, albite ($NaAlSi_3O_8$) and anorthite ($CaAl_2Si_2O_8$) respectively, but little is known about the solid-solution series other than that it is not conveniently linear as the plagioclase solid-solution (Kullerud & Erambert, 1999; Almeida & Jenkins, 2017). At Bennies Brook, scapolite composition (Table 4.2) is commonly more calcic than the plagioclase it replaces (Table 4.1) which demonstrates this non-linearity. Due to its relative abundance, scapolite represents the greatest sink of Cl along metasomatized zones. However, amphibole contains more chlorine by weight %, up to 5% (Table 4.3). Biotite and apatite are present in at least one sample each. Microstructural context gives little evidence as to the reactions responsible for their formation, but both minerals contain chlorine indicating that their formation is a result of the same fluid influx as the more prevalent scapolite and amphibole and is expected as part of a partial retrograde transition from the granulite facies to the amphibolite facies.

Previous workers have suggested that halogen concentrations and isotopic ratios can be used to identify sources of Cl-rich fluids such as sub-aerial evaporation of seawater (Hammerli et al., 2014), prograde metamorphism of marine sediments (Kusebauch et al., 2015), and

46

dehydration of a subducting slab (Kent et al., 2002; John et al., 2010). However, the quantitative thermodynamic modelling and isotopic measurements required are beyond the limits of this project. Therefore, though a slab-derived source is preferred based on the high salinity (Table 4.3) (Vanko, 1986) and tectonic context (Kent et al., 2002; John et al., 2010) this assumption cannot be quantitatively supported. Despite the lack of isotopic measurements to determine a fluid source, I do make some inferences of metasomatic conditions based on metasomatic mineral compositions. The increased Ca-content of scapolite with respect to plagioclase suggests that the system was locally in equilibrium with the fluid (Kullered & Erambert, 1999, Chan et al., 2016). Additionally, the Al- and Ti-contents of amphiboles act as a qualitative thermobarometer (Apted & Liou, 1983; Ernst & Liu, 1998) indicating that amphibole growth at 650ºC and 500 MPa is reasonable which correlates to prior pressure-temperature estimates during fluid influx (McLelland et al., 1996; McLelland et al., 2013; Peck et al., 2018, Regan et al., 2019).

5.4. Implications for Adirondack History

How does my hypothesis correlate to current geologic ideas concerning the Adirondack Highlands?

The full implications of intra-plutonic strain localization in the Marcy anorthosite lie beyond the limited reach of this work. To fully characterize the area would require many more sample locations and comprehensive mapping of the interior due to the size of the massif and the apparent heterogeneity in both igneous and metamorphic features. However, the observations I document in this work can shed light on several important aspects of local tectonics, geodynamics, and rheology in the Adirondack Highlands.

5.4.1. Tectonic Effects

The orientation and conjugate nature of the planar deformation features observed in outcrop at the Bennies Brook study site is consistent with a period of NW/SE extension in the Adirondack Highlands during late Ottawan orogenic collapse post-dating burial to granulite-facies conditions (Wong et al., 2012; Regan et al., 2019). The most definitive evidence of this extension lies in the kilometer-scale Carthage-Colton and East Adirondack shear zones that flank the Adirondack Highlands (McLelland et al., 1996; Rivers, 2008; McLelland & Selleck, 2011; Peck et al., 2018; Regan et al., 2019), as well as the presence of the intrusive Lyon Mountain granite and magnetite-apatite deposit series that have been dated to ca. 1050 Ma (Selleck, 2005; McLelland & Selleck, 2011; Valley et al., 2011: Chiarenzelli et al., 2018). However, these studies rarely advance hypotheses regarding the state of stress within the exhuming massif. My analysis and interpretations not only support this prior work but allow us to examine the stress state of the Marcy massif interior as exhumation occurred. Although I have no quantitative piezometer-based stress values, I suggest that the Marcy massif was deforming internally in response to the macroscale extension in the region during the late Ottawan. Furthermore, I suggest that brittle and viscous deformation mechanisms were operating essentially simultaneously within the same area, as evidenced by the presence of mutually offsetting dikes and shear zones. This shows that during exhumation, the massif existed in a dynamic deformation regime of mixed brittle and viscous behavior.

5.4.2. Massif Properties

The main hypothesis of this work depends on a sequence of events beginning with the nucleation of brittle fractures accompanied by an increase in permeability. Therefore, the

mechanism through which shear zones developed would alter the physical properties of the rock even without the localization of strain. The most important implications for the hydration of granulite bodies in Earth's crust are the changes in density and volume associated with the retrograde transition to lower-grade facies mineral assemblages evidenced both by theoretical calculations and seismic investigation (Austrheim, 1987; Tripathi et al., 2012; Centrella et al., 2015; Leslie et al., 2015; Pandey et al., 2016). Hydrous minerals like scapolite, biotite, and amphibole are less dense than the granulite-facies minerals like plagioclase and pyroxene that they replace (Deer et al., 1992). In dry anorthosite which comprises ~90% plagioclase, the replacement of plagioclase by scapolite is the dominant factor when determining bulk property changes. However, in this case, because of the difficulty inherent in calculating a change in volume from a solid + fluid reaction in addition to the lack of knowledge regarding non-endmember scapolite compositions, it is difficult to quantitatively determine the impact of the retrograde transition on the physical characteristics of the massif. Qualitative volume change calculations indicate a probable volume change of <1% under the assumptions of a solid-state interaction and linear relationships between endmembers (albite + halite + anorthosite + calcite → marialite + meionite) but due to the uncertainty of both assumptions, these calculations are preliminary (Table 5.1). A qualitative change in density can be more accurately constrained assuming pre- and post-fluid interaction scenarios in which the plagioclase within a given volume is replaced by less dense scapolite. In this case, the source of additional ions to complete the replacement reaction is ignored, simplifying the calculations. By comparing the density of typical Marcy anorthosite to the intermediate-composition scapolite I observed, I determined a hypothetical density reduction of >2% from 2.69 g/cm^3 (An$_{50}$ plagioclase) to 2.63 g/cm^3 (AnEq$_{65}$ scapolite) for a given volume (Table 5.1). Due to plagioclase being the dominant mineral, the

addition of amphibole and quartz replacing pyroxene to the calculation is less important, but

even if accounted for, this reaction would only reduce the density further due to the relatively

low density of quartz. Centrella et al. (2015) showed that this reaction is isovolumetric. Further

assuming that the Marcy massif was overlain by the same granitic gneisses, marbles, and other

igneous intrusive bodies that surround it (~2.70 g/cm^3), at this density change would exert

additional buoyancy forces and promote further exhumation. However, my observations

represent only a small fraction of the total massif volume, and there are few similar studies

within the massif. Therefore, I cannot hypothesize any significant geodynamic effects stemming

Volume and Density Calculations

Composition	100% Calcic	100% Calcic
Assumed Reaction	Pl » Scp	Pl + Cal » Scp
Density Change (%)	-2.29	2.20
Volume Change (%)	9.68	0.66
Composition	100% Sodic	100% Sodic
Assumed Reaction	Pl » Scp	Pl + Hl » Scp
Density Change (%)	0.00	0.36
Volume Change (%)	12.89	0.58
Composition	50An » 65AnEq	50An » 65AnEq
Assumed Reaction	Pl » Scp	Pl + Hl/Cal » Scp
Density Change (%)	-2.23	0.10
Volume Change (%)	10.68	0.67

Table 5.1.   Table showing calculated volume and density changes for various plagioclase and scapolite compositions. Reactions are assumed to take place under idealized conditions. Plagioclase (50An) reacting to scapolite (65AnEq) is representative of natural samples. If the reaction is Pl » Scp, the reaction does not account for the addition of fluid volume. If the reaction is Pl + Hl/Cal » Scp, the reaction treats Hl/Cal as solid reactants. Given these assumptions, the values shown serve only as preliminary end-member estimates.

50

from the hydration and retrograde transition of the anorthosite from granulite-facies assemblages to amphibolite assemblages, as I do not know the extent to which this transition took place in the Adirondack Highlands. However, depending on the exact replacement reactions that might occur, and the geologic context, this phenomenon could plausibly be geodynamically significant in certain instances.

CHAPTER 6

CONCLUSIONS

Based on observations made in the field and laboratory, this study shows that metamorphic weakening acted as the primary factor leading to the initiation of localized shear zones in the interior of a Mesoproterozoic meta-anorthosite pluton in the Adirondack Mountains, New York. Extensive brittle failure increased the permeability sufficiently to allow an influx of saline fluid to infiltrate the interior of the granulite-facies Marcy anorthosite massif along brittle fault planes at ~600-650°C and 500-600 MPa confining pressure. The addition of fluid under these conditions in which the granulite-facies assemblages were metastable triggered a partial retrograde transition to hydrous amphibolite-facies assemblages concentrated along fracture planes, creating a gradient of metamorphic replacement which represent a proxy for the fluid access gradient during infiltration. This metasomatic process weakened the rock through the growth of weak minerals and a net reduction in grain size, with the greatest weakening occurring along the plane of greatest fluid access. The weakening was sufficient such that as extensional stresses continued to be applied to the system, these weak, metasomatized planar zones allowed for the nucleation of shear zones deforming through grain-size-sensitive viscous creep. Strain then continued to localize as phase mixing and continued grain-size reduction kept the shear zone weak. This hypothesized sequence of deformational and metamorphic events correlates with other structures emplaced outside the massif margins as the Adirondack Highlands underwent tectonic extension during the Ottawan phase of the Grenville orogeny.

The geologic contribution of this work is two-fold. First, this study shows that a mixture of mechanical and chemical weakening processes drove the localization of strain within the

middle-lower crust and locally triggered a switch in deformation regime from brittle to viscous. This adds credence to the burgeoning understanding of the importance of fluids in the behavior of shear zones and also shows how complex the relationship between brittle and viscous deformation can be within the middle-lower crust. Second, this work is the first in-depth meso- to-microstructural study done in this area, and one of only few within the entire Marcy massif interior. My results support previous suggestions that the Adirondack Highlands underwent NW/SE extension during the late stages of the Grenville orogeny, most of which were based on work at the margins or outside of the Marcy massif. During this extension and exhumation, the massif itself was internally deformed through brittle damage and subsequent viscous strain localization through the influx of fluid. Therefore, in addition to the study of metamorphic weakening as a viable strain localization mechanism, this work serves as a novel contribution to the literature concerning the structure and tectonic history of the Adirondack Highlands.

REFERENCES

Almeida, K. M. F., Jenkins, D. M. (2017) 'Stability field of the Cl-rich scapolite marialite', *American Mineralogist,* 102, pp. 2484-2493.

Apted, M. J., Liou, J. G. (1983) 'Phase relations among greenschist, epidote-amphibolite, and amphibolite in a basaltic system', *American Journal of Science,* 283-A, pp. 328-354.

Austrheim, H. (1987) 'Eclogitization of lower crustal granulites by fluid migration through shear zones', *Earth and Planetary Science Letters,* 81, pp. 221-232.

Bercovici, D., Ricard, Y. (2012) 'Mechanisms for the generation of plate tectonics by two-phase grain-damage and pinning', *Physics of the Earth and Planetary Interiors,* 202-203, pp. 27-55.

Bohlen, S. R., Valley, J. W., Essene, E. J. (1985) 'Metamorphism in the Adirondack. I. Petrology, pressure, and temperature' *Journal of Petrology,* 26(4), pp. 971-992.

Brander, L., Svahnberg, H., Piazolo, S. (2012) 'Brittle-plastic deformation in initially dry rocks at fluid-present conditions: transient behavior of feldspar at mid-crustal levels', *Contributions to Mineralogy and Petrology,* 163, pp. 403-425.

Braun, J., Chéry, J., Poliakov, A., Mainprice, D., Vauchez, A., Tomassi, A., Daignières, M. (1999) 'A simple parameterization of strain localization in the ductile regime due to grain size reduction: a case study for olivine', *Journal of Geophysical Research,* 104(B11) , pp. 25167-15181.

Brodie, K. H., Rutter, E. H. (1987) 'The role of transiently fine-grained reaction products in syntectonic metamorphism: natural and experimental examples', *Canadian Journal of Earth Science,* 24, pp. 556-564.

Brown, W. L., Macaudière, J. (1984) 'Microfracturing in relation to atomic structure of plagioclase from a deformed meta-anorthosite', *Journal of Structural Geology,* 6(5), pp. 579-586.

Buddington, A. F. (1939) 'Anorthositic, gabbroic, and dioritic rocks. In: Adirondack igneous rocks and their metamorphism', *Geological Society of America,* pp. 19-72.

Bürgmann, R., Dresen, G. (2008) 'Rheology of the lower crust and upper mantle: evidence from rock mechanics, geodesy, and field observations', *Annual Review of Earth and Planetary Sciences,* 36, pp. 531-567.

Centrella, S., Austrheim, H., Putnis, A. (2015) 'Coupled mass transfer through a fluid phase and volume preservation during the hydration of granulite: an example from the Bergen Arcs, Norway', *Lithos,* 236-237, pp. 245-255.

Centrella, S., Putnis, A., Pierre, L., Austrheim, H. (2018) 'Textural and chemical evolution of pyroxene during hydration and deformation: A consequence of retrograde metamorphism', *Lithos,* 296-299, pp. 245-264.

Chan, A., Jenkins, D. M., Dyar, M. D. (2016) 'Partitioning of chlorine between NaCl brines and ferro-pargasite: Implications for the formation of chlorine-rich amphiboles in mafic rocks', *The Canadian Mineralogist,* 54, pp. 337-351.

Chiarenzelli, J. R., Lupulescu, M. V., Regan, S. P., Singer, J. W. (2018) 'Age and origin of the Mesoproterozoic iron oxide-apatite mineralization, Cheever Mine, eastern Adirondacks, NY', *Geosciences,* 8(9), pp. 345.

Clechenko, C. C., Valley, J. W. (2003) 'Oscillatory zoning in garnet from the Willsboro Wollastonite Skarn, Adirondack Mts, New York: a record of shallow hydrothermal processes preserved in a granulite facies terrane', *Journal of Metamorphic Geology,* 21, pp. 771–784.

Condit, C. B., Mahan, K. H. (2018) 'Fracturing, fluid flow and shear zone development: Relationships between chemical and mechanical processes in Proterozoic mafic dykes from southwestern Montana, USA', *Journal of Metamorphic Geology,* 36, pp. 195-223.

Cook, A. C., Vel, S. S., Gerbi, C., Johnson, S. E. (2014) 'Computational analysis of nonlinear creep of polyphase aggregates: influence of phase morphology', *Journal of Geophysical Research: Solid Earth,* 119, pp. 6877-6906.

Cross, A. J., Ellis, S., Prior, D. J. (2015) 'A phenomenological numerical approach for investigating grain size evolution in ductiley deforming rocks', *Journal of Structural Geology,* 76, pp. 22-34.

Culshaw, N., Gerbi, C., Marsh, J. (2010) 'Softening the lower crust: modes of syn-transport transposition around and adjacent to a deep crustal granulite nappe, Parry Sound domain, Grenville Province, Ontario, Canada', *Tectonics,* 29, TC5013.

Czaplińska, D., Piazolo, S., Zibra, I. (2015) 'The influence of phase and grain size distribution on the dynamics of strain localization in polymineralic rocks', *Journal of Structural Geology,* 72, pp. 15-32.

Davis, K. E. (1981) 'Magnetite rods in plagioclase as the primary carrier of stable NRM in ocean floor gabbros', *Earth and Planetary Science Letters,* 55, pp. 190-198.

De Ronde, A. A., Stünitz, H., Tullis, J., Heilbronner, R. (2005) 'Reaction-induced weakening of plagioclase-olivine composites', *Tectonophysics,* 409, pp. 85-106.

Deer, W. A., Howie, R. A., Zussman, J. (1992) 'An introduction to the rock-forming minerals', *Longman Scientific & Technical,* Harlow.

Drury, M. R., Urai, J. L. (1990) 'Deformation-related recrystallization process', *Tectonophysics,* 172, pp. 235-253.

Ernst, W. G., Liu, J. (1998) 'Experimental phase-equilibrium study of Al- and Ti-contents of calcic amphibole in MORB—a semiquantitative thermobarometer', *American Mineralogist,* 83, pp. 952-969.

Fitz Gerald, J. D., Stünitz, H. (1993) 'Deformation of granitoids at low metamorphic grade. I. Reactions and grain size reduction', *Tectonophysics,* 221, pp. 269-297.

Fossen, H., Cavalcante, G. C. G. (2017) 'Shear zones – A review', *Earth-Science Reviews,* 171, pp. 434-455.

Fusseis, F., Handy, M. R., Schrank, C. (2006) 'Networking of shear zones at the brittle-to-viscous transition (Cap de Creus, NE Spain)', *Journal of Structural Geology,* 28, 1228-1243.

Geake, J. E., Walker, G., Telfer, D. J., Mills, A. A. (1977) 'The cause and significance of luminescence in lunar plagioclase', *Philosophical Transactions of the Royal Society of London,* A285(1327), pp. 403-408.

Gerbi, C., Johnson, S. E., Shulman, D., Klepeis, K. (2016) 'Influence of microscale weak zones on bulk strength', *Geochemistry, Geophysics, Geosystems,* 17.

Goncalves, P., Oliot, E., Marquer, D., Connolly, J. A. D. (2012) 'Role of chemical processes on shear zone formation: an example from the Grimsel metagranodiorite (Aar massif, Central Alps)', *Journal of Metamorphic Geology,* 30, pp. 703-722.

Gueydan, F., Précigout, J., Montési, L. G. J. (2014) 'Strain weakening enables continental plate tectonics', *Tectonophysics,* 631, pp. 189-196.

Hammerli, J., Spandler, C., Oliver, N. H. S., Rusk, B. (2014) 'Cl/Br of scapolite as a fluid tracer in the Earth's crust: insights into fluid sources in the Mary Kathleen Fold Belt, Mt. Isa Inlier, Australia', *Journal of Metamorphic Geology,* 32, pp. 93-122.

Hertgen, S., Yamato, P., Morales, L. F. G., Angiboust, S. (2017) 'Evidence for brittle deformation events at eclogite-facies P-T conditions (example of the Mt. Emilius klippe, Western Alps)', *Tectonophysics,* 706-707, pp. 1-13.

Herwegh, M., Linckens, J., Ebert, A., Berger, A., Brodhag, S. H. (2011) 'The role of second phases for controlling microstructural evolution in polymineralic rocks: a review', *Journal of Structural Geology,* 33, pp. 1728-1750.

Holyoke, C. W., Tullis, J. (2006) 'The interaction between reaction and deformation: and experimental study using a biotite + plagioclase + quartz gneiss', *Journal of Metamorphic Geology,* 24, pp. 743-762.

Jamtveit, B., Austrheim, H., Putnis, A. (2016) 'Disequilibrium metamorphism of stressed lithosphere', *Earth-Science Reviews,* 154, pp. 1-13.

Ji, S., Mainprice, D. (1990) 'Recrystallization and Fabric Development in Plagioclase', *The Journal of Geology,* 98(1), pp. 65-79.

John, T., Layne, G. D., Haase, K. M., Barnes, J. D. (2010) 'Chlorine isotope evidence for crustal recycling into the Earth's mantle', *Earth and Planetary Science Letters,* 298, pp. 175-182.

Johnson, S., Vernon, R. H., Upton, P. (2004) 'Foliation development and progressive strain-rate partitioning in the crystallizing carapace of a tonalite pluton: microstructural evidence and numerical modeling', *Journal of Structural Geology,* 26, 1845-1865.

Kenkmann, T., Dresen, G. (2002) 'Dislocation microstructure and phase distribution in a lower crustal shear zone – an example from the Ivrea-Zone, Italy', *International Journal of Earth Science,* 91, pp. 445-458.'

Kent, A. J. R., Peate, D. W., Newman, S., Stolper, E. M., Pearce, J. A. (2002) 'Chlorine in submarine glasses from the Lau Basin: seawater contamination and constraints on the composition of slab-derived fluids', *Earth and Planetary Science Letters,* 202, pp. 361-377.

Kirby, S. H. (1985) 'Rock mechanics observations pertinent to the rheology of the continental lithosphere and the localization of strain along shear zones', *Tectonophysics,* 119, pp. 1-27.

Kruse, R., Stünitz, H., Kunze, K. (2001) 'Dynamic recrystallization process in plagioclase porphyroclasts', *Journal of Structural Geology,* 23, pp. 1781-1802.

Kullered, K., Erambert, M. (1999) 'Cl-scapolite, Cl-amphibole, and plagioclase equilibria in ductile shear zones at Nusfjord, Lofoten, Norway: implication for fluid compositional evolution during fluid-mineral interaction in the deep crust', *Geochimica et Cosmochimica Acta,* 63(22), pp. 3829-3844.

Kusebauch, C., John, T., Barnes, J. D., Klügel, A., Austrheim, H. O. (2015) 'Halogen element and stable chlorine isotope fractionation caused by fluid-rock interaction (Bamble Sector, SE Norway)', *Journal of Petrology,* 56(2), pp. 299-324.

Leslie, S. R., Mahan, K. H., Regan, S., Williams, M. L., Dumond, G. (2015) 'Contrasts in sillimanite deformation in felsic tectonites from anhydrous granulite- and hydrous amphibolite-facies shear zones, western Canadian Shield', *Journal of Structural Geology,* 71, pp. 112-124.

Mackenzie, K. B. (2017) 'Adirondack Landslides: history, exposures, and climbing', *Adirondack Journal of Environmental Sciences,* 21, pp. 167-193

Mancktelow, N. S. (2002) 'Finite-element modelling of shear zone development in viscoelastic material and its implications for localisation of partial melting', *Journal of Structural Geology,* 24, pp. 1045-1053.

Mancktelow, N. S., Pennacchioni, G. (2005) 'The control of precursor brittle fracture and fluid-rock interaction on the development of single and paired ductile shear zones', *Journal of Structural Geology,* 27, pp. 645-661.

Marsh, J. H., Johnson, S. E., Yates, M. G., West Jr., D. P. (2009) 'Coupling of deformation and reactions during mid-crustal shear zone development: an in-situ frictional-viscous transition', *Journal of Metamorphic Geology,* 27, pp. 531-553.

Marti, S., Stünitz, H., Heilbronner, R., Plümper, O., Kilian, R. (2018) 'Syn-kinematic hydration reactions, grain size reduction, and dissolution-precipitation creep in experimentally deformed plagioclase-pyroxene mixtures', *Solid Earth,* 9, pp. 985-1009.

McLelland, J. M. (1989) 'Crustal growth associated with anorogenic, mid-Proterozoic anorthosite massifs in northeastern North America', *Tectonophysics,* 161, pp. 331-341.

McLelland, J., Daly, J. S., McLelland, J. M. (1996) 'The Grenville Orogenic Cycle (ca. 1350-1000 Ma): an Adirondack perspective', *Tectonophysics,* 265, pp. 1-28.

McLelland, J. M., Bickford, M. E., Hill, B. M., Clechenko, C. C., Valley, J. W., Hamilton, M. A. (2004) 'Direct dating of Adirondack massif anorthosite by U-Pb SHRIMP analysis of igneous zircon: Implication for AMCG complexes', *GSA Bulletin,* 116(11-12), pp. 1299-1317.

McLelland, J. M., Selleck, B. W. (2011) 'Megacrystic Gore-Mountain-type garnets in the Adirondack Highlands: age, origin, and tectonic implications', *Geosphere,* 7(5) pp. 1194–1208.

Menegon, L., Stünitz, H., Nasipuri, P., Heilbronner, R., Svahnberg, H., (2013) 'Transition from fracturing to viscous flow in granulite facies perthitic feldspar (Lofoten, Norway)' *Journal of Structural Geology,* 48, pp. 95-112.

Mezger, K., Rawnsley, C. M., Bohlen, S. R., Hanson, G. N. (1991) 'U-Pb garnet, sphene, monazite, and rutile ages: implications for the duration of high-grade metamorphism and cooling histories, Adirondack Mts. New York', *The Journal of Geology,* 99(3), pp. 415-428.

Mills, S. G., Gerbi, C., Marsh, J. H., Yates, M. G., Seaman, S. J., White, J. C. (2017) 'Tectonic and chemical implications of cathodoluminescent microstructures in quartz, Parry Sound domain, Ontario, Canada', *Canadian Journal of Earth Sciences,* 54, pp. 677-692.

Misra, S., Mandal, N. (2007) 'Localization of plastic zones in rocks around rigid inclusions: insights from experimental and theoretical models', *Journal of Geophysical Research,* 112, B09206.

Mitra, G. (1978) 'Ductile deformation zones and mylonites: The mechanical processes involved in the deformation of crystalline basement rocks', *American Journal of Science,* 278, pp. 1057-1084.

Montési, L. G. J. (2013) 'Fabric development as the key for forming ductile shear zones and enabling plate tectonics', *Journal of Structural Geology,* 50, pp. 254-266.

Mora, C. I., Ramseyer, K. (1992) 'Cathodoluminescence of coexisting plagioclases, Boehls Butte anorthosite: CL activators and fluid flow paths', *American Mineralogist,* 77, pp. 1258-1265.

Morrison, J., Valley, J. W. (1988) 'Post-granulite facies fluid infiltration in the Adirondack Mountains', *Geology,* 16, pp. 513-516.

Morrison, J., Valley, J. W. (1991) 'Retrograde fluids in granulites: stable isotope evidence of fluid migration', *The Journal of Geology,* 99(4), pp. 559-570.

Mukai, H., Austrheim, H., Putnis, C. V., Putnis, A. (2014) 'Textural evolution of plagioclase feldspar across a shear zone: implications for deformation mechanism and rock strength', *Journal of Petrology,* 55(8), pp. 1457-1477.

Okudaira, T., Shigematsu, N., Harigane, Y., Yoshida, K. (2017) 'Grain size reduction due to fracturing and subsequent grain-size sensitive creep in a lower crustal shear Zone In the presence of a CO_2-bearing fluid', *Journal of Structural Geology,* 95, pp. 171-187.

Pandey, O. P., Tripathi, P., Vedanti, N., Sarma, S. (2016) 'Anomalous seismic velocity drop in iron and biotite rich amphibolite to granulite facies transitional rocks from Deccan volcanic covered 1993 Killari Earthquake Region, Maharashtra (India): a case study', *Pure and Applied Geophysics,* 173, pp. 2455-2471.

Passchier, C. W., Trouw, R. A. J. (2005) 'Microtectonics', *Springer,* New York, Berlin.

Peck, W. H., Selleck, B. W., Regan, S. P., Howard, G. E., Kozel, O. O. (2018) 'In-situ dating of metamorphism in Adirondack anorthosite', *American Mineralogist,* 103, pp. 1523-1529.

Platt, J. P., Behr, W. M. (2011) 'Grainsize evolution in ductile shear zones: Implication for strain localization and the strength of the lithosphere', *Journal of Structural Geology,* 33, pp. 537-550.

Platt, J. P. (2015) 'Rheology of two-phase systems: a microphysical and observational approach', *Tectonophysics,* 77, pp. 213-227.

Poirier, J. P. (1980) 'Shear localization and shear instability in materials in the ductile field', *Journal of Structural Geology,* 2(1-2), pp. 135-142.

Post, A., Tullis, J. (1999) 'A recrystallized grain size piezometer for experimentally deformed feldspar aggregates', *Tectonophysics*, 303(1-4), pp. 159-173.

Putnis, A., Jamtveit, B., Austrheim, H. (2017) 'Metamorphic processes and seismicity: the Bergen Arcs as a natural laboratory', *Journal of Petrology,* 58(10), pp. 1871-1898.

Ramsay, J. G. (1980) 'Shear zone geometry: a review', *Journal of Structural Geology,* 2(1-2), pp. 83-99.

Ree, J. H., Kim, H.S., Han, R., Jung, H. (2005) 'Grain-size reduction of feldspars by fracturing and neocrystallization in a low-grade granitic mylonite and its rheological effect', *Tectonophysics,* 407, pp. 227-237.

Regan, S. P., Walsh, G. J., Williams, M. L., Chiarenzelli, J. R., Toft, M., McAleer, R. (2019) 'Syn-collisional exhumation of hot middle crust in the Adirondack Mountains: implication for extensional orogenesis in the southern Grenville Province' *Geosphere,* 15.

Regenauer-Lieb, K., Yuen, D. (2004) 'Positive feedback of interacting ductile faults form coupling of equation of state, rheology and thermal-mechanics', *Physics of the Earth and Planetary Interiors,* 142, pp. 113-135.

Rivers, T., Corrigan, D. (2000) 'Convergent margin on southeastern Laurentia during the Mesoproterozoic: tectonic implications', *Canadian Journal of Earth Science,* 37, 359-383.

Rivers, T. (2008) 'Assembly and preservation of lower, mid, and upper orogenic crust in the Grenville Province – Implications for the evolution of large hot long-duration orogens', *Precambrian Research,* 167, pp. 237-259.

Rybacki, E., Dresen, G. (2004) 'Deformation mechanism maps for feldspar rocks', *Tectonics,* 382, pp. 173-187.

Segall, P., Simpson, C. (1986) 'Nucleation of ductile shear zones on dilatant fractures', *Geology,* 14,pp. 56-59. Find a place for this.

Seifert, K. E., Dymek, R. F., Whitney, P. R., Haskin, L. A. (2010) 'Geochemistry of massif anorthosite and associated rocks, Adirondack Mountains, New York', *Geosphere,* 6(6), pp. 855-899.

Selleck, B. W., McLelland, J. M., Bickford, M. E. (2005) 'Granite emplacement during tectonic exhumation: the Adirondack example', *Geology,* 33(10), pp. 781-784.

Sharp, Z. D., Barnes, J. D., Brearley, A. J., Chaussidon, M., Fischer, T. P., Kamentsky, V. S. (2007) 'Chlorine isotope homogeneity of the mantle, crust and carbonaceous chondrites', *Nature,* 446, pp. 1062-1065.

Shulman, D. J. (2016) 'Processes leading to the formation of deep granitic shear zones in the Grenville Front Tectonic Zone, Ontario, Canada', *Electronic Theses and Dissertations.* 2507.

Spear, F. S., Markussen, J. C. (1997) 'Mineral zoning, P-T-X-M phase relations, and metamorphic evolution of some Adirondack granulites, New York', *Journal of Petrology,* 38, pp. 757-783.

Stünitz, H., Tullis, J. (2001) 'Weakening and strain localization produced by syn-deformational reaction of plagioclase', *International Journal of Earth Sciences,* 90, pp. 136-148.

Stünitz, H., Fitz Gerald, J. D., Tullis, J. (2003) 'Dislocation generation, slip systems, and dynamic recrystallization in experimentally deformed plagioclase single crystals', *Tectonophysics,* 372, pp. 215-233.

Svahnberg, H., Piazolo, S. (2010) 'The initiation of strain localization in plagioclase-rich rocks: insight from detailed microstructural analyses', *Journal of Structural Geology,* 32, pp. 1404-1416.

Teertstra, D. K., Sherriff, B. L. (1997) 'Substitutional mechanisms, compositional trends and the end-member formulae of scapolite', *Chemical Geology,* 136, pp. 233-260.

Tripathi, P., Parthasarathy, G., Masood Ahmad, S., Pandey, O. P. (2012) 'Mantle-derived fluids in the basement of the Deccan Trap: evidence from stable carbon and oxygen isotopes of carbonates from the Killari borehole basement, Maharashtra, India', *International Journal of Science,* 101, pp. 1385-1395.

Tullis, J., Yund, R. A. (1987) 'Transition from cataclastic flow to dislocation creep of feldspar: Mechanisms and microstructures', *Geology,* 15, pp. 606-609.

Tullis, J., Yund, R. A. (1991) 'Diffusion Creep in feldspar aggregates: experimental evidence' , *Journal of Structural Geology,* 13(9) pp. 987-1000.

Valley, J. W., O'Neil, J. R. (1982) 'Oxygen isotope evidence for shallow emplacement of Adirondack anorthosite', *Nature,* 300, pp. 497-500.

Valley, P. M., Hanchar, J. M., Whitehouse, M. J. (2011) 'New insights on the evolution of the Lyon Mountain Granite and associated Kiruna-type magnetite-apatite deposits, Adirondack Mountains, New York State', *Geosphere,* 7, pp. 357-389.

Vanko, D. A. (1986) 'High-chlorine amphiboles from oceanic rocks: product of highly-saline hydrothermal fluids?', *American Mineralogist,* 71, pp. 51-59.

Vernon, R. H. (2004) 'Symplectic intergrowth. In: A practical guide to rock microstructure', *Cambridge University Press,* Cambridge, pp. 242-254.

Viegas, G., Menegon, L., Archanjo, C. (2016) 'Brittle grain-size reduction of feldspar, phase mixing and strain localization in granitoids at mid-crustal conditions (Pernambuco shear zone, NE Brazil', *Solid Earth,* 7, pp. 375-396.

Warren, J. M., Hirth, G. (2006) 'Grain size sensitive deformation mechanisms in naturally deformed peridotites', *Earth and Planetary Science Letters,* 248, pp. 438-450.

Wenk, H. R., Chen, K., Smith, R. (2011) 'Morphology and microstructure of magnetite and ilmenite inclusions in plagioclase from Adirondack anorthositic gneiss', *American Mineralogist,* 96, pp. 1316-1324.

White, S. H., Burrows, S. E., Carreras, J., Shaw, N. D., Humphreys, F. J. (1980) 'On mylonites in ductile shear zones', *Journal of Structural Geology,* 2(1), pp. 175-187.

Whitney, D. L., Evans, B. W. (2010) 'Abbreviations for names of rock-forming minerals', *American Mineralogist,* 95, pp. 185-187.

Wong, M. S., Williams, M. L., McLelland, J. M., Jercinovik, M. J., Kowalkoski, J. (2012) 'Late Ottawan extension in the eastern Adirondack Highlands: Evidence from structural studies and zircon and monazite geochronology' *GSA Bulletin,* 124(5-6), pp. 857-869.

Xiao, Y., Hoefs, J., Kronz, A. (2005) 'Compositionally zoned Cl-rich amphiboles from North Dabie Shan, China: monitor of high-pressure metamorphic fluid/rock interaction processes', *Lithos,* 81, pp. 279-295.

Xu, J., Zhang, B. (2018) 'Numerical study on stress heterogeneity development in two-phase rocks with large rheological contrast and implications in the lower crust', *Pure and Applied Geophysics,* 175, 963-976.

Figure A.1. 360° rose diagram showing orientations of anorthosite shear zones and sheared dikes at Bennies Brook.
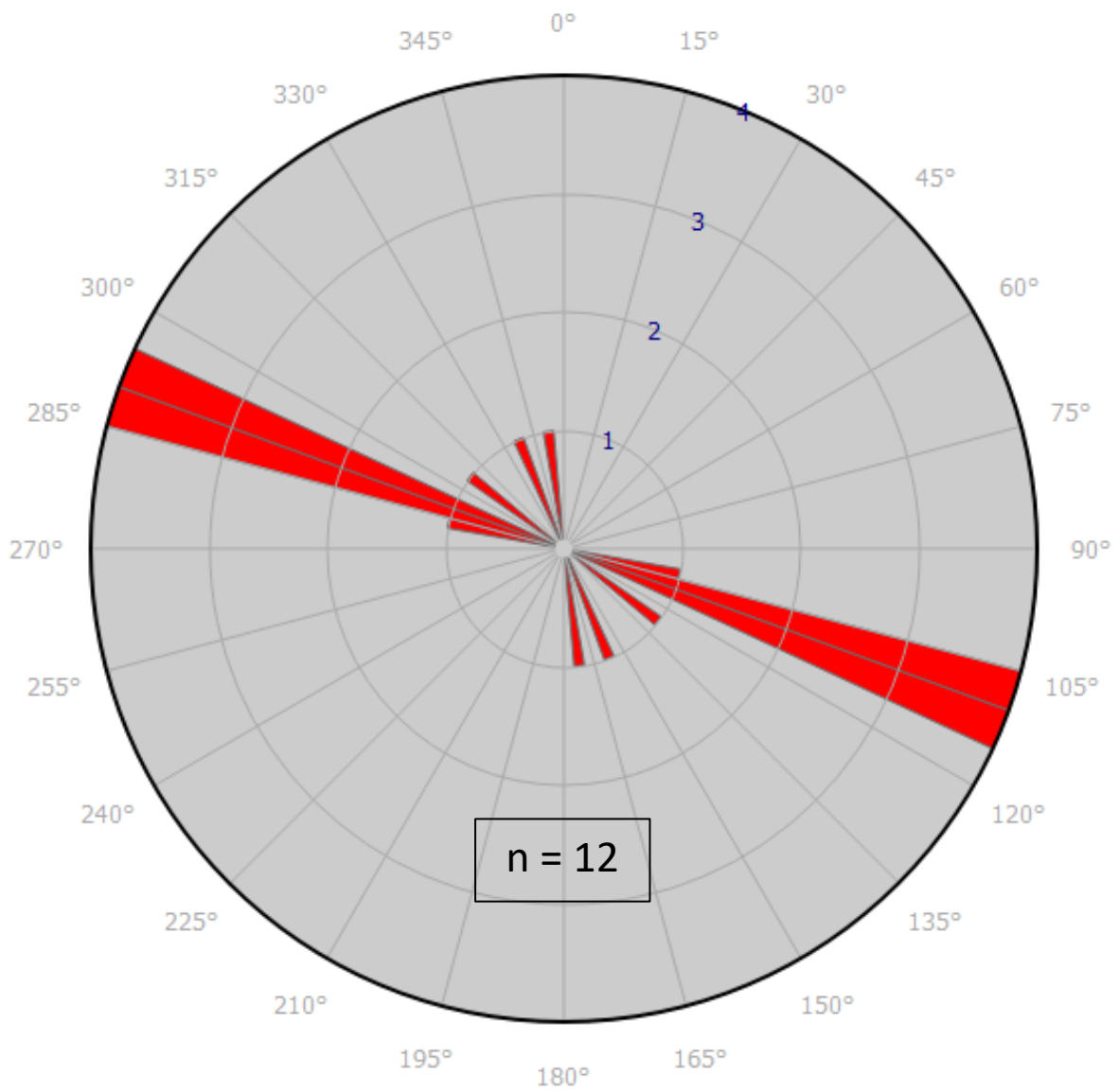
Table A.1. Plagioclase chemistries
*Analyses not used in mineral chemistry calculations

BB6-6 Plag	Wt% Oxide											
Formula	Cl	Na2O	K2O	MgO	CaO	MnO	FeO	BaO	Al2O3	SiO2	SO2	Total
1 / 1 .	0.01	6.56	0.51	-0.01	8.05	-0.02	0.08	-0.20	27.07	59.40	-0.01	101.67
1 / 2 .	0.00	6.63	0.56	0.01	8.11	-0.06	0.10	-0.12	27.30	58.32	-0.01	101.02
1 / 3 .	0.00	6.49	0.47	0.01	8.06	-0.04	0.05	-0.20	26.56	58.43	-0.01	100.08
1 / 4 .	0.00	6.32	0.51	0.00	8.21	-0.03	0.08	-0.20	26.62	58.75	-0.01	100.49
1 / 5 .	-0.01	6.72	0.54	0.00	8.05	-0.06	0.11	-0.14	27.63	58.93	-0.01	101.98
1 / 6 .	0.00	6.49	0.53	0.01	8.17	-0.03	0.08	0.08	27.76	59.28	0.01	102.40
1 / 7 .	-0.01	6.56	0.54	0.00	8.00	-0.05	0.11	-0.34	27.98	59.03	-0.03	102.23
1 / 8 .	0.00	6.60	0.51	0.00	8.06	-0.02	0.06	-0.29	27.86	58.72	-0.01	101.81
1 / 9 .	0.00	6.47	0.54	0.00	8.06	-0.04	0.06	-0.11	26.91	59.04	-0.01	101.08
1 / 10 .	0.00	6.44	0.58	-0.01	8.10	-0.04	0.12	-0.20	26.69	58.71	-0.01	100.63
Average	0.00	6.53	0.53	0.00	8.09	-0.04	0.08	-0.17	27.24	58.86	-0.01	101.34
2 / 1 .	0.01	6.26	0.42	0.00	8.30	-0.04	0.07	0.05	26.79	58.74	-0.01	100.63
2 / 2 .	0.01	6.40	0.44	-0.01	8.15	-0.04	0.10	-0.23	26.22	57.65	-0.01	98.97
2 / 3 .	0.00	6.66	0.43	0.00	8.14	-0.02	0.08	-0.09	26.27	57.77	-0.02	99.35
2 / 4 .	0.01	6.59	0.44	0.00	8.18	-0.01	0.09	-0.23	26.54	58.61	-0.01	100.47
2 / 5 .	0.00	6.43	0.47	-0.01	8.13	-0.04	0.08	-0.18	26.31	57.56	-0.01	98.98
2 / 6 .	0.00	6.53	0.49	0.00	8.10	-0.01	0.07	-0.15	28.11	58.30	0.00	101.59
2 / 7 .	0.00	6.42	0.46	0.00	8.30	-0.02	0.09	-0.14	27.04	57.84	-0.01	100.14
2 / 8 .	-0.01	6.57	0.45	-0.01	8.17	-0.02	0.09	-0.21	26.44	57.64	0.00	99.36
2 / 9 .	-0.01	6.54	0.45	0.00	8.24	0.00	0.10	-0.11	27.02	57.34	0.00	99.68
2 / 10 .	0.02	6.98	0.45	0.00	7.63	-0.03	0.10	-0.29	26.56	58.40	0.00	100.15
Average	0.00	6.54	0.45	0.00	8.13	-0.02	0.09	-0.16	26.73	57.99	-0.01	99.93

Table A.1.   Plagioclase chemistries
*Analyses not used in mineral chemistry calculations

BB6-6 Plag	Wt% Oxide											
Formula	Cl	Na2O	K2O	MgO	CaO	MnO	FeO	BaO	Al2O3	SiO2	SO2	Total
3 / 1 .	0.00	6.82	0.42	0.01	8.21	0.00	0.07	-0.29	27.36	57.76	0.00	100.64
3 / 2 .	0.00	6.70	0.42	-0.01	8.06	-0.03	0.10	-0.18	27.48	59.01	-0.02	101.77
3 / 3 .	0.00	6.50	0.41	0.00	8.05	-0.02	0.11	0.22	26.86	58.92	-0.01	101.08
3 / 4 .	0.00	6.62	0.43	0.00	8.07	-0.04	0.10	0.02	27.05	58.47	0.00	100.77
3 / 5 .	0.00	6.55	0.43	0.00	8.02	-0.02	0.09	0.22	26.47	58.06	-0.01	99.83
3 / 6 .	-0.01	6.75	0.46	0.00	8.13	-0.03	0.10	-0.17	26.37	57.69	0.00	99.49
3 / 7 .	0.00	6.76	0.45	-0.01	7.93	-0.02	0.09	-0.20	26.59	58.11	0.00	99.94
3 / 8 .	0.00	6.70	0.45	0.01	8.00	-0.05	0.07	-0.20	26.79	58.16	-0.01	100.17
3 / 9 .	0.01	6.47	0.43	0.00	8.01	-0.03	0.09	-0.09	26.36	58.25	-0.01	99.62
3 / 10 .	0.01	6.75	0.49	0.00	8.12	-0.01	0.11	0.28	26.37	58.79	0.00	100.92
Average	0.00	6.66	0.44	0.00	8.06	-0.03	0.09	-0.04	26.77	58.32	-0.01	100.42
4 / 1 .	0.00	6.41	0.43	0.00	7.99	-0.04	0.09	-0.12	26.63	57.62	-0.03	99.17
4 / 2 .	0.00	6.48	0.50	0.00	8.20	-0.05	0.10	-0.24	26.03	58.08	0.00	99.40
4 / 3 .	0.00	6.56	0.46	0.00	8.04	-0.04	0.09	-0.06	26.54	57.65	0.00	99.34
4 / 4 .	0.00	6.46	0.51	0.00	8.22	-0.02	0.11	0.02	26.17	57.86	-0.02	99.35
4 / 5 .	0.01	6.46	0.54	0.00	8.01	0.00	0.10	-0.17	26.32	58.18	0.00	99.63
4 / 6 .	0.01	6.61	0.57	-0.01	7.98	-0.01	0.06	-0.17	25.95	58.65	-0.03	99.83
4 / 7 .	0.00	6.59	0.58	0.00	8.02	0.00	0.05	-0.03	27.08	57.70	0.00	100.02
4 / 8 .	0.00	6.43	0.54	0.00	8.07	-0.02	0.08	-0.18	26.28	58.45	0.00	99.85
4 / 9 .	0.00	6.39	0.59	0.00	7.68	-0.01	0.09	-0.28	26.28	57.71	-0.01	98.74
4 / 10 .	0.01	6.57	0.63	-0.01	7.63	-0.01	0.10	-0.23	26.61	57.88	0.00	99.43
Average	0.00	6.50	0.54	0.00	7.98	-0.02	0.09	-0.15	26.39	57.98	-0.01	99.48

Table A.1.   Plagioclase chemistries
*Analyses not used in mineral chemistry calculations

BB6-6 Plag	Wt% Oxide											
Formula	Cl	Na2O	K2O	MgO	CaO	MnO	FeO	BaO	Al2O3	SiO2	SO2	Total
5 / 1 .	-0.01	6.29	0.53	-0.01	7.94	-0.03	0.11	-0.18	26.02	58.47	0.00	99.37
5 / 2 .	0.00	6.64	0.51	0.00	8.04	-0.02	0.08	-0.14	26.44	58.34	0.01	100.07
5 / 3 .	0.00	6.57	0.49	-0.01	7.78	-0.05	0.10	-0.18	26.65	58.45	-0.01	100.04
5 / 4 .	-0.01	6.53	0.52	0.00	7.84	-0.02	0.11	-0.07	26.19	58.19	0.00	99.37
5 / 5 .	-0.01	6.48	0.47	0.00	7.93	0.00	0.12	-0.26	25.99	58.08	-0.01	99.08
5 / 6 .	0.00	6.78	0.51	0.01	7.97	-0.02	0.11	-0.04	27.34	58.82	-0.02	101.54
5 / 7 .	0.00	6.62	0.45	0.00	7.84	-0.03	0.12	0.02	26.28	58.76	-0.01	100.08
5 / 8 .	0.00	6.53	0.44	0.00	7.92	-0.01	0.12	-0.01	26.09	58.95	-0.02	100.05
5 / 9 .	0.00	6.80	0.41	0.00	7.87	-0.03	0.13	-0.24	26.38	58.88	0.00	100.47
5 / 10 .	0.00	6.68	0.45	-0.01	8.00	-0.04	0.09	-0.12	26.36	58.95	-0.01	100.53
Average	0.00	6.59	0.48	0.00	7.91	-0.03	0.11	-0.12	26.38	58.59	-0.01	100.06
6 / 1 .	0.00	6.66	0.41	-0.01	8.04	-0.02	0.10	0.25	26.20	58.94	-0.01	100.60
6 / 2 .	-0.01	6.73	0.43	0.01	7.94	-0.03	0.06	-0.21	26.71	58.20	0.00	100.08
6 / 3 .	0.00	6.63	0.47	0.01	7.92	-0.03	0.11	-0.18	27.42	58.78	-0.01	101.34
6 / 4 .	-0.01	6.55	0.48	-0.01	8.02	-0.03	0.12	-0.26	26.42	58.76	-0.01	100.35
6 / 5 .	0.00	6.49	0.43	-0.01	7.94	-0.05	0.10	0.00	26.37	58.92	0.00	100.26
6 / 6 .	0.00	6.79	0.49	0.00	7.96	-0.03	0.08	-0.18	26.07	57.90	-0.01	99.29
6 / 7 .	0.00	6.49	0.46	-0.01	7.79	-0.04	0.09	0.11	26.06	59.28	0.00	100.28
6 / 8 .	0.01	6.67	0.50	0.00	7.49	-0.03	0.08	-0.26	25.65	59.02	0.00	99.42
6 / 9 .	0.00	6.57	0.52	0.00	7.98	0.00	0.08	-0.28	26.17	58.92	-0.02	100.24
6 / 10 .	-0.01	6.79	0.51	0.00	7.99	-0.02	0.08	-0.15	26.40	58.31	0.01	100.09
Average	0.00	6.64	0.47	0.00	7.91	-0.03	0.09	-0.12	26.35	58.70	0.00	100.20

Table A.1. Plagioclase chemistries
*Analyses not used in mineral chemistry calculations

BB6-6 Plag	Wt% Oxide											
Formula	Cl	Na2O	K2O	MgO	CaO	MnO	FeO	BaO	Al2O3	SiO2	SO2	Total
7 / 1 .	-0.01	6.41	0.48	0.00	8.51	-0.03	0.10	0.02	26.68	56.65	0.01	98.86
7 / 2 .	0.01	6.13	0.45	0.00	8.65	-0.01	0.10	-0.20	26.66	57.74	0.00	99.75
7 / 3 .	-0.01	6.19	0.47	0.00	8.54	0.00	0.10	-0.18	27.03	58.03	0.00	100.37
7 / 4 .	0.00	6.41	0.44	0.00	8.68	-0.01	0.09	-0.17	26.83	58.20	-0.01	100.65
7 / 5 .	0.00	6.03	0.43	0.00	8.62	0.00	0.11	-0.17	26.71	57.44	0.00	99.34
7 / 6 .	0.00	6.33	0.45	0.00	8.68	-0.01	0.10	0.07	26.93	57.57	-0.02	100.13
7 / 7 .	0.00	6.35	0.45	0.00	8.50	-0.02	0.08	-0.06	26.95	56.89	-0.01	99.21
7 / 8 .	0.00	6.07	0.41	0.01	8.56	0.00	0.12	-0.37	26.77	57.42	0.01	99.35
7 / 9 .	0.00	6.25	0.45	0.00	8.47	0.02	0.10	-0.29	26.76	57.95	0.00	100.00
7 / 10 .	0.00	6.18	0.43	-0.01	8.51	-0.02	0.13	-0.14	27.29	57.69	0.01	100.24
Average	0.00	6.23	0.45	0.00	8.57	-0.01	0.10	-0.15	26.86	57.56	0.00	99.79
8 / 1 .	0.00	6.50	0.42	-0.01	8.63	-0.03	0.08	-0.26	27.32	57.86	-0.01	100.81
8 / 2 .	-0.01	6.15	0.40	0.00	8.63	-0.03	0.08	-0.10	26.89	57.72	-0.01	99.87
8 / 3 .	-0.01	6.19	0.42	0.00	8.68	-0.01	0.08	0.02	27.14	58.21	-0.02	100.73
8 / 4 .	0.00	6.32	0.45	0.01	8.73	-0.02	0.09	-0.23	26.92	57.84	0.00	100.36
8 / 5 .	0.00	6.24	0.42	0.00	8.69	-0.03	0.07	-0.15	28.08	57.95	-0.01	101.46
8 / 6 .	0.00	6.33	0.45	0.00	8.54	-0.03	0.06	0.38	26.84	57.30	-0.02	99.91
8 / 7 .	-0.01	6.08	0.50	0.00	8.78	-0.01	0.04	-0.24	28.00	56.68	-0.02	100.08
8 / 8 .	0.00	6.21	0.48	0.00	8.74	-0.02	0.09	0.11	27.07	57.36	-0.01	100.07
8 / 9 .	0.00	6.12	0.45	-0.01	8.80	-0.04	0.10	-0.18	28.08	58.00	0.00	101.55
8 / 10 .	0.00	6.10	0.45	0.01	8.71	-0.04	0.09	-0.12	26.75	57.51	-0.01	99.62
Average	0.00	6.22	0.45	0.00	8.69	-0.03	0.08	-0.08	27.31	57.64	-0.01	100.45

Table A.1.   Plagioclase chemistries
*Analyses not used in mineral chemistry calculations

BB6-6 Plag	Wt% Oxide											
Formula	Cl	Na2O	K2O	MgO	CaO	MnO	FeO	BaO	Al2O3	SiO2	SO2	Total
9 / 1 .	0.00	6.36	0.50	0.00	8.20	-0.01	0.10	-0.15	27.10	57.61	-0.01	99.86
9 / 2 .	0.00	6.17	0.47	0.00	8.23	-0.02	0.13	-0.23	27.02	58.69	0.00	100.71
9 / 3 .	0.01	6.27	0.46	0.00	8.14	-0.01	0.10	0.03	27.18	57.18	-0.01	99.38
9 / 4 .	0.00	6.50	0.47	0.01	8.24	-0.04	0.09	-0.21	26.31	58.66	-0.02	100.28
9 / 5 .	-0.01	6.19	0.46	-0.01	8.34	-0.03	0.07	0.07	26.59	58.11	0.00	99.83
9 / 6 .	0.01	6.43	0.48	0.00	8.32	-0.02	0.05	-0.06	26.52	58.21	0.01	100.03
9 / 7 .	0.00	6.28	0.51	0.00	8.26	-0.04	0.04	-0.03	27.12	58.04	-0.01	100.25
9 / 8 .	0.00	6.47	0.49	0.00	8.39	-0.03	0.10	-0.10	26.57	58.12	0.00	100.13
9 / 9 .	0.01	6.34	0.49	-0.01	8.19	-0.03	0.08	-0.32	27.98	58.30	0.01	101.39
9 / 10 .	0.00	6.32	0.47	-0.01	8.35	-0.05	0.09	-0.20	26.65	58.07	-0.02	99.95
Average	0.00	6.33	0.48	0.00	8.27	-0.03	0.08	-0.12	26.90	58.10	-0.01	100.18
10 / 1 .	0.00	6.55	0.46	0.00	7.97	-0.01	0.11	-0.11	27.37	57.98	-0.01	100.45
10 / 2 .	0.01	6.67	0.47	-0.01	7.95	0.00	0.09	-0.10	26.49	58.60	-0.02	100.28
10 / 3 .	-0.01	6.74	0.50	0.00	7.99	-0.04	0.08	-0.18	26.29	58.46	-0.01	100.06
10 / 4 .	0.00	6.67	0.48	-0.01	7.96	-0.04	0.10	-0.29	26.65	58.74	-0.02	100.60
10 / 5 .	-0.01	6.39	0.49	0.00	8.08	-0.04	0.09	0.16	26.74	59.05	-0.01	100.99
10 / 6 .	-0.01	6.70	0.52	0.00	7.85	-0.03	0.11	-0.01	26.17	59.16	-0.01	100.51
10 / 7 .	0.01	6.59	0.49	0.00	7.85	-0.01	0.10	-0.01	26.64	58.62	-0.01	100.29
10 / 8 .	0.00	6.78	0.49	-0.01	8.04	0.00	0.08	-0.31	26.31	59.24	0.00	100.94
10 / 9 .	0.00	6.54	0.48	0.00	7.84	-0.05	0.08	-0.14	26.58	59.23	-0.02	100.73
10 / 10 .	-0.01	6.56	0.49	0.00	8.03	-0.02	0.07	0.04	26.69	59.29	0.00	101.16
Average	0.00	6.62	0.49	0.00	7.96	-0.03	0.09	-0.10	26.59	58.84	-0.01	100.60

Table A.1. Plagioclase chemistries
*Analyses not used in mineral chemistry calculations

BB8-2 Plag	Wt% Oxide											
Formula	Cl	Na2O	K2O	MgO	CaO	MnO	FeO	BaO	Al2O3	SiO2	SO2	Total
1 / 1 .	-0.01	5.29	0.35	-0.12	10.18	-0.02	0.10	-0.02	28.50	56.20	-0.01	100.63
1 / 2 .	-0.01	5.29	0.40	-0.12	10.51	0.00	0.09	0.06	28.23	55.56	-0.02	100.13
1 / 3 .	-0.01	5.13	0.40	-0.12	10.40	-0.03	0.09	0.07	28.40	55.45	-0.02	99.95
1 / 4 .	-0.01	5.37	0.36	-0.12	10.44	-0.02	0.14	0.07	28.48	55.63	-0.03	100.49
1 / 5 .	0.00	5.23	0.35	-0.11	10.29	-0.02	0.16	0.13	30.10	55.67	-0.03	101.94
1 / 6 .	0.01	5.17	0.32	-0.11	10.12	-0.01	0.08	0.15	28.55	55.28	-0.01	99.68
1 / 7 .	0.00	5.18	0.39	-0.12	10.35	0.00	0.08	0.12	28.68	55.33	-0.03	100.13
1 / 8 .	-0.01	5.22	0.39	-0.11	10.15	0.00	0.52	0.15	27.81	55.08	-0.04	99.31
1 / 9 .	0.00	5.39	0.40	-0.11	10.53	-0.01	0.12	0.09	28.12	56.06	-0.03	100.70
1 / 10 .	0.00	5.34	0.38	-0.12	10.19	-0.03	0.10	0.26	28.43	55.68	-0.03	100.38
Average	0.00	5.26	0.37	-0.12	10.32	-0.01	0.15	0.11	28.53	55.59	-0.02	100.34
2 / 1 .	-0.01	5.64	0.35	-0.11	9.91	-0.03	0.08	0.07	27.91	55.71	-0.03	99.67
2 / 2 .	0.00	5.65	0.38	-0.11	9.96	-0.03	0.10	0.07	28.15	55.43	-0.03	99.75
2 / 3 .	-0.02	5.53	0.36	-0.11	9.91	-0.05	0.07	0.04	27.87	55.71	-0.04	99.49
2 / 4 .	0.01	5.42	0.39	-0.12	9.93	-0.02	0.08	0.07	27.56	56.04	-0.01	99.51
2 / 5 .	0.00	5.53	0.35	-0.12	9.80	-0.02	0.76	0.18	27.36	55.18	-0.03	99.15
2 / 6 .	0.00	5.76	0.37	-0.12	9.89	-0.02	0.14	0.09	28.09	55.11	-0.01	99.45
2 / 7 .	0.00	5.64	0.37	-0.12	10.01	-0.05	0.09	0.07	27.93	56.07	-0.03	100.20
2 / 8 .	-0.01	5.29	0.36	-0.13	9.92	-0.02	0.07	0.26	27.59	55.19	-0.01	98.68
2 / 9 .	-0.01	5.61	0.36	-0.12	9.78	-0.01	0.11	0.20	27.84	56.01	-0.02	99.90
2 / 10 .	0.00	5.55	0.38	-0.11	9.89	-0.02	0.07	0.18	28.22	56.42	-0.02	100.71
Average	0.00	5.56	0.37	-0.12	9.90	-0.03	0.16	0.12	27.85	55.69	-0.02	99.65

Table A.1.   Plagioclase chemistries
*Analyses not used in mineral chemistry calculations

BB8-2 Plag	Wt% Oxide											
Formula	Cl	Na2O	K2O	MgO	CaO	MnO	FeO	BaO	Al2O3	SiO2	SO2	Total
3 / 1 .	-0.01	5.29	0.33	-0.11	10.19	0.00	0.06	0.03	28.33	55.41	-0.04	99.64
3 / 2 .	0.00	5.10	0.34	-0.11	10.34	0.01	0.12	0.06	28.23	54.21	-0.02	98.41
3 / 3 .	0.00	5.09	0.35	-0.11	10.48	-0.01	0.09	0.04	28.33	54.88	-0.03	99.27
3 / 4 .	0.00	5.34	0.36	-0.12	10.47	-0.02	0.08	0.12	28.26	55.80	-0.01	100.43
3 / 5 .	-0.01	5.12	0.36	-0.12	10.43	-0.03	0.06	0.20	28.27	54.99	-0.02	99.44
3 / 6 .	-0.01	5.22	0.35	-0.11	10.38	-0.02	0.08	0.00	28.30	54.63	-0.03	98.96
3 / 7 .	0.00	5.25	0.34	-0.12	10.16	0.00	0.10	0.07	28.14	54.36	-0.03	98.44
3 / 8 .	-0.01	5.12	0.35	-0.12	10.48	-0.01	0.10	-0.11	27.81	54.86	-0.04	98.71
3 / 9 .	0.00	5.24	0.36	-0.12	10.48	0.01	0.04	0.21	28.35	54.15	-0.03	98.84
3 / 10 .	-0.01	5.35	0.34	-0.12	10.33	-0.02	0.10	-0.02	27.87	54.28	-0.03	98.26
Average	0.00	5.21	0.35	-0.12	10.38	-0.01	0.08	0.06	28.19	54.76	-0.03	99.04
4 / 1 .	0.01	5.54	0.38	-0.10	9.48	-0.02	0.21	0.13	27.23	55.58	-0.01	98.56
4 / 2 .	-0.01	5.74	0.35	-0.12	9.47	0.00	0.39	-0.07	27.13	55.36	-0.02	98.45
4 / 3 .	0.00	5.66	0.34	-0.12	9.54	0.00	0.05	0.12	27.62	56.23	-0.01	99.57
4 / 4 .	-0.01	5.63	0.34	-0.11	9.55	-0.03	0.06	0.07	27.19	55.62	-0.01	98.45
4 / 5 .	0.01	5.66	0.33	-0.12	9.53	-0.02	0.08	0.04	27.81	55.60	-0.02	99.04
4 / 6 .	0.00	5.66	0.36	-0.12	9.40	0.01	0.05	-0.01	28.13	56.57	-0.02	100.18
4 / 7 .	-0.01	5.66	0.37	-0.12	9.48	0.00	0.10	0.15	27.87	56.00	-0.01	99.63
4 / 8 .	0.00	5.62	0.33	-0.12	9.42	0.03	0.06	-0.11	27.73	56.39	0.00	99.58
4 / 9 .	-0.01	5.80	0.36	-0.12	9.45	-0.04	0.07	-0.02	27.78	55.79	-0.02	99.25
4 / 10 .	-0.01	5.48	0.34	-0.12	9.39	-0.02	0.06	0.21	27.16	56.26	-0.04	98.92
Average	0.00	5.64	0.35	-0.12	9.47	-0.01	0.11	0.05	27.56	55.94	-0.02	99.16

Table A.1.   Plagioclase chemistries
*Analyses not used in mineral chemistry calculations

BB8-2 Plag	Wt% Oxide											
Formula	Cl	Na2O	K2O	MgO	CaO	MnO	FeO	BaO	Al2O3	SiO2	SO2	Total
5 / 1 .	0.00	6.20	0.36	-0.12	8.78	-0.01	0.07	0.04	26.91	56.37	-0.03	98.73
5 / 2 .	0.00	6.28	0.34	-0.12	8.74	-0.03	0.07	-0.19	27.18	57.62	0.00	100.24
5 / 3 .	0.00	6.16	0.34	-0.13	8.76	-0.01	0.05	0.10	27.06	57.17	0.00	99.64
5 / 4 .	-0.01	6.28	0.36	-0.12	8.87	-0.02	0.07	-0.11	27.42	56.89	-0.01	99.90
5 / 5 .	-0.01	6.09	0.40	-0.12	8.69	-0.04	0.05	0.03	26.86	57.98	-0.04	100.09
5 / 6 .	-0.01	6.15	0.36	-0.12	9.09	-0.02	0.07	0.10	27.12	56.92	-0.04	99.82
5 / 7 .	-0.02	5.97	0.36	-0.12	8.72	-0.04	0.07	-0.01	27.08	56.44	-0.03	98.64
5 / 8 .	0.00	6.22	0.37	-0.13	8.90	-0.01	0.04	-0.07	26.99	57.12	-0.02	99.65
5 / 9 .	0.00	6.07	0.39	-0.12	8.86	0.01	0.05	-0.11	26.73	57.13	-0.02	99.25
5 / 10 .	-0.01	5.90	0.40	-0.12	8.97	-0.01	0.06	0.26	26.94	57.52	-0.01	100.04
Average	0.00	6.13	0.37	-0.12	8.84	-0.02	0.06	0.00	27.03	57.12	-0.02	99.60
BB12-8 Plag	Wt% Oxide											
Formula	Cl	Na2O	K2O	MgO	CaO	MnO	FeO	BaO	Al2O3	SiO2	SO2	Total
1 / 1 .	-0.01	5.06	0.35	0.01	10.56	0.00	0.08	-0.26	27.43	57.01	-0.01	100.51
1 / 2 .	0.00	5.09	0.35	0.00	10.48	-0.03	0.09	-0.25	26.96	55.29	-0.02	98.26
1 / 3 .	0.00	5.17	0.34	0.01	10.39	-0.01	0.12	-0.26	26.81	56.72	-0.02	99.55
1 / 4 .	0.00	5.08	0.34	0.00	10.47	0.01	0.06	-0.13	27.58	56.14	-0.01	99.69
1 / 5 .	0.00	5.12	0.34	0.01	10.59	-0.01	0.11	-0.08	27.57	55.85	-0.02	99.59
1 / 6 .	0.00	5.06	0.32	0.00	10.36	0.02	0.07	-0.46	27.18	55.68	-0.02	98.68
1 / 7 .	-0.01	5.21	0.30	0.00	10.49	-0.02	0.07	-0.17	27.50	55.59	-0.03	99.17
1 / 8 .	-0.01	5.13	0.32	0.01	10.46	0.01	0.08	-0.01	27.19	55.57	-0.02	98.77
1 / 9 .	0.00	5.11	0.35	0.01	10.38	0.00	0.06	-0.44	27.57	56.07	-0.02	99.55
1 / 10 .	-0.01	5.09	0.30	0.00	10.39	-0.01	0.04	-0.41	27.34	56.05	-0.02	99.20
Average	0.00	5.11	0.33	0.01	10.46	-0.01	0.08	-0.25	27.31	56.00	-0.02	99.30

Table A.1.   Plagioclase chemistries
*Analyses not used in mineral chemistry calculations

BB12-9 Plag	Wt% Oxide											
Formula	Cl	Na2O	K2O	MgO	CaO	MnO	FeO	BaO	Al2O3	SiO2	SO2	Total
1 / 1 .	0.00	5.12	0.36	0.00	10.45	0.03	0.10	0.18	28.30	55.51	0.01	100.04
1 / 2 .	-0.01	5.33	0.34	0.02	10.18	0.03	1.25	0.45	27.74	55.02	-0.01	100.33
1 / 3 .	0.00	5.39	0.37	0.01	10.45	0.01	0.10	0.14	28.20	55.38	-0.01	100.04
1 / 4 .	0.00	5.24	0.30	0.00	10.41	0.01	0.10	0.27	28.05	55.57	-0.01	99.95
1 / 5 .	-0.01	5.30	0.35	0.00	10.30	0.05	0.12	0.29	28.63	55.10	0.00	100.13
1 / 6 .	0.00	5.40	0.35	0.01	10.41	0.01	0.07	0.24	28.70	54.94	-0.01	100.11
1 / 7 .	0.01	5.28	0.36	0.00	10.52	0.03	0.08	0.23	28.57	55.51	-0.02	100.57
1 / 8 .	-0.01	5.24	0.30	0.00	10.42	0.03	0.07	0.15	28.34	55.35	-0.02	99.89
1 / 9 .	0.00	5.23	0.21	0.01	10.41	0.01	0.12	0.24	28.41	54.84	-0.01	99.47
1 / 10 .	0.01	5.31	0.26	0.00	10.31	0.00	0.12	0.29	28.35	55.53	0.00	100.18
1 / 11 .	0.01	5.58	0.19	0.07	10.20	0.00	0.39	0.23	28.42	55.18	-0.01	100.25
1 / 12 .	0.00	5.19	0.17	0.00	10.05	0.02	0.10	0.12	28.83	56.47	0.01	100.97
1 / 13 .	-0.01	5.46	0.27	0.01	10.17	0.04	0.12	0.11	28.49	55.76	0.01	100.44
1 / 14 .	0.00	5.33	0.28	0.00	10.18	0.02	0.12	0.29	28.01	55.17	-0.01	99.39
1 / 15 .	0.00	5.48	0.29	0.00	10.38	0.02	0.12	0.29	28.26	54.87	-0.01	99.69
1 / 16 .	-0.01	5.23	0.28	0.00	10.36	0.02	0.11	0.26	28.60	56.19	0.00	101.05
1 / 17 .	0.00	5.41	0.30	0.00	10.21	0.03	0.14	0.19	28.97	55.87	-0.01	101.10
1 / 18 .	0.00	5.34	0.27	0.01	10.21	0.04	0.13	0.00	28.27	55.86	-0.01	100.13
1 / 19 .	-0.01	5.41	0.32	0.01	10.20	0.02	0.11	0.08	28.39	56.00	-0.01	100.53
1 / 20 .	0.00	5.69	0.27	0.00	10.16	0.01	0.12	0.24	28.34	55.34	-0.01	100.18
1 / 21 .	0.00	5.31	0.25	0.00	10.14	0.03	0.14	0.34	28.41	55.53	-0.01	100.13
1 / 22 .	0.00	5.27	0.26	0.17	9.86	0.03	0.37	0.15	27.89	55.77	0.01	99.79
Average	0.00	5.34	0.29	0.01	10.27	0.02	0.19	0.22	28.37	55.49	-0.01	100.20

Table A.1. Plagioclase chemistries
*Analyses not used in mineral chemistry calculations

BB12-9 Plag	Wt% Oxide											
Formula	Cl	Na2O	K2O	MgO	CaO	MnO	FeO	BaO	Al2O3	SiO2	SO2	Total
2 / 1 .	-0.01	5.43	0.26	0.00	10.01	0.03	0.06	0.32	27.96	55.28	-0.02	99.97
2 / 2 .	-0.01	5.52	0.31	0.00	10.24	0.02	0.10	0.29	28.15	55.25	-0.01	99.98
2 / 3 .	-0.01	5.34	0.32	0.01	10.18	0.03	0.08	0.24	27.98	55.55	0.00	99.99
2 / 4 .	0.00	5.28	0.27	0.00	10.34	0.04	0.11	0.25	28.31	55.56	0.00	100.17
2 / 5 .	-0.01	5.32	0.32	0.01	10.17	0.00	0.09	-0.06	27.97	55.06	0.00	99.93
2 / 6 .	0.00	5.52	0.31	0.00	10.27	0.04	0.11	0.31	28.14	55.69	-0.02	100.39
2 / 7 .	0.00	5.37	0.31	0.01	10.24	0.00	0.08	0.24	28.29	56.06	0.00	100.59
2 / 8 .	0.00	5.25	0.31	0.05	10.18	0.02	0.12	0.20	28.34	55.61	0.01	100.08
2 / 9 . *	0.01	4.68	0.21	1.51	9.02	0.06	4.75	0.51	25.31	52.42	0.01	100.00
2 / 10 .	0.00	5.23	0.31	0.00	10.22	0.04	0.07	0.30	28.11	55.35	-0.01	99.99
2 / 11 .	-0.01	5.23	0.31	0.01	10.22	0.01	0.12	0.20	28.14	55.02	-0.01	99.99
2 / 12 .	-0.01	5.29	0.32	0.01	10.14	0.01	0.13	0.09	28.01	55.07	-0.01	99.98
2 / 13 .	0.00	5.52	0.30	0.01	10.16	0.04	0.14	0.20	27.98	55.36	-0.01	99.99
2 / 14 .	0.00	5.45	0.30	0.00	10.05	0.05	0.10	0.20	27.99	55.72	-0.01	99.99
2 / 15 .	-0.01	5.27	0.33	0.00	10.18	0.02	0.11	0.20	28.25	55.98	-0.02	100.34
2 / 16 .	-0.01	5.39	0.33	0.00	10.04	0.02	0.11	0.29	28.14	55.67	-0.03	99.99
2 / 17 .	0.00	5.26	0.36	0.00	10.17	0.01	0.12	0.41	28.24	56.23	-0.01	100.80
2 / 18 .	-0.01	5.30	0.34	0.01	10.09	0.04	0.08	0.38	28.37	55.80	0.00	100.40
2 / 19 .	-0.01	5.35	0.31	0.00	10.09	0.03	0.11	0.29	28.10	55.58	0.00	99.99
2 / 20 .	0.00	5.37	0.51	0.00	9.95	0.04	0.11	0.23	28.47	56.19	-0.01	100.87
2 / 21 . *	-0.01	4.64	0.46	0.01	8.18	0.00	0.12	0.18	29.01	55.87	0.00	99.99
2 / 22 .	0.00	5.40	0.31	0.00	10.15	0.03	0.14	-0.03	28.04	54.88	0.01	99.97
2 / 23 .	0.01	5.40	0.29	0.01	10.24	0.05	0.12	0.24	28.36	55.98	0.01	100.71
Average	0.00	5.30	0.32	0.07	10.02	0.03	0.31	0.24	28.07	55.44	-0.01	100.18

Table A.1. Plagioclase chemistries
*Analyses not used in mineral chemistry calculations

BB12-9 Plag	Wt% Oxide											
Formula	Cl	Na2O	K2O	MgO	CaO	MnO	FeO	BaO	Al2O3	SiO2	SO2	Total
3 / 1 .	0.00	5.47	0.34	0.00	10.18	0.02	0.12	0.39	28.54	55.90	-0.02	100.97
3 / 2 .	-0.02	5.51	0.35	0.01	10.23	0.02	0.13	0.20	27.86	56.04	0.00	100.35
3 / 3 .	-0.01	5.54	0.34	0.00	10.22	0.04	0.11	0.24	27.51	54.96	-0.02	99.98
3 / 4 .	0.00	5.42	0.37	0.01	10.23	0.03	0.10	0.38	27.77	56.20	-0.02	100.51
3 / 5 .	-0.01	5.69	0.30	0.00	10.21	0.03	0.13	0.36	27.54	55.82	-0.02	100.08
3 / 6 .	0.00	5.31	0.35	0.01	10.25	0.01	0.13	-0.03	28.86	55.89	-0.01	100.81
3 / 7 .	-0.01	5.36	0.32	0.00	10.28	0.04	0.09	0.19	27.75	54.91	0.00	99.99
3 / 8 .	0.00	5.33	0.31	0.01	10.40	0.01	0.07	0.29	27.76	55.13	-0.01	99.99
3 / 9 .	0.00	5.80	0.31	0.02	10.36	0.04	0.11	0.38	27.67	54.00	0.00	100.00
3 / 10 .	-0.01	5.12	0.31	0.01	10.53	0.04	0.13	0.21	27.86	55.14	-0.02	99.97
3 / 11 .	0.01	5.50	0.25	0.01	10.32	0.05	0.12	0.25	28.15	55.23	0.00	100.00
3 / 12 .	0.00	5.35	0.29	0.01	10.32	-0.01	0.10	0.48	28.41	55.71	-0.02	100.67
3 / 13 .	-0.01	5.34	0.31	-0.01	10.28	0.01	0.11	0.29	28.24	55.20	0.00	99.98
3 / 14 .	0.00	5.48	0.34	0.01	10.27	0.03	0.10	-0.01	27.67	55.31	-0.01	99.98
3 / 15 .	-0.01	5.32	0.33	0.01	10.20	0.04	0.14	0.20	28.60	56.04	0.00	100.88
3 / 16 .	-0.01	5.40	0.32	0.01	10.36	0.02	0.13	-0.03	28.09	56.38	-0.03	100.71
3 / 17 .	0.00	5.33	0.30	0.06	10.39	0.05	0.17	0.43	28.15	55.04	-0.01	99.99
3 / 18 .	0.00	5.28	0.34	0.00	10.28	0.05	0.12	0.15	27.92	56.14	0.00	100.29
3 / 19 .	0.00	5.37	0.32	0.00	10.44	0.00	0.12	0.32	28.21	55.73	-0.01	100.52
3 / 20 .	-0.01	5.43	0.34	0.01	10.35	0.02	0.14	0.29	28.51	55.33	0.00	100.40
3 / 21 .	0.00	5.18	0.33	0.01	10.38	0.02	0.11	0.14	28.86	55.97	0.00	101.01
3 / 22 .	0.00	5.35	0.33	0.01	10.45	0.04	0.13	0.09	28.55	54.96	-0.01	99.99
3 / 23 .	0.00	5.48	0.31	0.00	10.33	0.02	0.10	0.18	28.75	55.85	-0.03	101.03
Average	0.00	5.41	0.32	0.01	10.32	0.03	0.12	0.24	28.14	55.52	-0.01	100.35

Table A.1. Plagioclase chemistries
*Analyses not used in mineral chemistry calculations

BB12-9 Plag	Wt% Oxide											
Formula	Cl	Na2O	K2O	MgO	CaO	MnO	FeO	BaO	Al2O3	SiO2	SO2	Total
4 / 1 .	0.00	5.75	0.29	0.01	10.17	-0.02	0.14	0.45	28.00	56.30	0.00	101.11
4 / 2 .	0.01	5.61	0.30	0.01	10.09	0.02	0.07	0.10	27.95	55.65	-0.01	99.99
4 / 3 .	-0.01	5.65	0.31	0.00	10.12	-0.01	0.12	0.36	28.62	56.13	-0.02	101.31
4 / 4 . *	0.00	5.29	0.26	0.82	9.42	0.05	1.31	0.44	28.19	54.85	0.01	100.65
4 / 5 . *	0.01	4.52	0.19	3.14	8.39	0.03	4.74	0.23	25.50	50.54	0.00	100.00
4 / 6 .	0.00	5.39	0.30	0.00	10.03	0.02	0.11	0.11	28.44	55.56	0.00	100.00
4 / 7 .	-0.01	5.13	0.31	0.01	9.91	0.05	0.20	0.06	27.83	56.55	-0.01	100.05
4 / 8 .	0.01	5.65	0.38	0.00	10.01	0.00	0.13	0.44	27.86	56.09	-0.01	100.58
4 / 9 .	-0.01	5.73	0.35	0.00	10.03	0.01	0.11	0.50	28.06	56.12	-0.01	100.91
4 / 10 .	0.00	5.73	0.34	0.01	9.99	0.03	0.11	0.22	27.88	56.09	-0.02	100.39
4 / 11 .	0.04	5.50	0.35	0.02	10.06	0.03	0.10	0.35	27.78	56.31	0.01	100.54
4 / 12 .	0.08	5.54	0.34	0.02	10.27	0.03	0.10	0.25	28.07	56.40	0.01	101.09
4 / 13 .	0.03	5.71	0.33	0.02	10.20	0.01	0.17	0.34	28.02	55.77	0.00	100.59
4 / 14 .	0.01	5.72	0.35	0.01	10.18	0.02	0.09	0.11	27.84	55.90	0.01	100.24
4 / 15 .	0.02	5.56	0.38	0.02	10.18	0.02	0.09	0.35	29.55	55.54	0.00	101.71
4 / 16 .	0.00	5.58	0.36	0.00	10.23	0.05	0.11	0.23	27.51	55.82	-0.02	99.98
4 / 17 .	0.00	5.59	0.37	0.01	10.02	0.02	0.14	0.58	29.02	55.96	0.00	101.70
4 / 18 .	0.00	5.68	0.39	0.00	10.24	0.02	0.08	0.26	27.66	55.48	-0.01	99.99
4 / 19 .	0.00	5.61	0.33	0.00	10.16	0.04	0.13	0.19	27.88	55.83	0.00	100.17
4 / 20 .	0.00	5.76	0.41	0.00	10.25	0.02	0.12	0.36	27.90	56.13	-0.02	100.96
Average	0.01	5.54	0.33	0.21	10.00	0.02	0.41	0.30	27.98	55.65	-0.01	100.60

Table A.1.   Plagioclase chemistries
*Analyses not used in mineral chemistry calculations

BB12-9 Plag	Wt% Oxide											
Formula	Cl	Na2O	K2O	MgO	CaO	MnO	FeO	BaO	Al2O3	SiO2	SO2	Total
5 / 1 . *	0.01	5.05	0.40	0.57	9.50	0.00	2.04	-0.17	31.22	55.74	-0.01	104.54
5 / 2 . *	0.00	5.22	0.36	0.24	9.96	0.00	0.86	-0.37	28.31	56.41	-0.02	101.37
5 / 3 .	-0.01	5.31	0.38	0.01	10.09	0.01	0.09	-0.07	28.86	57.71	-0.02	102.47
5 / 4 .	0.00	5.38	0.40	0.01	10.04	-0.01	0.04	-0.07	29.58	57.99	-0.02	103.44
5 / 5 .	-0.01	5.29	0.38	0.01	10.13	-0.02	0.08	-0.34	29.40	56.68	-0.02	101.97
5 / 6 .	0.01	5.35	0.40	0.01	10.03	0.01	0.09	-0.19	29.45	57.45	-0.02	102.81
5 / 7 .	0.00	5.30	0.39	0.01	10.12	0.02	0.09	-0.43	29.59	57.77	-0.04	103.29
5 / 8 .	-0.01	5.42	0.36	0.00	10.11	0.02	0.07	-0.40	28.97	57.75	-0.03	102.71
5 / 9 .	0.00	5.34	0.41	0.00	10.05	0.01	0.06	-0.25	29.11	57.57	-0.01	102.56
5 / 10 .	0.01	5.36	0.38	0.01	9.88	-0.02	0.05	-0.24	28.81	57.23	-0.03	101.74
Average	0.00	5.35	0.38	0.01	10.06	0.00	0.07	-0.25	29.22	57.52	-0.02	102.62

Table A.2.   Scapolite chemistries
CO2 calculated by difference. *Analyses not used in mineral chemistry calculations

BB6-6 Scap Formula	Wt% Oxide Cl	Na2O	K2O	MgO	CaO	MnO	FeO	BaO	Al2O3	CO2	SiO2	SO2	Total
1 / 1 .	2.90	6.13	2.04	-0.12	10.22	0.01	0.09	-0.21	23.97	1.73	53.21	0.01	100.00
1 / 2 . *	0.05	0.34	0.11	-0.06	0.78	0.15	59.22	0.59	1.47		4.38	76.54	143.55
1 / 3 .	2.77	6.31	2.04	-0.11	10.68	0.00	0.09	0.32	24.14	0.78	52.95	0.03	100.00
1 / 4 .	2.76	5.97	2.06	-0.12	10.60	0.03	0.04	0.07	25.15	0.66	52.74	0.02	100.00
1 / 5 .	2.87	6.33	2.05	-0.11	10.44	0.00	0.03	-0.05	24.26	1.26	52.92	0.00	100.00
1 / 6 .	2.97	6.22	2.06	-0.12	10.24	0.02	0.07	-0.04	24.42	1.26	52.87	0.01	100.00
1 / 7 .	2.93	6.21	2.00	-0.12	10.27	-0.01	0.08	0.31	24.72	0.17	53.41	0.03	100.00
1 / 8 . *	0.01	6.59	0.39	-0.11	8.78	0.00	0.05	-0.32	27.74		57.11	-0.03	100.21
1 / 9 . *	-0.01	6.36	0.43	-0.13	8.58	-0.03	0.08	0.09	27.11		58.38	-0.03	100.84
1 / 10 . *	1.07	5.23	0.84	-0.12	10.41	-0.02	0.06	-0.05	25.70		51.95	-0.01	95.06
Average	2.87	6.20	2.04	-0.12	10.41	0.01	0.07	0.07	24.44	0.98	53.02	0.02	100.00
2 / 1 .	2.80	6.11	2.12	-0.12	10.67	0.03	0.04	0.24	23.94	1.50	52.62	0.04	100.00
2 / 2 .	2.67	6.17	2.10	-0.12	10.71	0.00	0.05	0.38	24.14	0.80	53.08	0.01	100.00
2 / 3 .	2.76	5.95	2.13	-0.12	10.72	0.02	0.07	0.30	23.98	1.74	52.44	0.01	100.00
2 / 4 .	2.76	6.05	2.13	-0.11	10.65	-0.02	0.07	0.26	24.20	1.64	52.35	0.02	100.00
2 / 5 .	2.85	5.98	2.06	-0.12	10.66	0.00	0.01	0.27	24.17	1.52	52.59	0.01	100.00
2 / 6 .	2.77	5.97	2.16	-0.12	10.68	0.00	0.07	0.21	24.36	1.11	52.76	0.03	100.00
2 / 7 .	2.80	6.17	2.09	-0.12	10.60	0.03	0.04	-0.10	24.26	2.32	51.90	0.01	100.00
2 / 8 .	2.79	5.80	2.14	-0.11	10.69	0.00	0.08	0.10	24.21	0.69	53.61	-0.01	100.00
2 / 9 .	2.83	5.99	2.17	-0.12	10.43	0.01	0.04	0.04	24.62	0.98	52.99	0.01	100.00
2 / 10 .	2.77	6.22	2.16	-0.12	10.67	0.00	0.05	0.21	24.33	0.41	53.29	0.02	100.00
Average	2.78	6.04	2.13	-0.12	10.65	0.01	0.05	0.19	24.22	1.27	52.76	0.02	100.00

Table A.2. Scapolite chemistries
CO2 calculated by difference. *Analyses not used in mineral chemistry calculations

BB6-6 Scap Formula	Wt% Oxide Cl	Na2O	K2O	MgO	CaO	MnO	FeO	BaO	Al2O3	CO2	SiO2	SO2	Total
3 / 1 .	2.89	6.08	2.12	-0.11	10.29	0.01	0.04	-0.08	24.28	2.10	52.36	0.02	100.00
3 / 2 .	2.91	6.10	2.12	-0.10	10.48	-0.01	0.06	0.06	24.36	1.53	52.46	0.04	100.00
3 / 3 .	2.83	5.91	2.08	-0.12	10.63	-0.02	0.06	0.15	24.24	1.69	52.52	0.01	100.00
3 / 4 .	2.89	5.90	2.13	-0.12	10.62	-0.04	0.02	0.04	24.40	1.98	52.16	0.01	100.00
3 / 5 .	2.79	6.02	2.07	-0.12	10.64	0.01	0.06	0.13	24.98	1.01	52.39	0.02	100.00
3 / 6 .	2.83	6.14	2.09	-0.10	10.45	0.00	0.03	0.18	24.46	1.54	52.38	0.00	100.00
3 / 7 .	2.89	6.06	2.08	-0.12	10.47	0.00	0.06	-0.04	24.15	1.19	53.27	-0.02	100.00
3 / 8 .	2.72	6.12	2.09	-0.11	10.52	-0.03	0.04	0.12	24.39	0.57	53.55	0.01	100.00
3 / 9 .	2.85	6.18	2.02	-0.11	10.55	0.02	0.04	-0.05	24.53	0.92	53.06	0.00	100.00
3 / 10 .	2.78	6.07	2.06	-0.12	10.53	-0.01	0.06	0.07	24.09	1.86	52.58	0.02	100.00
Average	2.84	6.06	2.09	-0.11	10.52	-0.01	0.05	0.06	24.39	1.44	52.67	0.01	100.00
4 / 1 .	2.86	6.03	2.12	-0.11	10.29	0.00	0.05	0.35	24.03	0.53	53.84	0.00	100.00
4 / 2 .	2.80	6.32	2.07	-0.11	10.37	0.00	0.05	0.07	23.99	2.62	51.80	0.02	100.00
4 / 3 .	2.89	6.28	2.04	-0.12	10.40	0.01	0.06	0.18	23.94	1.91	52.42	-0.01	100.00
4 / 4 .	2.80	6.29	2.08	-0.12	10.61	-0.01	0.03	0.12	24.02	1.39	52.78	0.00	100.00
4 / 5 .	2.80	6.06	2.13	-0.12	10.37	0.00	0.05	0.01	24.25	2.04	52.39	0.01	100.00
4 / 6 .	2.83	5.96	2.13	-0.11	10.43	0.00	0.06	-0.08	24.21	2.07	52.50	0.01	100.00
4 / 7 .	2.83	6.07	2.07	-0.11	10.34	-0.01	0.07	0.15	24.72	0.97	52.91	0.00	100.00
4 / 8 .	2.75	6.02	2.03	-0.11	10.29	0.02	0.05	0.12	24.18	1.72	52.91	0.01	100.00
4 / 9 .	2.81	6.35	2.14	-0.11	10.51	0.02	0.09	-0.08	24.55	1.50	52.22	0.01	100.00
4 / 10 .	2.83	6.11	2.05	-0.12	10.58	0.02	0.08	0.09	24.06	0.91	53.37	0.00	100.00
Average	2.82	6.15	2.09	-0.11	10.42	0.01	0.06	0.09	24.20	1.57	52.72	0.00	100.00

Table A.2. Scapolite chemistries
CO2 calculated by difference. *Analyses not used in mineral chemistry calculations

BB6-6 Scap Formula	Wt% Oxide Cl	Na2O	K2O	MgO	CaO	MnO	FeO	BaO	Al2O3	CO2	SiO2	SO2	Total
5 / 1 .	3.11	6.53	2.04	-0.12	9.83	0.00	0.07	-0.10	24.05	1.47	53.13	-0.01	100.00
5 / 2 .	2.96	6.37	2.09	-0.12	10.09	0.01	0.06	0.20	24.08	0.78	53.49	-0.01	100.00
5 / 3 .	2.89	5.81	2.01	-0.11	10.39	-0.01	0.07	0.01	24.52	1.51	52.93	-0.02	100.00
5 / 4 .	2.82	6.09	2.07	-0.12	10.65	-0.02	0.05	-0.02	24.41	1.48	52.58	0.01	100.00
5 / 5 .	2.82	5.82	1.98	-0.10	10.86	0.02	0.06	-0.13	24.65	1.39	52.63	0.00	100.00
5 / 6 .	2.83	5.81	2.01	-0.12	10.73	0.01	0.08	0.03	24.65	1.43	52.55	-0.01	100.00
5 / 7 .	2.85	5.99	2.00	-0.12	10.72	0.02	0.09	0.15	24.25	1.77	52.29	-0.01	100.00
5 / 8 .	2.77	6.20	1.99	-0.11	10.64	0.02	0.09	0.27	24.69	1.00	52.46	-0.02	100.00
5 / 9 .	2.90	6.14	2.03	-0.12	10.64	0.01	0.06	0.10	24.88	0.97	52.39	0.01	100.00
5 / 10 .	2.87	6.06	1.99	-0.12	10.64	-0.02	0.04	0.06	24.44	1.56	52.47	0.01	100.00
Average	2.88	6.08	2.02	-0.12	10.52	0.01	0.07	0.06	24.46	1.34	52.69	-0.01	100.00
BB8-2 Scap Formula	Wt% Oxide Cl	Na2O	K2O	MgO	CaO	MnO	FeO	BaO	Al2O3	CO2	SiO2	SO2	Total
1 / 1 .	1.80	5.06	1.40	-0.07	13.04	0.02	0.13	-0.01	25.31	3.54	49.80	-0.03	100.00
1 / 2 .	1.83	4.72	1.37	-0.08	12.86	0.00	0.16	0.31	25.10	3.55	50.19	0.01	100.00
1 / 3 .	1.85	4.73	1.34	-0.08	12.99	-0.02	0.18	0.24	25.25	3.34	50.21	-0.02	100.00
1 / 4 .	1.90	4.85	1.41	-0.08	13.07	0.04	0.17	-0.11	25.42	2.23	51.11	0.01	100.00
1 / 5 .	1.93	4.62	1.42	-0.08	13.05	-0.01	0.17	0.14	25.31	4.47	48.97	0.01	100.00
1 / 6 .	1.83	4.72	1.41	-0.09	13.33	0.00	0.16	0.28	25.51	2.59	50.27	0.00	100.00
1 / 7 .	1.83	4.73	1.36	-0.07	13.25	0.01	0.15	0.03	25.58	2.84	50.31	-0.01	100.00
1 / 8 .	1.81	4.81	1.44	-0.08	13.22	0.00	0.17	0.20	25.47	2.93	50.05	-0.01	100.00
1 / 9 .	1.84	4.67	1.41	-0.07	13.05	0.01	0.15	0.29	25.30	2.58	50.79	-0.02	100.00
1 / 10 .	1.84	4.76	1.42	-0.08	13.12	0.04	0.19	0.12	25.55	3.53	49.51	0.01	100.00
Average	1.85	4.77	1.40	-0.08	13.10	0.01	0.16	0.15	25.38	3.16	50.12	-0.01	100.00

Table A.2. Scapolite chemistries
CO2 calculated by difference. *Analyses not used in mineral chemistry calculations

BB8-2 Scap Formula	Wt% Oxide Cl	Na2O	K2O	MgO	CaO	MnO	FeO	BaO	Al2O3	CO2	SiO2	SO2	Total
2 / 1 .	1.97	4.85	1.50	-0.08	12.55	0.02	0.13	0.04	25.47	2.46	51.09	0.00	100.00
2 / 2 .	1.99	4.98	1.49	-0.09	12.62	-0.03	0.11	0.00	25.08	2.75	51.11	0.00	100.00
2 / 3 .	1.95	4.90	1.42	-0.10	12.60	0.01	0.14	0.01	24.97	4.06	50.02	0.01	100.00
2 / 4 .	1.98	5.09	1.44	-0.07	12.59	0.00	0.18	-0.04	24.85	3.23	50.74	0.00	100.00
2 / 5 .	2.03	4.98	1.44	-0.08	12.59	0.00	0.17	0.04	25.00	3.64	50.20	-0.02	100.00
2 / 6 .	1.94	4.99	1.43	-0.08	12.68	0.01	0.18	0.20	24.88	3.36	50.41	0.01	100.00
2 / 7 .	2.00	4.96	1.45	-0.09	12.65	0.04	0.18	0.03	24.67	2.56	51.57	-0.01	100.00
2 / 8 .	1.96	4.94	1.44	-0.08	12.74	-0.02	0.12	0.09	24.80	3.63	50.39	0.00	100.00
2 / 9 .	1.95	5.05	1.44	-0.08	12.68	-0.02	0.18	0.17	24.91	3.59	50.15	-0.03	100.00
2 / 10 .	1.95	4.96	1.45	-0.08	12.75	-0.04	0.18	-0.05	24.91	2.86	51.09	0.01	100.00
Average	1.97	4.97	1.45	-0.08	12.65	0.00	0.16	0.05	24.95	3.22	50.68	0.00	100.00
3 / 1 .	1.64	4.49	1.36	-0.09	13.77	0.00	0.17	-0.13	25.67	2.97	50.19	-0.03	100.00
3 / 2 .	1.70	4.29	1.36	-0.10	13.53	0.00	0.12	-0.08	25.25	4.82	49.12	-0.02	100.00
3 / 3 .	1.67	4.44	1.37	-0.09	13.59	0.03	0.11	0.24	25.77	3.11	49.76	-0.01	100.00
3 / 4 .	1.72	4.46	1.34	-0.10	13.75	0.00	0.10	0.21	25.82	3.68	49.04	-0.03	100.00
3 / 5 .	1.62	4.24	1.76	-0.02	12.79	0.00	0.29	0.23	26.26	2.97	49.87	-0.01	100.00
3 / 6 .	1.55	4.16	1.28	-0.05	14.12	-0.03	0.21	0.40	26.32	2.38	49.68	-0.03	100.00
3 / 7 .	1.55	4.05	1.29	-0.10	14.08	0.01	0.13	-0.02	26.10	3.14	49.79	-0.02	100.00
3 / 8 .	1.64	4.44	1.31	-0.09	13.90	0.01	0.13	0.06	25.62	2.92	50.09	-0.02	100.00
3 / 9 .	1.73	4.57	1.37	-0.09	13.64	-0.01	0.12	-0.07	25.85	2.96	49.94	-0.01	100.00
3 / 10 .	1.56	4.42	1.28	-0.10	14.07	0.02	0.12	-0.15	25.93	3.02	49.85	-0.02	100.00
Average	1.64	4.36	1.37	-0.08	13.73	0.00	0.15	0.07	25.86	3.20	49.73	-0.02	100.00

Table A.2.   Scapolite chemistries
CO2 calculated by difference. *Analyses not used in mineral chemistry calculations

BB8-2 Scap Formula	Wt% Oxide Cl	Na2O	K2O	MgO	CaO	MnO	FeO	BaO	Al2O3	CO2	SiO2	SO2	Total
4 / 1 .	1.89	4.75	1.37	-0.10	12.79	-0.02	0.16	0.20	25.19	3.56	50.22	0.00	100.00
4 / 2 .	1.89	4.83	1.46	-0.08	12.75	0.00	0.13	-0.04	24.76	4.13	50.17	0.00	100.00
4 / 3 .	1.89	5.15	1.38	-0.08	12.55	0.01	0.14	0.23	25.17	2.73	50.82	0.01	100.00
4 / 4 .	2.05	5.17	1.40	-0.09	12.48	0.00	0.13	-0.02	24.81	3.82	50.25	0.00	100.00
4 / 5 .	1.95	5.17	1.36	-0.09	12.54	0.00	0.17	0.28	24.41	4.06	50.16	0.00	100.00
4 / 6 .	1.89	5.12	1.31	-0.09	12.61	-0.01	0.12	-0.05	25.51	3.89	49.70	0.00	100.00
4 / 7 .	1.93	5.20	1.38	-0.08	12.59	0.00	0.13	0.14	24.97	4.05	49.69	0.00	100.00
4 / 8 .	1.96	5.37	1.37	-0.09	12.66	0.00	0.20	0.06	24.97	3.42	50.09	-0.01	100.00
4 / 9 .	2.00	5.23	1.35	-0.08	12.54	0.04	0.14	0.12	24.82	3.52	50.32	0.01	100.00
4 / 10 .	2.00	5.05	1.39	-0.09	12.66	0.02	0.15	-0.07	24.97	2.94	50.99	-0.01	100.00
Average	1.95	5.10	1.38	-0.08	12.62	0.00	0.15	0.08	24.96	3.61	50.24	0.00	100.00
5 / 1 .	1.95	5.53	1.35	-0.09	12.21	-0.01	0.14	0.10	24.64	2.74	51.44	-0.01	100.00
5 / 2 .	2.06	5.39	1.34	-0.09	12.16	0.01	0.15	-0.08	24.67	2.98	51.42	0.00	100.00
5 / 3 .	2.03	5.57	1.31	-0.10	11.94	0.01	0.11	0.14	24.59	2.74	51.67	-0.01	100.00
5 / 4 .	1.95	5.73	1.32	-0.12	11.87	-0.01	0.16	0.10	24.70	2.95	51.35	-0.01	100.00
5 / 5 .	1.94	5.46	1.35	0.21	11.69	0.01	0.80	0.24	24.10	4.29	49.90	0.00	100.00
5 / 6 .	2.01	5.31	1.35	-0.10	12.23	0.00	0.13	-0.02	24.78	3.58	50.75	-0.01	100.00
5 / 7 .	2.04	5.47	1.35	-0.05	12.05	-0.02	0.29	0.46	24.64	3.19	50.60	-0.02	100.00
5 / 8 .	2.01	5.30	1.34	0.01	12.04	0.00	0.30	-0.15	24.61	3.85	50.69	-0.02	100.00
5 / 9 .	1.98	5.55	1.41	-0.09	12.22	-0.02	0.16	-0.07	24.79	3.41	50.65	-0.01	100.00
5 / 10 .	1.99	5.46	1.32	-0.08	12.12	0.01	0.15	-0.14	24.57	3.95	50.67	-0.01	100.00
Average	1.99	5.48	1.34	-0.05	12.05	0.00	0.24	0.06	24.61	3.37	50.92	-0.01	100.00

Table A.2.   Scapolite chemistries

CO2 calculated by difference. *Analyses not used in mineral chemistry calculations

BB12-9 Scap Formula	Wt% Oxide Cl	Na2O	K2O	MgO	CaO	MnO	FeO	BaO	Al2O3	CO2	SiO2	SO2	Total
1 / 1 .	1.04	3.69	0.94	0.01	15.32	-0.01	0.26	0.05	27.08	1.75	49.87	0.00	100.00
1 / 2 .	0.94	3.77	0.91	0.06	15.50	0.00	0.28	0.06	26.07	3.04	49.35	0.03	100.00
1 / 3 .	0.97	3.76	0.89	0.00	15.49	0.02	0.24	0.00	26.51	1.94	50.15	0.02	100.00
1 / 4 .	1.02	3.73	0.87	0.01	15.41	0.02	0.25	0.03	26.69	2.20	49.76	0.01	100.00
1 / 5 .	0.98	3.72	0.90	0.00	15.35	0.03	0.21	0.23	26.71	2.02	49.82	0.02	100.00
1 / 6 .	0.98	3.65	0.89	0.01	15.24	0.03	0.20	0.08	26.18	2.28	50.45	0.02	100.00
1 / 7 .	1.01	3.72	0.91	0.00	15.30	-0.01	0.23	0.10	26.42	3.12	49.21	-0.01	100.00
1 / 8 .	0.97	3.74	0.91	0.00	15.55	0.02	0.25	0.09	26.24	2.88	49.32	0.03	100.00
1 / 9 .	0.96	3.77	0.92	-0.01	15.24	0.02	0.23	0.43	26.14	2.24	50.02	0.02	100.00
1 / 10 .	0.96	3.77	0.94	0.01	15.37	0.03	0.26	0.17	26.15	1.82	50.52	0.01	100.00
Average	0.98	3.73	0.91	0.01	15.38	0.02	0.24	0.12	26.42	2.33	49.85	0.01	100.00
2 / 1 .	0.98	3.82	1.13	0.03	15.17	0.02	0.43	0.55	26.41	2.67	48.83	-0.01	100.00
2 / 2 .	1.28	4.19	1.24	0.03	14.42	0.06	0.24	0.47	26.87	1.44	49.74	0.02	100.00
2 / 3 .	1.32	4.46	1.25	0.04	14.11	0.06	0.23	0.06	25.45	3.36	49.66	0.00	100.00
2 / 4 .	1.34	4.45	1.34	0.04	13.88	0.09	0.24	0.14	25.44	3.33	49.70	0.01	100.00
2 / 5 .	1.34	4.52	1.31	0.06	14.01	0.06	0.30	0.33	26.30	1.62	50.15	0.01	100.00
2 / 6 .	1.32	4.40	1.33	0.05	13.91	0.05	0.23	0.20	25.82	2.24	50.46	0.00	100.00
2 / 7 .	1.36	4.75	1.29	0.04	13.86	0.04	0.23	0.15	25.07	3.32	49.86	0.01	100.00
2 / 8 .	1.23	4.18	1.20	0.93	12.68	0.02	3.61	0.29	23.62	3.77	48.45	0.01	100.00
2 / 9 .	1.39	4.61	1.27	0.03	14.05	0.07	0.26	0.12	25.10	3.33	49.78	-0.03	100.00
Average	1.29	4.38	1.26	0.14	14.01	0.05	0.64	0.26	25.56	2.79	49.62	0.00	100.00

Table A.2. Scapolite chemistries

CO2 calculated by difference. *Analyses not used in mineral chemistry calculations

BB12-9 Scap Formula	Wt% Oxide Cl	Na2O	K2O	MgO	CaO	MnO	FeO	BaO	Al2O3	CO2	SiO2	SO2	Total
3 / 1 .	1.07	3.99	0.98	0.02	15.38	0.04	0.22	0.18	26.25	3.79	48.02	0.04	100.00
3 / 2 .	1.31	4.16	1.01	0.05	15.30	0.04	0.25	0.11	26.21	2.80	48.74	0.03	100.00
3 / 3 .	1.09	3.83	1.37	0.09	14.76	0.04	0.29	-0.03	26.82	3.24	48.44	0.04	100.00
3 / 4 .	1.10	4.00	1.05	0.04	15.49	0.01	0.18	0.24	26.56	2.29	49.04	0.01	100.00
3 / 5 .	1.10	4.09	1.00	0.05	15.36	0.04	0.26	0.23	26.19	2.52	49.13	0.03	100.00
3 / 6 .	1.06	3.91	1.03	0.04	15.24	0.09	0.19	0.14	26.14	3.85	48.26	0.04	100.00
3 / 7 .	1.06	4.00	1.01	0.04	15.15	0.07	0.19	0.24	26.15	3.39	48.66	0.05	100.00
3 / 8 .	1.08	3.88	1.05	0.04	15.36	0.04	0.22	0.37	26.49	3.49	47.96	0.03	100.00
3 / 9 .	1.08	4.11	1.04	0.03	15.28	0.02	0.18	-0.07	26.57	2.82	48.92	0.03	100.00
3 / 10 .	1.11	3.81	1.04	0.04	14.98	0.05	0.20	0.09	26.18	4.24	48.22	0.03	100.00
3 / 11 .	1.09	3.97	0.99	0.05	15.13	0.05	0.23	0.29	25.94	3.60	48.65	0.02	100.00
3 / 12 .	1.10	3.92	0.99	0.05	15.12	0.04	0.24	0.23	26.21	3.67	48.39	0.02	100.00
3 / 13 .	1.08	4.12	0.99	0.04	15.04	0.03	0.20	-0.07	26.37	3.92	48.24	0.04	100.00
3 / 14 .	1.10	4.17	0.96	0.04	14.92	0.03	0.23	0.35	26.38	2.40	49.37	0.04	100.00
3 / 15 .	1.06	4.17	1.04	0.05	15.04	0.03	0.24	0.03	26.29	4.21	47.81	0.02	100.00
3 / 16 .	1.05	3.91	0.96	0.05	15.08	0.05	0.26	0.12	26.27	4.60	47.61	0.04	100.00
3 / 17 .	1.06	4.02	0.97	0.11	15.10	0.03	0.31	-0.03	26.28	3.95	48.16	0.04	100.00
3 / 18 .	1.08	3.84	0.96	0.05	15.22	0.04	0.26	0.05	26.50	3.21	48.77	0.03	100.00
3 / 19 .	1.00	4.02	0.94	0.04	15.19	0.03	0.25	0.31	26.28	3.71	48.22	0.00	100.00
3 / 20 .	1.01	3.85	0.92	0.05	15.41	0.06	0.27	-0.01	26.60	3.52	48.30	0.02	100.00
3 / 21 .	1.03	3.80	0.93	0.04	15.22	0.04	0.29	0.08	26.49	4.13	47.92	0.02	100.00
Average	1.08	3.98	1.01	0.05	15.18	0.04	0.24	0.14	26.34	3.49	48.42	0.03	100.00

Table A.2. Scapolite chemistries

CO2 calculated by difference. *Analyses not used in mineral chemistry calculations

BB12-9 Scap Formula	Wt% Oxide Cl	Na2O	K2O	MgO	CaO	MnO	FeO	BaO	Al2O3	CO2	SiO2	SO2	Total
4 / 1 .	0.86	3.67	0.91	0.04	15.81	0.05	0.22	0.00	26.55	3.55	48.31	0.01	100.00
4 / 2 .	0.93	3.56	0.87	0.04	16.06	0.03	0.25	0.20	26.16	4.57	47.30	0.01	100.00
4 / 3 .	0.92	3.88	0.93	0.04	15.92	0.05	0.20	0.17	27.73	2.20	47.96	-0.01	100.00
4 / 4 .	0.91	3.73	0.95	0.04	16.06	0.06	0.26	0.08	26.42	3.54	47.94	0.01	100.00
4 / 5 .	0.89	3.83	0.86	0.03	15.92	0.05	0.19	0.03	26.84	3.85	47.47	0.02	100.00
4 / 6 .	0.89	3.77	0.88	0.04	15.93	0.03	0.25	0.16	26.31	3.92	47.81	0.02	100.00
4 / 7 .	0.91	3.91	0.91	0.05	16.03	0.04	0.20	0.15	26.19	4.00	47.59	0.01	100.00
4 / 8 .	0.90	3.71	0.90	0.04	16.00	0.03	0.24	0.17	25.94	4.53	47.53	0.00	100.00
4 / 9 .	0.94	3.88	0.94	0.05	15.93	0.03	0.21	0.40	26.37	2.75	48.48	0.01	100.00
4 / 10 .	0.95	3.82	0.91	0.05	16.01	0.06	0.24	0.28	26.01	3.79	47.89	0.00	100.00
4 / 11 .	0.96	4.03	0.94	0.05	15.82	0.06	0.24	0.32	26.23	3.50	47.82	0.02	100.00
4 / 12 .	0.88	3.93	0.97	0.05	15.93	0.05	0.20	0.15	26.59	3.32	47.90	0.02	100.00
4 / 13 .	0.94	3.67	0.94	0.04	15.84	0.04	0.25	0.15	26.12	4.31	47.69	0.00	100.00
4 / 14 .	1.01	4.01	0.96	0.04	15.88	0.05	0.23	0.15	27.61	1.71	48.36	-0.01	100.00
4 / 15 .	0.97	3.88	0.99	0.05	15.87	0.05	0.24	0.17	26.44	3.41	47.92	0.01	100.00
4 / 16 .	0.97	4.01	0.97	0.04	15.71	0.05	0.20	0.53	26.45	3.00	48.06	0.01	100.00
4 / 17 .	0.98	3.85	1.03	0.04	15.87	0.06	0.19	0.50	26.49	2.93	48.03	0.01	100.00
4 / 18 .	0.97	3.92	0.98	0.04	15.96	0.02	0.21	0.38	26.35	2.83	48.29	0.03	100.00
4 / 19 .	0.71	2.67	0.69	3.97	11.31	0.08	8.39	0.23	22.58	5.79	43.59	0.00	100.00
4 / 20 .	0.99	3.81	0.94	0.03	15.57	0.00	0.25	0.24	25.85	4.31	47.99	0.00	100.00
4 / 21 .	1.00	3.87	0.94	0.03	15.74	0.04	0.21	0.24	26.68	3.38	47.84	0.02	100.00
4 / 22 .	1.03	3.78	0.94	0.03	15.92	0.07	0.26	0.24	26.63	2.09	48.98	0.02	100.00
Average	0.94	3.79	0.93	0.23	15.68	0.05	0.61	0.24	26.29	3.51	47.74	0.01	100.00

Table A.2.   Scapolite chemistries

CO2 calculated by difference. *Analyses not used in mineral chemistry calculations

BB12-9 Scap Formula	Wt% Oxide Cl	Na2O	K2O	MgO	CaO	MnO	FeO	BaO	Al2O3	CO2	SiO2	SO2	Total
5 / 1 .	1.01	3.90	0.90	0.05	15.43	0.02	0.22	0.20	26.22	4.44	47.57	0.02	100.00
5 / 2 .	0.94	3.96	0.93	0.05	15.69	0.03	0.25	0.09	26.00	4.68	47.35	0.02	100.00
5 / 3 .	0.98	3.93	0.90	0.04	15.48	0.04	0.25	0.15	26.13	4.12	47.91	0.06	100.00
5 / 4 .	0.99	3.89	0.92	0.04	15.40	0.05	0.25	0.16	26.16	4.44	47.68	0.03	100.00
5 / 5 .	0.57	2.15	0.46	6.36	7.80	0.10	13.08	0.19	20.76	7.83	40.70	0.01	100.00
5 / 6 .	1.01	3.90	0.88	0.03	15.56	0.03	0.24	0.31	26.24	2.37	49.41	0.02	100.00
5 / 7 .	1.00	3.78	0.92	0.03	15.26	0.04	0.20	0.31	26.45	3.81	48.19	0.02	100.00
5 / 8 .	0.95	3.81	0.87	0.04	15.70	0.05	0.21	0.12	26.60	3.06	48.53	0.05	100.00
5 / 9 .	0.95	3.56	0.88	0.04	15.63	0.06	0.23	0.21	26.51	4.65	47.28	0.01	100.00
5 / 10 .	0.90	3.89	0.84	0.03	15.81	0.05	0.24	0.21	26.83	3.30	47.86	0.04	100.00
5 / 11 .	0.96	3.74	0.81	0.04	16.04	0.04	0.25	0.08	27.65	3.15	47.21	0.03	100.00
5 / 12 .	0.89	3.72	0.83	0.04	15.75	0.05	0.23	0.22	26.46	4.59	47.18	0.05	100.00
5 / 13 .	0.87	3.89	0.77	0.04	15.92	0.04	0.27	0.15	26.54	3.46	48.02	0.03	100.00
5 / 14 .	0.89	3.55	0.85	0.04	15.98	0.04	0.24	0.21	26.89	3.40	47.86	0.04	100.00
5 / 15 .	0.89	3.75	0.86	0.04	15.87	0.03	0.25	0.09	26.68	4.39	47.10	0.05	100.00
5 / 16 .	0.89	3.66	0.80	0.06	15.85	0.06	0.24	0.19	26.52	4.96	46.74	0.04	100.00
5 / 17 .	1.09	4.18	0.86	0.07	15.70	0.03	0.23	0.28	26.51	4.31	46.68	0.05	100.00
5 / 18 .	0.91	3.77	0.82	0.04	15.76	0.05	0.17	0.26	26.83	2.96	48.38	0.06	100.00
5 / 19 .	0.93	3.68	0.82	0.04	15.73	0.02	0.25	0.26	26.64	3.40	48.18	0.04	100.00
5 / 20 .	0.89	3.71	0.85	0.05	15.66	0.06	0.27	0.20	26.57	4.24	47.47	0.03	100.00
5 / 21 .	0.83	3.53	0.79	0.66	15.38	0.04	0.82	0.18	25.59	4.39	47.75	0.04	100.00
Average	0.92	3.71	0.84	0.37	15.30	0.04	0.88	0.19	26.23	4.09	47.38	0.04	100.00

Table A.3.   Pyroxene chemistries
*Analyses not used in mineral chemistry calculations

BB6-6 Pyx Formula	Wt% Oxide Na2O	K2O	MgO	CaO	MnO	FeO	Al2O3	V2O3	Cr2O3	SiO2	TiO2	Total
1 / 1 .	0.56	0.02	9.53	22.05	0.49	13.82	3.32	-0.05	0.07	48.74	0.48	99.08
1 / 2 .	0.51	0.02	10.18	22.29	0.44	13.48	1.98	-0.07	0.02	49.84	0.29	99.05
1 / 3 .	0.53	0.00	10.13	22.22	0.56	13.87	2.16	-0.02	0.04	50.21	0.20	99.92
1 / 4 .	0.60	0.00	9.67	21.98	0.47	13.90	3.07	-0.08	0.02	48.70	0.37	98.77
1 / 5 .	0.59	0.01	9.65	21.84	0.50	13.78	3.22	-0.07	0.01	49.20	0.41	99.21
1 / 6 .	0.63	0.00	9.73	22.17	0.45	13.94	3.19	-0.09	0.04	49.33	0.38	99.86
1 / 7 .	0.64	0.00	9.75	22.01	0.46	13.82	3.12	-0.10	0.02	49.65	0.44	99.91
1 / 8 .	0.56	0.01	10.00	22.32	0.50	13.62	2.61	-0.05	0.07	50.72	0.33	100.74
1 / 9 .	0.48	0.01	9.69	22.15	0.47	13.66	3.06	-0.06	0.01	49.01	0.40	98.94
1 / 10 .	0.58	0.01	9.79	22.17	0.53	13.67	2.80	-0.05	0.01	50.28	0.39	100.22
Average	0.57	0.01	9.81	22.12	0.49	13.75	2.85	-0.06	0.03	49.57	0.37	99.57
2 / 1 .	0.68	0.01	9.61	21.21	0.48	14.15	3.41	-0.05	0.06	50.12	0.41	100.14
2 / 2 .	0.64	0.00	9.96	21.39	0.48	13.88	3.43	-0.06	0.06	50.42	0.47	100.74
2 / 3 .	0.58	0.00	10.01	21.49	0.49	13.67	3.31	-0.08	0.01	49.84	0.42	99.82
2 / 4 .	0.66	0.01	10.15	21.57	0.48	13.12	3.38	-0.08	0.06	50.38	0.40	100.19
2 / 5 .	0.55	0.01	10.26	21.78	0.46	12.98	3.38	-0.06	0.03	50.26	0.44	100.15
2 / 6 .	0.50	0.00	10.15	21.78	0.48	12.74	3.57	-0.06	0.05	50.05	0.42	99.73
2 / 7 .	0.59	0.00	10.32	21.83	0.45	12.81	3.32	-0.02	-0.01	50.34	0.40	100.05
2 / 8 .	0.43	0.00	10.35	21.80	0.47	12.79	3.43	-0.07	0.06	50.09	0.40	99.82
2 / 9 .	0.54	0.00	10.75	21.56	0.41	12.76	3.04	-0.04	0.02	50.60	0.28	99.98
2 / 10 .	0.57	0.01	10.57	21.78	0.44	12.14	3.24	-0.07	0.07	50.54	0.34	99.70
Average	0.57	0.00	10.21	21.62	0.46	13.10	3.35	-0.06	0.04	50.26	0.40	100.03

Table A.3. Pyroxene chemistries
*Analyses not used in mineral chemistry calculations

BB6-6 Pyx Formula	Wt% Oxide Na2O	K2O	MgO	CaO	MnO	FeO	Al2O3	V2O3	Cr2O3	SiO2	TiO2	Total
3 / 1 .	0.53	0.00	10.45	22.09	0.45	12.57	2.96	-0.08	0.03	50.74	0.37	100.21
3 / 2 .	0.58	0.00	10.20	21.73	0.46	12.85	3.07	-0.06	0.02	50.18	0.39	99.46
3 / 3 .	0.50	0.01	10.06	21.79	0.44	13.36	3.33	-0.04	0.03	49.81	0.33	99.67
3 / 4 .	0.55	0.01	10.04	21.80	0.53	13.58	3.45	-0.09	0.04	50.36	0.45	100.81
3 / 5 .	0.61	0.01	10.02	21.93	0.51	13.49	3.19	-0.05	0.03	50.16	0.44	100.38
3 / 6 .	0.68	0.00	9.94	21.73	0.48	13.77	3.17	-0.04	0.00	50.15	0.41	100.33
3 / 7 .	0.51	0.02	9.83	21.66	0.47	13.87	3.64	-0.07	0.00	49.75	0.46	100.20
3 / 8 .	0.57	0.00	9.86	21.71	0.46	13.81	3.19	-0.05	0.05	49.79	0.42	99.87
3 / 9 .	0.58	0.00	9.78	21.73	0.45	14.10	3.38	-0.04	0.04	50.19	0.41	100.66
3 / 10 .	0.60	0.01	9.70	21.54	0.44	13.96	3.41	-0.07	0.02	49.97	0.36	100.00
Average	0.57	0.01	9.99	21.77	0.47	13.54	3.28	-0.06	0.03	50.11	0.40	100.16
4 / 1 .	0.66	-0.01	10.29	21.54	0.43	12.93	3.28	-0.06	0.02	50.09	0.44	99.68
4 / 2 .	0.71	0.01	10.12	21.53	0.41	13.00	3.27	-0.03	0.00	50.05	0.39	99.47
4 / 3 .	0.55	0.01	10.16	21.32	0.45	13.60	3.66	-0.06	0.01	50.37	0.48	100.62
4 / 4 .	0.55	-0.01	10.10	21.39	0.41	13.61	3.35	-0.08	0.05	50.31	0.57	100.35
4 / 5 .	0.60	-0.01	10.10	21.58	0.46	13.52	3.42	-0.06	0.04	50.03	0.48	100.23
4 / 6 .	0.57	0.00	10.01	21.47	0.46	13.41	3.50	-0.07	0.01	49.71	0.55	99.70
4 / 7 .	0.69	0.00	10.11	21.44	0.51	13.26	3.55	-0.09	0.00	49.91	0.52	99.99
4 / 8 .	0.55	0.00	10.13	21.54	0.44	13.15	3.59	-0.07	0.04	50.06	0.50	100.01
4 / 9 .	0.50	0.00	10.15	21.47	0.43	13.28	3.66	-0.07	0.03	50.30	0.51	100.32
4 / 10 .	0.48	0.00	10.28	21.66	0.46	13.07	3.61	-0.08	0.06	50.22	0.48	100.32
Average	0.58	0.00	10.14	21.49	0.45	13.28	3.49	-0.07	0.03	50.11	0.49	100.07

Table A.3. Pyroxene chemistries
*Analyses not used in mineral chemistry calculations

BB6-6 Pyx Formula	Wt% Oxide Na2O	K2O	MgO	CaO	MnO	FeO	Al2O3	V2O3	Cr2O3	SiO2	TiO2	Total
5 / 1 .	0.49	0.00	12.13	22.63	0.42	10.09	2.59	-0.07	0.03	51.41	0.28	100.08
5 / 2 .	0.45	0.00	11.94	22.58	0.41	10.22	2.89	-0.02	0.00	50.99	0.25	99.72
5 / 3 .	0.47	0.01	11.98	22.48	0.38	10.39	2.77	-0.05	0.01	51.19	0.26	99.95
5 / 4 .	0.49	0.01	11.66	22.49	0.38	10.79	3.12	-0.06	0.04	50.96	0.29	100.24
5 / 5 .	0.51	0.01	11.52	22.41	0.42	10.66	2.93	-0.04	0.04	50.96	0.31	99.78
5 / 6 .	0.49	0.01	11.43	22.25	0.46	11.23	3.16	-0.07	0.02	50.99	0.33	100.38
5 / 7 .	0.57	0.00	11.19	22.16	0.42	11.46	3.10	-0.02	0.02	50.75	0.32	99.98
5 / 8 .	0.53	0.00	11.10	22.26	0.45	11.37	3.11	-0.07	0.03	51.00	0.25	100.12
5 / 9 .	0.61	0.01	10.96	22.15	0.40	11.67	3.11	-0.05	0.03	50.39	0.31	99.65
5 / 10 .	0.61	0.01	10.86	22.25	0.47	11.85	3.33	-0.03	-0.01	51.06	0.36	100.80
Average	0.52	0.01	11.48	22.37	0.42	10.97	3.01	-0.05	0.02	50.97	0.30	100.07
6 / 1 .	0.38	0.00	12.12	22.64	0.42	10.18	2.86	0.01	0.01	51.63	0.15	100.39
6 / 2 .	0.44	0.00	11.91	22.46	0.42	10.90	3.13	-0.02	0.02	51.05	0.15	100.48
6 / 3 .	0.44	-0.01	11.25	22.39	0.43	11.38	3.31	0.00	0.01	51.08	0.26	100.55
6 / 4 .	0.55	0.00	10.85	22.21	0.48	11.87	3.46	-0.02	0.03	50.42	0.27	100.13
6 / 5 .	0.48	0.00	10.70	22.20	0.50	12.17	3.48	-0.02	0.03	50.63	0.32	100.50
6 / 6 .	0.55	-0.01	10.57	22.16	0.47	12.55	3.24	-0.01	0.04	50.15	0.30	100.02
6 / 7 .	0.45	-0.01	10.37	22.06	0.49	12.62	3.45	-0.03	0.03	50.06	0.36	99.88
6 / 8 .	0.52	-0.01	10.34	21.76	0.47	12.91	3.25	-0.04	0.01	50.41	0.37	100.05
6 / 9 .	0.59	-0.01	10.09	21.91	0.50	13.12	3.37	-0.02	0.03	50.10	0.40	100.11
6 / 10 .	0.52	-0.01	10.26	21.98	0.50	12.87	3.10	-0.05	0.02	50.00	0.45	99.70
Average	0.49	-0.01	10.85	22.18	0.47	12.06	3.26	-0.02	0.02	50.55	0.30	100.18

Table A.3.   Pyroxene chemistries
*Analyses not used in mineral chemistry calculations

BB6-6 Pyx Formula	Wt% Oxide Na2O	K2O	MgO	CaO	MnO	FeO	Al2O3	V2O3	Cr2O3	SiO2	TiO2	Total
7 / 1 .	0.47	-0.01	11.03	22.05	0.50	12.08	3.55	-0.03	-0.01	50.90	0.32	100.90
7 / 2 .	0.45	-0.01	10.66	21.96	0.55	12.70	3.48	-0.07	0.00	50.39	0.41	100.60
7 / 3 .	0.57	-0.01	10.42	21.92	0.51	13.19	3.32	-0.04	0.01	50.46	0.41	100.82
7 / 4 .	0.48	0.01	10.38	21.85	0.53	13.36	3.36	-0.07	-0.03	50.07	0.44	100.47
7 / 5 .	0.59	0.00	10.23	21.73	0.47	13.79	3.43	-0.06	0.00	50.38	0.40	101.03
7 / 6 .	0.58	-0.01	10.10	21.80	0.51	13.62	3.31	-0.11	-0.02	49.79	0.45	100.17
7 / 7 .	0.53	-0.01	9.99	21.68	0.59	13.88	3.42	-0.09	0.00	50.04	0.48	100.61
7 / 8 .	0.48	0.00	9.99	21.76	0.48	14.18	3.44	-0.04	0.02	50.13	0.42	100.92
7 / 9 .	0.54	0.00	9.87	21.77	0.52	14.13	3.33	-0.09	0.02	50.05	0.45	100.69
7 / 10 .	0.69	-0.01	9.97	21.49	0.50	14.10	3.25	-0.05	-0.04	50.71	0.43	101.14
Average	0.54	0.00	10.27	21.80	0.52	13.50	3.39	-0.06	0.00	50.29	0.42	100.73
8 / 1 .	0.45	0.00	11.84	23.02	0.46	9.97	3.53	-0.04	0.00	50.12	0.45	99.82
8 / 2 .	0.52	0.00	11.57	22.52	0.43	10.67	3.63	-0.04	-0.01	50.20	0.42	99.95
8 / 3 .	0.58	-0.01	11.15	22.43	0.49	11.30	4.34	-0.03	0.01	50.35	0.48	101.12
8 / 4 .	0.43	0.00	11.04	22.17	0.41	11.46	4.27	-0.06	0.02	49.59	0.59	99.97
8 / 5 .	0.42	0.00	10.82	22.13	0.51	11.81	4.19	-0.08	0.01	49.70	0.54	100.13
8 / 6 .	0.51	0.00	10.93	22.12	0.48	11.79	3.94	-0.03	-0.03	50.09	0.47	100.33
8 / 7 .	0.54	0.00	10.52	22.04	0.48	12.41	3.71	-0.05	0.02	49.85	0.58	100.15
8 / 8 .	0.44	-0.01	10.50	21.88	0.58	12.49	3.71	-0.08	0.02	49.92	0.46	99.99
8 / 9 .	0.57	0.00	10.17	21.69	0.53	12.65	4.05	-0.07	0.04	49.38	0.59	99.67
8 / 10 .	0.54	-0.01	10.12	21.62	0.50	12.89	3.98	-0.11	-0.02	49.82	0.57	100.04
Average	0.50	0.00	10.87	22.16	0.49	11.74	3.94	-0.06	0.01	49.90	0.52	100.12

Table A.3. Pyroxene chemistries
*Analyses not used in mineral chemistry calculations

BB6-6 Pyx Formula	Wt% Oxide Na2O	K2O	MgO	CaO	MnO	FeO	Al2O3	V2O3	Cr2O3	SiO2	TiO2	Total
9 / 1 .	0.52	-0.01	11.13	22.05	0.43	11.91	3.08	0.00	-0.01	50.60	0.35	100.07
9 / 2 .	0.53	0.00	10.62	21.96	0.52	12.77	3.24	-0.04	0.03	50.71	0.31	100.69
9 / 3 .	0.52	0.00	10.50	21.74	0.49	12.93	3.28	-0.04	0.01	49.94	0.32	99.72
9 / 4 .	0.63	0.00	10.36	21.60	0.51	13.17	3.08	-0.04	0.02	50.26	0.36	99.99
9 / 5 .	0.43	0.00	10.10	21.56	0.47	13.52	3.27	-0.02	0.04	50.24	0.33	99.95
9 / 6 .	0.53	0.00	10.06	21.53	0.48	13.65	3.21	-0.03	-0.04	50.25	0.35	100.07
9 / 7 .	0.58	0.00	9.96	21.72	0.53	13.89	3.12	-0.03	0.05	50.06	0.34	100.26
9 / 8 .	0.56	0.01	10.11	21.54	0.54	13.58	3.10	-0.01	0.02	50.10	0.33	99.90
9 / 9 .	0.49	0.00	10.21	21.66	0.51	13.62	3.14	-0.05	0.00	50.66	0.32	100.60
9 / 10 .	0.63	0.00	10.35	21.78	0.48	13.60	2.83	-0.07	-0.03	50.39	0.36	100.42
Average	0.54	0.00	10.34	21.71	0.49	13.26	3.14	-0.03	0.01	50.32	0.34	100.17
10 / 1 .	0.58	0.01	9.84	21.48	0.50	14.08	3.15	-0.02	-0.01	50.08	0.38	100.10
10 / 2 .	0.43	0.01	9.79	21.38	0.49	13.94	3.33	-0.02	-0.05	50.14	0.34	99.84
10 / 3 .	0.59	0.01	9.86	21.29	0.52	14.33	3.22	-0.05	-0.02	49.96	0.41	100.19
10 / 4 .	0.57	0.01	9.86	21.57	0.52	14.27	3.17	-0.03	0.01	50.03	0.34	100.34
10 / 5 .	0.51	0.00	9.74	21.46	0.53	14.08	3.12	-0.02	-0.03	50.16	0.39	99.98
10 / 6 .	0.69	0.01	9.76	21.43	0.52	14.14	3.14	-0.03	-0.02	50.15	0.28	100.12
10 / 7 .	0.67	0.01	9.85	21.41	0.56	14.24	3.31	0.00	0.01	50.35	0.27	100.67
10 / 8 .	0.54	0.01	9.80	21.24	0.55	14.21	3.46	-0.06	0.02	50.33	0.36	100.53
10 / 9 .	0.49	0.01	9.83	21.40	0.51	14.36	3.20	-0.02	-0.01	50.32	0.32	100.43
10 / 10 .	0.46	0.00	9.87	21.27	0.50	14.32	3.02	-0.03	0.01	49.94	0.29	99.69
Average	0.55	0.01	9.82	21.39	0.52	14.20	3.21	-0.03	-0.01	50.15	0.34	100.19

Table A.4.   Amphibole chemistries
*Analyses not used in mineral chemistry calculations

BB6-6 Amp	Wt% Oxide																	
Formula	F	Cl	H2O	Na2O	K2O	MgO	CaO	MnO	FeO	BaO	Al2O3	V2O3	Cr2O3	SiO2	TiO2	Total	O=F , Cl	Total
1 / 1 .	0.17	4.59	0.53	0.93	3.39	4.28	11.31	0.29	24.26	0.07	14.16	0.03	0.01	35.19	1.82	101.03	1.11	99.93
1 / 2 .	0.16	4.58	0.53	0.91	3.41	4.26	11.30	0.30	23.96	0.20	14.12	0.00	0.02	35.23	1.76	100.76	1.10	99.66
1 / 3 .	0.13	4.62	0.54	0.91	3.40	4.28	11.35	0.31	24.13	0.26	14.15	0.01	0.04	35.18	1.74	101.06	1.10	99.96
1 / 4 .	0.14	4.66	0.52	0.83	3.48	4.12	11.29	0.30	24.35	0.20	14.30	0.04	-0.04	34.91	1.92	101.06	1.11	99.95
1 / 5 .	0.16	4.68	0.50	0.82	3.49	4.06	11.26	0.31	24.11	0.23	14.39	0.02	0.05	34.81	1.91	100.78	1.12	99.66
1 / 6 .	0.14	4.64	0.52	0.86	3.42	4.15	11.17	0.29	24.03	0.36	14.39	0.05	-0.01	34.74	1.75	100.52	1.11	99.41
1 / 7 .	0.15	4.70	0.50	0.86	3.48	4.13	11.26	0.32	24.26	0.30	14.31	0.03	0.01	34.93	1.89	101.13	1.13	100.00
1 / 8 .	0.14	4.60	0.54	0.92	3.38	4.26	11.32	0.30	24.29	0.16	14.19	0.06	-0.02	34.96	1.85	100.96	1.10	99.86
1 / 9 .	0.19	4.63	0.51	0.94	3.36	4.30	11.22	0.31	24.33	0.22	14.17	0.05	0.00	35.17	1.77	101.17	1.13	100.05
1 / 10 .	0.21	4.51	0.52	0.99	3.38	4.35	11.26	0.33	24.02	0.22	14.07	0.04	0.00	35.17	1.74	100.82	1.11	99.72
Average	0.16	4.62	0.52	0.90	3.42	4.22	11.27	0.31	24.17	0.22	14.22	0.03	0.00	35.03	1.81	100.93	1.11	99.82
2 / 1 .	0.22	4.65	0.50	1.02	3.38	4.90	11.22	0.25	24.32	0.11	13.66	0.04	-0.01	36.16	0.97	101.39	1.14	100.26
2 / 2 .	0.24	4.76	0.45	0.99	3.37	4.80	11.19	0.27	24.04	0.17	13.74	-0.01	0.03	36.01	0.96	101.02	1.17	99.84
2 / 3 .	0.24	4.73	0.46	0.97	3.31	4.76	11.15	0.28	24.11	0.16	13.81	0.01	-0.01	35.99	0.90	100.88	1.17	99.71
2 / 4 .	0.27	4.75	0.43	0.98	3.40	4.75	11.24	0.30	24.21	0.17	13.87	0.02	-0.03	35.78	0.84	101.02	1.19	99.83
2 / 5 .	0.25	4.80	0.43	0.93	3.32	4.73	11.24	0.30	24.09	0.08	13.86	0.02	-0.01	35.81	0.91	100.77	1.19	99.58
2 / 6 .	0.23	4.70	0.48	0.97	3.39	4.69	11.14	0.31	24.10	0.22	14.13	0.03	0.06	35.87	0.96	101.27	1.16	100.12
2 / 7 .	0.18	4.75	0.47	0.99	3.42	4.65	11.12	0.37	24.15	0.09	13.96	0.06	-0.01	35.68	0.86	100.75	1.15	99.60
2 / 8 .	0.23	4.77	0.45	0.96	3.40	4.59	11.24	0.31	24.25	0.14	13.87	-0.01	0.01	35.71	1.02	100.95	1.17	99.77
2 / 9 .	0.22	4.67	0.48	0.98	3.34	4.62	11.21	0.29	24.13	0.17	13.95	0.02	0.01	35.81	0.98	100.88	1.14	99.73
2 / 10 .	0.27	4.70	0.45	1.01	3.36	4.68	11.22	0.29	24.30	0.26	13.92	0.06	0.02	35.81	0.94	101.27	1.17	100.10
Average	0.23	4.73	0.46	0.98	3.37	4.72	11.20	0.30	24.17	0.16	13.88	0.02	0.00	35.86	0.93	101.02	1.16	99.85

Table A.4. Amphibole chemistries
*Analyses not used in mineral chemistry calculations

BB6-6 Amp	Wt% Oxide																	
Formula	F	Cl	H2O	Na2O	K2O	MgO	CaO	MnO	FeO	BaO	Al2O3	V2O3	Cr2O3	SiO2	TiO2	Total	O=F , Cl	Total
3 / 1 .	0.21	5.00	0.39	0.82	3.48	4.37	11.18	0.29	24.05	0.25	14.61	0.02	-0.01	35.11	0.77	100.55	1.21	99.34
3 / 2 .	0.16	5.09	0.39	0.85	3.44	4.48	11.22	0.30	24.12	0.34	14.48	-0.01	0.01	35.27	0.83	100.96	1.22	99.75
3 / 3 .	0.18	4.98	0.41	0.90	3.42	4.47	11.24	0.29	24.29	0.17	14.31	0.04	-0.01	35.35	0.86	100.91	1.20	99.71
3 / 4 .	0.20	4.87	0.43	0.87	3.38	4.62	10.98	0.29	24.73	0.30	14.30	0.02	-0.01	35.16	0.88	101.01	1.18	99.83
3 / 5 .	0.17	4.98	0.41	0.88	3.47	4.26	11.19	0.32	24.42	0.32	14.38	0.02	0.00	34.92	0.96	100.70	1.19	99.51
3 / 6 .	0.17	4.92	0.42	0.88	3.42	4.43	10.95	0.30	24.22	0.34	14.31	0.01	0.00	35.00	0.85	100.22	1.18	99.04
3 / 7 .	0.19	5.07	0.39	0.91	3.41	4.56	11.18	0.38	24.34	0.22	14.18	0.04	0.02	35.40	0.89	101.18	1.22	99.96
3 / 8 .	0.22	5.08	0.35	0.90	3.42	4.46	11.04	0.31	24.28	0.14	14.25	0.00	0.01	35.19	0.83	100.49	1.24	99.25
3 / 9 .	0.22	4.99	0.39	0.94	3.37	4.52	11.15	0.32	24.13	0.29	14.28	0.01	-0.01	35.29	0.83	100.72	1.22	99.50
3 / 10 .	0.18	4.95	0.42	0.91	3.36	4.52	11.16	0.31	24.30	0.27	14.45	-0.02	0.05	35.18	0.92	100.98	1.19	99.78
Average	0.19	4.99	0.40	0.89	3.42	4.47	11.13	0.31	24.29	0.26	14.35	0.01	0.01	35.19	0.86	100.77	1.21	99.56
4 / 1 .	0.25	4.32	0.56	1.01	3.26	4.49	11.08	0.28	24.78	0.22	13.44	0.01	0.02	35.88	1.48	101.08	1.08	100.00
4 / 2 .	0.21	4.07	0.66	1.01	3.10	4.64	11.15	0.30	25.08	0.09	12.82	0.01	-0.04	36.56	1.46	101.17	1.01	100.16
4 / 3 .	0.23	4.32	0.58	1.05	3.20	4.57	11.28	0.30	24.54	0.01	13.30	0.06	-0.02	36.13	1.54	101.11	1.07	100.04
4 / 4 .	0.18	4.31	0.60	1.06	3.22	4.61	11.03	0.31	24.38	0.21	13.23	-0.02	-0.03	36.02	1.64	100.79	1.05	99.74
4 / 5 .	0.28	4.25	0.57	1.08	3.26	4.63	11.16	0.31	24.47	0.17	13.25	0.01	0.01	36.07	1.69	101.22	1.08	100.14
4 / 6 .	0.24	4.29	0.58	1.08	3.20	4.69	11.13	0.28	24.42	0.15	13.21	0.01	0.00	35.90	1.68	100.86	1.07	99.79
4 / 7 .	0.23	4.25	0.59	1.09	3.22	4.61	11.18	0.33	24.57	0.04	13.19	0.06	0.00	35.91	1.66	100.94	1.06	99.89
4 / 8 .	0.20	4.26	0.61	1.05	3.16	4.62	11.16	0.29	24.64	0.15	13.25	0.01	-0.03	36.02	1.68	101.10	1.04	100.06
4 / 9 .	0.23	4.28	0.58	1.05	3.20	4.56	11.08	0.31	24.53	0.19	13.29	0.05	-0.01	35.86	1.57	100.79	1.06	99.73
4 / 10 .	0.22	4.23	0.60	1.05	3.19	4.51	11.21	0.31	24.52	0.11	13.31	0.01	0.06	35.94	1.56	100.83	1.05	99.78
Average	0.23	4.26	0.59	1.05	3.20	4.59	11.15	0.30	24.59	0.13	13.23	0.02	0.00	36.03	1.60	100.99	1.06	99.93

Table A.4. Amphibole chemistries
*Analyses not used in mineral chemistry calculations

BB6-6 Amp	Wt% Oxide																
Formula	F	Cl	H2O	Na2O	K2O	MgO	CaO	MnO	FeO	BaO	Al2O3	V2O3	Cr2O3	SiO2	TiO2	Total	O=F , Cl	Total
5 / 1 .	0.22	4.83	0.42	0.70	3.58	4.02	11.27	0.30	25.11	0.09	13.83	0.02	0.01	35.46	0.65	100.51	1.18	99.33
5 / 2 .	0.22	4.65	0.47	0.96	3.36	4.11	11.21	0.28	25.41	0.18	13.69	0.01	-0.02	35.46	0.79	100.80	1.14	99.66
5 / 3 .	0.21	4.71	0.45	0.94	3.21	4.16	11.13	0.29	25.23	0.16	13.61	0.02	-0.02	35.38	0.95	100.46	1.15	99.31
5 / 4 .	0.22	4.70	0.45	1.01	3.25	4.17	11.10	0.25	25.07	0.17	13.63	0.01	0.00	35.43	0.94	100.44	1.15	99.28
5 / 5 .	0.18	4.56	0.52	1.05	3.18	4.20	11.15	0.29	25.15	0.10	13.52	0.01	-0.01	35.65	0.94	100.52	1.11	99.41
5 / 6 .	0.22	4.52	0.51	1.04	3.13	4.16	11.09	0.32	25.51	0.26	13.50	-0.03	-0.05	35.58	0.92	100.75	1.11	99.64
5 / 7 .	0.26	4.62	0.46	1.03	3.22	4.18	11.05	0.33	24.94	0.18	13.47	0.04	-0.04	35.55	0.98	100.31	1.15	99.15
5 / 8 .	0.18	4.49	0.54	1.06	3.16	4.29	11.14	0.30	25.15	0.12	13.42	-0.01	-0.02	35.64	1.11	100.60	1.09	99.51
5 / 9 .	0.24	4.58	0.49	1.06	3.18	4.27	11.22	0.33	25.49	0.25	13.39	0.02	0.00	35.51	1.20	101.24	1.13	100.10
5 / 10 .	0.24	4.47	0.51	1.09	3.13	4.23	11.09	0.29	24.89	0.25	13.43	0.02	-0.03	35.60	0.99	100.23	1.11	99.12
Average	0.22	4.61	0.48	0.99	3.24	4.18	11.15	0.30	25.20	0.18	13.55	0.01	-0.02	35.53	0.95	100.58	1.13	99.45

BB12-3 Amp	Wt% Oxide																
Formula	F	Cl	H2O	Na2O	K2O	MgO	CaO	MnO	FeO	BaO	Al2O3	V2O3	Cr2O3	SiO2	TiO2	Total	O=F , Cl	Total
6 / 1 .	0.38	2.94	0.90	1.06	3.16	5.33	11.12	0.11	23.55	0.08	13.32	0.11	0.04	36.83	2.01	100.94	0.82	100.12
6 / 2 .	0.34	2.94	0.92	1.09	3.16	5.42	11.21	0.14	23.75	0.22	13.30	0.06	-0.01	36.84	1.87	101.28	0.81	100.47
6 / 3 .	0.33	3.00	0.90	1.09	3.18	5.23	11.11	0.12	23.64	0.03	13.27	0.09	0.03	36.87	1.78	100.67	0.82	99.85
6 / 4 .	0.35	2.96	0.91	1.06	3.13	5.31	11.22	0.14	23.64	0.03	13.26	0.08	-0.04	36.99	1.82	100.89	0.82	100.07
6 / 5 .	0.36	2.99	0.89	1.08	3.17	5.36	11.12	0.12	23.52	- 0.01	13.35	0.04	0.03	36.85	1.82	100.71	0.83	99.88
6 / 6 .	0.37	2.94	0.89	1.04	3.12	5.30	11.07	0.12	23.55	0.09	13.22	0.10	-0.03	36.88	1.71	100.41	0.82	99.59
6 / 7 .	0.38	2.99	0.88	1.06	3.14	5.29	11.16	0.13	23.70	0.02	13.22	0.07	0.00	36.93	1.91	100.89	0.84	100.06
6 / 8 .	0.34	2.95	0.91	1.09	3.06	5.27	11.23	0.14	23.91	- 0.06	13.37	0.11	0.03	36.71	1.95	101.07	0.81	100.26
6 / 9 .	0.29	2.97	0.94	1.03	3.16	5.24	11.20	0.15	23.88	0.00	13.36	0.11	0.03	36.82	1.98	101.17	0.79	100.37
6 / 10 .	0.37	3.01	0.88	1.01	3.22	5.18	11.23	0.13	23.57	- 0.06	13.57	0.07	0.02	36.60	2.01	100.87	0.83	100.03
Average	0.35	2.97	0.90	1.06	3.15	5.29	11.17	0.13	23.67	0.03	13.33	0.08	0.01	36.83	1.89	100.89	0.82	100.07

Table A.4. Amphibole chemistries
*Analyses not used in mineral chemistry calculations

BB12-3 Amp — Wt% Oxide

Formula	F	Cl	H2O	Na2O	K2O	MgO	CaO	MnO	FeO	BaO	Al2O3	V2O3	Cr2O3	SiO2	TiO2	Total	O=F , Cl	Total
7 / 1 .	0.28	2.84	0.98	1.16	3.11	5.22	11.15	0.13	24.02	0.05	12.75	0.07	0.05	37.08	2.28	101.15	0.76	100.39
7 / 2 .	0.34	2.82	0.95	1.13	3.07	5.31	11.05	0.19	24.03	0.01	12.75	0.09	-0.02	37.10	2.29	101.14	0.78	100.36
7 / 3 .	0.32	2.79	0.97	1.13	3.04	5.27	11.15	0.16	23.73	0.03	12.82	0.10	-0.02	37.05	2.40	100.93	0.76	100.17
7 / 4 .	0.33	2.80	0.96	1.16	3.01	5.29	11.04	0.15	23.70	0.03	12.77	0.12	0.01	37.17	2.15	100.69	0.77	99.91
7 / 5 .	0.30	2.80	0.98	1.11	3.06	5.29	11.14	0.15	23.95	0.09	12.78	0.06	0.01	37.20	2.35	101.26	0.76	100.50
7 / 6 .	0.30	2.92	0.94	1.12	3.02	5.24	11.07	0.10	23.81	0.02	12.85	0.07	0.05	36.98	2.24	100.70	0.79	99.91
7 / 7 .	0.29	2.91	0.96	1.16	3.05	5.24	11.08	0.18	24.04	0.11	12.91	0.08	0.07	37.17	2.33	101.57	0.78	100.79
7 / 8 .	0.33	2.88	0.94	1.12	3.04	5.25	11.04	0.11	23.90	0.08	12.82	0.07	0.03	37.13	2.29	100.95	0.79	100.16
7 / 9 .	0.31	2.91	0.95	1.16	3.11	5.40	11.10	0.16	24.12	0.09	12.86	0.13	0.08	37.06	2.36	101.79	0.79	101.00
7 / 10 .	0.31	2.82	0.97	1.16	3.07	5.32	11.04	0.18	23.66	0.04	12.82	0.09	0.02	37.04	2.31	100.83	0.77	100.06
Average	0.31	2.85	0.96	1.14	3.06	5.28	11.09	0.15	23.90	0.03	12.81	0.09	0.03	37.10	2.30	101.10	0.77	100.33
8 / 1 .	0.34	2.68	0.99	1.10	3.05	5.56	11.30	0.16	23.05	0.01	12.88	0.06	0.05	36.81	2.42	100.45	0.75	99.70
8 / 2 .	0.32	2.66	1.00	1.08	3.07	5.49	11.22	0.15	23.23	0.13	12.96	0.12	0.00	37.10	2.16	100.69	0.74	99.95
8 / 3 .	0.34	2.68	0.99	1.09	3.09	5.62	11.17	0.17	23.48	0.05	12.89	0.10	0.02	36.94	2.21	100.83	0.75	100.08
8 / 4 .	0.37	2.71	0.97	1.12	3.09	5.58	11.29	0.16	23.05	0.01	12.99	0.07	-0.01	36.95	2.29	100.63	0.77	99.87
8 / 5 .	0.36	2.75	0.96	1.07	3.10	5.55	11.41	0.16	23.17	0.20	12.86	0.09	0.04	36.93	2.29	100.95	0.77	100.17
8 / 6 .	0.35	2.73	0.97	1.11	3.12	5.49	11.26	0.17	23.05	0.07	12.93	0.12	0.02	37.00	2.35	100.75	0.76	99.99
8 / 7 .	0.32	2.72	0.98	1.10	3.09	5.52	11.24	0.16	23.15	0.17	12.90	0.09	0.04	36.94	2.19	100.62	0.75	99.87
8 / 8 .	0.33	2.67	1.00	1.16	3.04	5.48	11.24	0.17	23.26	0.06	12.88	0.09	0.07	36.96	2.53	100.94	0.74	100.20
8 / 9 .	0.36	2.76	0.96	1.14	3.02	5.51	11.25	0.16	22.97	0.13	12.95	0.10	0.03	36.91	2.40	100.63	0.77	99.86
8 / 10 .	0.34	2.73	0.99	1.08	3.04	5.52	11.18	0.16	23.27	0.07	12.97	0.07	0.04	37.15	2.44	101.04	0.76	100.28
Average	0.34	2.71	0.98	1.11	3.07	5.53	11.26	0.16	23.17	0.09	12.92	0.09	0.03	36.97	2.33	100.75	0.76	100.00

Table A.4.   Amphibole chemistries
*Analyses not used in mineral chemistry calculations

BB12-3 Amp	Wt% Oxide																	
Formula	F	Cl	H2O	Na2O	K2O	MgO	CaO	MnO	FeO	BaO	Al2O3	V2O3	Cr2O3	SiO2	TiO2	Total	O=F , Cl	Total
9 / 1 .	0.40	2.96	0.88	1.17	2.92	5.76	11.18	0.17	22.69	0.09	13.15	0.07	0.00	36.94	1.85	100.22	0.84	99.38
9 / 2 .	0.39	2.90	0.91	1.19	2.99	5.79	11.20	0.18	23.19	0.15	13.17	0.07	0.02	36.89	1.82	100.87	0.82	100.05
9 / 3 .	0.40	2.94	0.89	1.18	2.99	5.79	11.10	0.13	22.95	0.11	13.20	0.09	-0.01	36.95	1.79	100.49	0.83	99.66
9 / 4 .	0.39	2.96	0.89	1.19	3.02	5.80	11.28	0.14	22.79	0.08	13.10	0.08	0.05	36.89	1.95	100.61	0.83	99.77
9 / 5 .	0.39	2.84	0.92	1.19	2.95	5.76	11.29	0.14	22.71	0.01	13.20	0.07	0.02	36.87	1.93	100.28	0.81	99.48
9 / 6 .	0.34	2.90	0.92	1.18	2.96	5.78	11.19	0.19	22.96	0.08	13.13	0.05	0.03	36.92	1.87	100.52	0.80	99.72
9 / 7 .	0.39	2.88	0.91	1.22	3.01	5.71	11.18	0.15	22.99	0.01	13.21	0.08	0.01	36.76	1.91	100.40	0.81	99.59
9 / 8 .	0.38	2.96	0.89	1.16	3.01	5.59	11.11	0.17	23.14	0.15	13.36	0.06	0.03	36.58	1.90	100.48	0.83	99.65
9 / 9 .	0.36	2.92	0.91	1.17	3.02	5.53	11.20	0.16	23.41	0.11	13.26	0.03	-0.02	36.66	1.86	100.60	0.81	99.79
9 / 10 .	0.33	3.03	0.90	1.15	3.02	5.59	11.33	0.14	23.40	0.01	13.27	0.09	-0.01	36.71	1.86	100.82	0.82	100.00
Average	0.38	2.93	0.90	1.18	2.99	5.71	11.21	0.16	23.02	0.07	13.20	0.07	0.01	36.82	1.87	100.53	0.82	99.71
10 / 1 .	0.35	3.37	0.79	1.01	3.20	5.60	11.26	0.15	23.25	0.05	13.52	0.05	0.00	36.58	1.36	100.55	0.91	99.64
10 / 2 .	0.32	3.34	0.82	1.03	3.23	5.58	11.28	0.15	23.49	0.02	13.55	0.06	0.05	36.63	1.39	100.93	0.89	100.04
10 / 3 .	0.38	3.35	0.78	1.02	3.24	5.56	11.32	0.18	23.17	0.01	13.49	0.08	0.05	36.66	1.41	100.70	0.92	99.78
10 / 4 .	0.37	3.35	0.79	0.99	3.22	5.54	11.33	0.18	23.55	0.09	13.58	0.08	-0.02	36.67	1.40	101.14	0.91	100.23
10 / 5 .	0.40	3.34	0.74	1.01	3.20	5.32	11.22	0.14	23.55	0.02	13.15	0.06	-0.02	35.87	1.44	99.46	0.92	98.54
10 / 6 .	0.33	3.44	0.78	0.97	3.27	5.40	11.35	0.13	23.71	0.13	13.66	0.04	0.03	36.35	1.37	100.95	0.92	100.03
10 / 7 .	0.36	3.48	0.75	0.94	3.32	5.19	11.26	0.18	24.34	0.07	13.93	0.06	0.01	35.92	1.41	101.22	0.94	100.28
10 / 8 .	0.32	3.44	0.78	0.89	3.35	5.39	11.32	0.13	23.58	0.05	13.41	0.06	0.03	36.46	1.28	100.44	0.91	99.53
10 / 9 .	0.34	3.42	0.78	0.90	3.31	5.55	11.30	0.21	23.63	0.05	13.26	0.07	0.01	36.63	1.33	100.79	0.91	99.88
10 / 10 .	0.38	3.34	0.77	0.83	3.33	5.54	11.25	0.15	23.76	0.03	13.05	0.06	0.00	36.68	1.26	100.42	0.91	99.50
Average	0.36	3.39	0.78	0.96	3.27	5.47	11.29	0.16	23.60	0.04	13.46	0.06	0.01	36.44	1.37	100.66	0.91	99.74

Table A.5. Summary of samples gathered from Bennies Brook, NY.

Sample #	In Situ	Thin Sections Made
BB1	Y	3
BB2	Y	4
BB3	Y	3
BB4	Y	-
BB5	Y	3
BB6	Y	6
BB7	Y	2
BB8	Y	4
BB9	Y	6
BB10	Y	2
BB11	Y	-
BB12	Y	8
BB14	Y	-
ADK1	N	2
ADK4	N	-
ADK5	N	2
ADK6	N	-
ADK7	N	6

BIOGRAPHY OF THE AUTHOR

James Hodge was born November 27th, 1990 in Stamford, CT. He was homeschooled alongside his two siblings until deciding to enroll part time at Schenectady County Community College, NY, where he dabbled in various subjects until finding interest in science in an introductory chemistry class. From there, he transitioned to the College of Saint Rose in Albany, NY, where he worked as a student researcher in Colorado and New York before graduating with a Bachelor of Science degree in Geology. His continued interest in Earth sciences led him to graduate school, and he was accepted into the University of Maine to pursue a master's degree in microstructural geology. James plans to continue to reside in Maine with his fiancée Ashley, a fellow geologist, and work in the field of environmental science. James is a candidate for the Master of Science degree in Earth and Climate Sciences from the University of Maine in August 2019.